THE ASTROPHYSICAL JOURNAL SUPPLEMENT SERIES, 100:37–68, 1995 September

MULTIFREQUENCY SPECTRA OF *EXOSAT* BLAZARS

K. K. GHOSH AND S. SOUNDARARAJAPERUMAL
Indian Institute of Astrophysics, Vainu Bappu Observatory, Kavalur, Alangayam, N.A., T.N., 635701 India
Received 1993 July 22; accepted 1995 January 3

ABSTRACT

Blazars have been divided into two groups: radio-selected blazars (RBLs) and X-ray–selected blazars (XBLs). Results of the X-ray spectral analysis of 28 such blazars which were observed with *EXOSAT* are presented in this paper, and in four these are new results which were not published earlier. X-ray results suggest that XBLs are steep-spectrum sources and RBLs are relatively flat-spectrum sources. Even though the RBLs are, in general, higher redshift objects than XBLs, they are slightly more luminous (by a factor of 4–7) in X-rays than XBLs. However, the RBLs are much more luminous (by two to three orders of magnitude) in radio than the XBLs. Using simultaneous/quasi-simultaneous and nonsimultaneous observations, we have constructed the multifrequency spectra (radio through X-ray continuum fluxes) of 28 blazars, and they can be well represented with a single parabolic curve for XBLs and with two parabolic curves for RBLs. One of the important differences between the multifrequency spectra of RBLs and XBLs is the spectral discontinuity in the UV–X-ray region of RBLs. This result has been confirmed by only using simultaneous UV and X-ray observations of 50% of the sources of the present sample. Luminosities at different bands have also been computed for all the blazars in the present sample, and a bimodal character of the distribution of these objects has been found in the radio and X-ray luminosity plane. All these results will be discussed in the framework of a "wide-jet" model.

Subject headings: BL Lacertae objects: general — quasars: general — radiation mechanisms: nonthermal — X-rays: galaxies

1. INTRODUCTION

The term "blazar" was coined by E. Speigel in a banquet speech at the Pittsburgh meeting on BL Lacertae objects (Wolfe 1978), which was the topic of the first conference after the discovery of the first example (Schmitt 1968). Around that time the characteristics of BL Lac objects were reviewed by Kinman (1975), Stein, O'Dell, & Strittmatter (1976), and Stein (1978), and more than 50 objects were classified as BL Lac objects based on the following characteristics: (1) strong variability at radio, optical, infrared, and X-ray frequencies; (2) strong and variable linear polarization in the radio, infrared, and optical bands; and (3) featureless (or weak emission and/or absorption) optical spectrum. The featureless optical continuum may be due to the absence of gas around the BL Lac objects, which was suggested based on the radio (Jones & O'Dell 1977), optical (Strittmatter et al. 1974; Wills & Wills 1976; Miller, French, & Hawley 1978), ultraviolet (Boksenberg et al. 1978), and X-ray (Mushotzky et al. 1978) observations. However, several BL Lac objects which are embedded in the nuclei of galaxies were also detected (Ulrich et al. 1975).

In 1980 Angel & Stockman (1980) made a list of blazars, which were usually variable and highly polarized objects. Later Moore & Stockman (1981, 1984) produced a list of highly polarized quasars (HPQs), and around that time the term "optically violent variable" (OVV) was also introduced (Angel & Stockman 1980; Ledden & O'Dell 1985). Presently, BL Lac objects, HPQs, and OVVs are classed as blazars. They are core-dominated radio sources, displaying superluminal motion, rapid variability, and relatively high optical polarization (Stickel et al. 1991; Urry, Padovani, & Stickel 1991b; Padovani & Urry 1992; and references therein). Also, these objects have displayed variable optical polarization, which often shows various types of frequency dependence on the polarization (Smith et al. 1987; Sitko 1989; Mead et al. 1990; Valtaoja et al. 1991). Recently Impey (1992) studied a sample of 65 blazars using the VLBI and optical spectroscopic and polarimetric data. He has suggested that BL Lac objects with measured VLBI kinematics have slower apparent superluminal motion ($v/c < 4$) than HPQs/OVVs ($v/c > 8$). Also, it has been suggested by him that BL Lac objects differ significantly from HPQs/OVVs in terms of luminosity, continuum shape, and apparent superluminal motions.

It can be seen from the literature that the strength of the emission lines (5 Å equivalent width) was used to classify a sample of flat-spectrum radio sources from the Parkes catalog (Wilkes 1986) and a sample of X-ray–selected BL Lac objects (XBLs) from the *Einstein* Extended Medium-Sensitivity Survey (EMSS) (Stocke et al. 1990). It is also evident from the literature that the same object displayed weak and strong emission lines during its brighter and fainter states, respectively (Stein et al. 1976; Moore & Stockman 1981, 1984). Thus the classification of blazars based on the line emission strength criteria may be arbitrary. However, they may be classified based on their detection technique, because most of the blazars have been discovered either at radio or at X-ray frequencies, which has led to a subdivision of the blazars into radio-selected blazars (RBLs) and X-ray–selected blazars (XBLs). RBLs and XBLs have common characteristics, but important differences have also been detected in their core dominance, optical polarization, radio luminosity, and variability properties (Perlman & Stocke 1993; Jannuzi, Smith, & Elston 1994). Also, the number counts and cosmological evolution of RBLs appear to

be different from those of the XBLs (Morris et al. 1991; Wolter et al. 1994).

In this paper we present the results of the X-ray (0.04–10 keV) spectral analysis of 28 blazars (Table 1) which were observed with *EXOSAT*. We present the X-ray spectra of four blazars (AO 0235+164, 0754+10, OJ 287, 1921−293 [OV 236]) which were not published earlier. Also, the multifrequency spectra and the luminosities at different frequencies of 28 blazars will be used for the analysis. A brief discussion about the completeness of the sample is given in § 2, and we describe the observations and analysis of the X-ray and multifrequency spectra in § 3. The results are given in § 4, and the discussion is given in § 5. Throughout this paper, the values of $H_0 = 50$ km s^{-1} Mpc^{-1} and $q_0 = 0$ have been used.

2. THE *EXOSAT* BLAZAR SAMPLE

We have selected all the BL Lac objects, HPQs, and OVVs from the *EXOSAT* database system (ESA TM-13 [1991]). Our selection led to a total of 49 blazars observed by *EXOSAT*. All the objects in our sample are contained in the list of Burbidge & Hewitt (1992) and in the catalog of Véron-Cetty & Véron (1993). A number of criteria were then imposed on this sample to make sure that the spectra analyzed were good and were uncontaminated. The criteria followed to reject the spectra are as follows: (1) a flux less than 4 times its error and (2) a data-quality factor less than 3 (the data-quality flag takes account of solar contamination, high background, and other factors that would affect the quality of the detection (for details see ESA TM-12 [1991]). Based on the above criteria, we have rejected the spectra (2–10 keV) of 16 blazars (GC 0109+224, 0300+470 [4C 47.08], PKS 0537−44, 0855+143 [3CR 212], 0923+39, MC 1057+100 [S5 1150+812], 1150+812, B2 1156+295, 1E 1235+63, 3C 279, B2 1308+326, OQ 530, AP Lib, 4C 14.60, BL Lac, and PHL 5200) whose signal-to-noise ratios were too poor to derive any spectral parameters. Also, the spectra of five blazars (PKS 0735+17, 1E 1207.9+3945, ON 325, 2A 1218+304, and 3C 446) were rejected because they were contaminated by other bright sources in the field. Finally, we are left with 28 blazars, and they are listed in Table 1. These 28 objects form the complete sample of *EXOSAT* blazars (for spectroscopic studies), because we have not excluded any object for which good spectrum (at least at the level of 4 σ signal significance) is available from *EXOSAT* observations. Most of the objects of this sample (except NRAO 140, 3C 120, 3C 273, PKS 1510−089, OV 236, 3C 390.3 and 1928+73 [4C 73.18]) have already been classified into RBLs and XBLs by Giommi et al. (1990), and we have followed the same classification. NRAO 140, 3C 273, PKS 1510−089, OV 236, and 1928+73 (4C 73.18) have been classified as RBLs following

TABLE 1

INFORMATION ABOUT THE BLAZARS

Object Name	R.A. (1950)	Decl. (1950)	z	$F_{5\,\mathrm{GHz}}$ (Jy)	5 HGz Reference	M_{abs}	Selection[a]
3C 66A	$02^h19^m30^s$	42°48′30″	0.444	1.04	1	−27.2	R
AO 0235+164	02 35 53	16 2405	0.940	2.79	2	−28.7	R
1E 0317+18	03 17 01	18 3445	0.190	0.01	3	−22.1	X
H0323+022	03 23 38	02 1447	0.147	0.04	4	−23.1	X
NRAO 140	03 33 22	32 0836	1.263	2.50	5	−27.6	R
1H 0414+009	04 14 18	00 5803	0.287	0.08	6	−24.9	X
3C 120	04 30 32	05 1459	0.033	5.09	5	−21.4	R
PKS 0521−36	05 21 13	−36 3016	0.061	8.89	7	−23.2	R
PKS 0548−32	05 48 50	−32 1656	0.069	0.08	3	−22.6	X
PKS 0754+10	07 54 23	10 0440	...	1.48	1	...	R
OJ 287	08 51 57	20 1758	0.306	3.60	8	−26.0	R
Mrk 421	11 01 41	38 2843	0.031	0.53	9	−22.8	X
Mrk 180	11 33 30	70 2500	0.046	0.25	10	−22.7	X
B2 1147+245	11 47 44	24 3435	...	1.00	11	...	R
3C 273	12 26 33	02 1943	0.158	43.41	5	−27.0	R
1E 1402+04	14 02 20	04 1621	...	0.018	12	...	X
1E 1415+259	14 15 41	25 5715	0.237	0.05	13	−24.8	X
1H 1427+42	14 26 36	42 5346	0.129	0.03	14	−22.9	X
PKS 1510−089	15 10 09	−08 5448	0.361	4.36	5	−25.3	R
Mrk 501	16 52 12	39 5026	0.034	1.20	15	−22.6	X
4U 1722+119	17 22 44	11 5452	...	0.08	16	...	X
I Zw 186	17 27 04	50 1531	0.055	0.15	1	−21.6	X
3C 371	18 07 18	69 4858	0.051	1.45	17	−23.2	R
3C 390.3	18 45 37	79 4306	0.057	4.48	5	−22.3	R
OV 236	19 21 42	−29 2027	0.352	8.00	18	−24.3	R
1928+73 (4C 73.18)	19 28 49	73 5145	0.302	3.34	10	−25.9	R
PKS 2005−489	20 05 47	−48 5843	0.071	1.19	19	−24.8	X
PKS 2155−304	21 55 58	−30 2752	0.341	0.31	20	−26.1	X

[a] R = radio-selected BL Lac objects and X = X-ray–selected BL Lac objects.

REFERENCES.—(1) Weiler & Johnston 1980; (2) Pauliny-Toth et al. 1972; (3) Stocke et al. 1985; (4) Feigelson et al. 1986; (5) Pauliny-Toth & Kellermann 1968; (6) Ulmer et al. 1983; (7) Shimmins & Bolton 1972; (8) Laundau et al. 1983; (9) Ulvestad, Johnston, & Weiler 1983; (10) Kuhr et al. 1981b; (11) Pauliny-Toth & Kellermann 1972; (12) Feigelson, Maccacaro, & Zamorani 1982; (13) Halpern et al. 1986; (14) Remillard et al. 1989; (15) Mufson et al. 1984; (16) Griffiths et al. 1989; (17) Perley 1982; (18) Giacani & Colomb 1988; (19) Wall et al. 1975; (20) Shimmins & Bolton 1974.

the classification of the Revised and Updated Catalog of Quasistellar Objects of Hewitt & Burbidge (1993). 3C 120 and 3C 390.3 are radio galaxies with superluminal motions (Zensus 1989; Porcas 1987) and also known as blazars (Angel & Stockman 1980; Webb et al. 1988; Ledden & O'Dell 1985). We have classified these two radio-loud blazars as RBLs. It can be seen from Table 1 that there are 14 XBLs and 14 RBLs in the present sample. Two-point spectral indices between the radio and optical bands (α_{RO}) and between the optical and X-ray bands (α_{OX}) are plotted in Figure 1. The indices α_{RO} and α_{OX} are defined as $\alpha_{RO} = -\log(F_R/F_O)/\log(\nu_R/\nu_O)$ and $\alpha_{OX} = -\log(F_O/F_X)/\log(\nu_O/\nu_X)$, where F_R, F_O, and F_X are the fluxes at 5 GHz (ν_R), 5560 Å (ν_O), and 1 keV (ν_X), respectively. Circles with crosses correspond to RBLs, and circles with dots to XBLs. The solid line shows the correlation between α_{RO} and α_{OX}, which is similar to that found by Ledden & O'Dell (1985) in a sample of blazars observed with the *Einstein Observatory*. From this figure it can also be seen that the XBLs are located to a region of the plane defined by $0.2 < \alpha_{RO} < 0.6$ and $0.7 < \alpha_{OX} < 1.2$. This clearly shows the bimodal nature of the distribution of blazars in the present sample, which was also noted in other samples observed with *Einstein* (Ledden & O'Dell 1985; Stocke et al. 1985; Stocke et al. 1988; Worrall et al. 1987). Note that the same distribution, as found with *EXOSAT* blazars, is also present in the two complete samples of radio- and X-ray–selected blazars (Stickel et al. 1991; Morris et al. 1991).

3. OBSERVATIONS AND ANALYSIS

3.1. *X-Ray Spectra*

EXOSAT observations of these sources were carried out with *EXOSAT* using low- and medium-energy (LE and ME) detectors. The LE (0.04–2 keV) observations used Lexan 3000 (LX3) and aluminum/parylene (Al/P) filters (White & Peacock 1988) with the CMA detectors (de Korte et al. 1981). Background-subtracted LE count rates with errors were obtained from the *EXOSAT* database (White & Giommi 1991). The X-Ray Analysis and Data Utilization (XANADU) software package was used to convert the background-subtracted LE count rates to obtain the LE pulse-height analyzer (PHA) spectra. Eight argon-filled proportional counters were used as the ME detectors (Turner, Smith, & Zimmermann 1981) to obtain the ME spectra. These detectors were divided into two groups of four, which could either be aligned with the pointing axis or offset by up to 2° to obtain background emissions. The ME observation mode for the above blazars was with the two detector groups offset to obtain simultaneous background data, which were used to eliminate background effects from the source data.

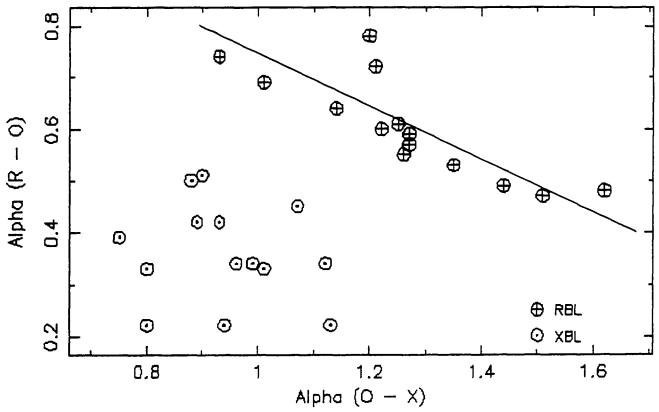

FIG. 1.—Plot of two-point spectral indices of 28 blazars between radio and optical bands (α_{RO}) and between the optical and X-ray bands (α_{OX}).

The observations flagged 3 or above with flux $\geq 4\ \sigma$ were retrieved from the *EXOSAT* database. A log of the LE and ME observations and the corresponding count rates are given in Table 2. The last two columns of this table show the channel range and the signal significance of the blazars. In this table we have included only those observations of *EXOSAT* which have signal significances at the level of 4 σ and above.

The LE and ME spectra of 28 blazars were analyzed with the X-Ray Spectral Fitting (XSPEC) fitting program (Shafer, Haberl, & Arnaud 1991). A number of trial models, folded with the instrumental responses, were used to fit the data, and the best-fitting parameters were obtained by minimizing χ^2_r. A simple power-law plus uniform absorption model with the effective photoelectric cross sections given by Morrison & McCammon (1983) and with the absorption column density N_H was used to fit the spectra. This model fits well with the spectra of most of the sources. However, the best-fit parameters of this model for two sources (3C 273, PKS 2155−304) show that the derived values of N_H are smaller than the corresponding Galactic N_H values. In the next model we have fitted the spectra of these two sources by freezing the values of N_H with the corresponding Galactic N_H values. The Galactic values of N_H are taken from the *EXOSAT* database by using the GETNH program, which runs under the XANADU system. This covers the whole sky and uses various 21 cm radio surveys for its source data (Stark et al. 1992 and others). Errors on the quoted Galactic absorbing columns are typically of the order of 10^{19} cm^{-2} (Elvis, Lockman, & Wilkes 1989). The best-fitting parameters of the above models are listed in Table 3 along with the computed fluxes for the 0.1–2 and 2–10 keV ranges. These fluxes were obtained from the spectral fit using the power-law plus absorption model, and they have not been corrected for the absorption. The 90% confidence error bars, which were computed for each parameter keeping the rest of the parameters free following the procedure detailed by Lampton, Margon, & Bowyer (1976) ($\chi^2_{min} + 4.61$ for two free parameters), of the fit parameters are also listed in Table 3 along with the χ^2_r values. It may be noted from Table 3 that the X-ray spectra of few sources (Mrk 421, 3C 273, and PKS 2155−304) cannot be well represented by the power-law plus absorption model ($\chi^2_r > 2$). To fit the spectra of these sources, we have added other spectral components, such as blackbody, thermal bremsstrahlung, high-energy cutoff, and absorption edge, with the power-law plus fixed absorption model. Also, we have used the broken power-law and double power-law models to fit the spectra of Mrk 421, 3C 273, and PKS 2155−304. The power-law plus fixed absorption plus absorption-edge model or high-energy cutoff model fits the spectra of Mrk 421 better than the power-law plus fixed absorption model, the power-law plus fixed absorption plus blackbody model, the power-law plus fixed absorption plus thermal bremsstrahlung model, the bro-

TABLE 2

LOG OF OBSERVATIONS OF THE LE AND ME SPECTRA AND COUNT RATES OF BLAZARS

SOURCE	START TIME[a]	END TIME[b]	LE COUNT RATE (10^{-4} cm^{-2} s^{-1}) LX3	LE COUNT RATE (10^{-4} cm^{-2} s^{-1}) Al/P	ME[c] COUNT RATE (10^{-3} cm^{-2} s^{-1})	ME SIGNAL SIGNIFICANCE Channel Range	ME SIGNAL SIGNIFICANCE Signal
3C 66A	1986, 006, 10:24	006, 15:29	0.51 ± 0.09	...	0.43 ± 0.04	5–13	~4 σ
	1986, 032, 08:12	032, 19:25	0.33 ± 0.06	...	0.47 ± 0.02	5–20	≥4 σ
AO 0235+164	1984, 214, 03:22	214, 07:49	0.08 ± 0.02	...	0.25 ± 0.04	6–30	≥4 σ
1E 0317+18	1985, 013, 18:55	013, 23:14	0.95 ± 0.21	...	1.04 ± 0.09	5–14	≥4 σ
	1985, 039, 22:08	040, 03:05	0.89 ± 0.14	0.97 ± 0.16	0.70 ± 0.04	5–18	≥4 σ
H0323+022	1984, 265, 06:47	265, 12:16	3.58 ± 0.42	...	1.33 ± 0.12	5–15	≥4 σ
	1984, 267, 06:26	267, 12:16	3.07 ± 0.22	...	0.89 ± 0.04	4–16	≥4 σ
NRAO 140	1985, 025, 14:43	025, 22:43	0.31 ± 0.04	...	0.77 ± 0.03	4–23	≥4 σ
	1985, 025, 23:56	026, 08:56	0.31 ± 0.04	...	0.80 ± 0.03	5–25	≥4 σ
1H 0414+009	1984, 253, 09:16	253, 02:45	3.99 ± 0.50	2.68 ± 0.36	2.16 ± 0.05	4–24	≥4 σ
	1984, 258, 07:48	258, 11:20	4.25 ± 0.40	3.00 ± 0.28	2.57 ± 0.05	3–25	≥4 σ
	1984, 266, 10:16	266, 13:16	4.31 ± 0.50	2.45 ± 0.25	1.70 ± 0.05	4–19	≥4 σ
	1984, 274, 09:01	274, 11:49	4.37 ± 0.46	2.81 ± 0.34	1.29 ± 0.05	5–16	≥4 σ
3C 120	1983, 228, 08:47	229, 07:35	4.37 ± 0.23	3.22 ± 0.23	3.34 ± 0.04	3–33	≥4 σ
	1983, 305, 08:20	305, 13:50	4.83 ± 0.34	3.57 ± 0.34	3.16 ± 0.04	3–24	≥4 σ
	1984, 249, 11:53	249, 19:41	4.48 ± 0.48	3.95 ± 0.45	4.25 ± 0.04	3–33	≥4 σ
	1984, 276, 06:36	276, 18:28	3.92 ± 0.23	3.25 ± 0.33	4.44 ± 0.03	3–32	≥4 σ
	1984, 277, 10:24	277, 15:48	3.18 ± 0.19	2.79 ± 0.28	3.83 ± 0.08	4–31	≥4 σ
	1984, 278, 13:02	278, 18:34	3.21 ± 0.39	3.13 ± 0.31	3.40 ± 0.04	4–29	≥4 σ
	1984, 280, 13:48	280, 20:35	3.12 ± 0.17	2.44 ± 0.27	2.87 ± 0.04	4–31	≥4 σ
	1984, 284, 03:27	284, 08:46	3.29 ± 0.23	2.29 ± 0.26	3.27 ± 0.04	3–27	≥4 σ
	1984, 286, 01:26	286, 06:33	3.88 ± 0.30	2.33 ± 0.33	3.61 ± 0.04	3–29	≥4 σ
	1985, 044, 23:35	045, 05:46	3.29 ± 0.22	...	3.07 ± 0.05	4–26	≥4 σ
	1985, 283, 19:59	284, 10:00	4.05 ± 0.27	2.44 ± 0.39	3.87 ± 0.04	3–30	≥4 σ
	1986, 044, 15:02	044, 21:00	2.83 ± 0.44	2.10 ± 0.36	2.43 ± 0.04	4–26	≥4 σ
PKS 0521−36	1983, 306, 10:30	306, 15:00	1.29 ± 0.20	1.27 ± 0.20	0.97 ± 0.04	6–20	≥4 σ
	1983, 334, 10:06	334, 14:59	1.36 ± 0.30	1.08 ± 0.25	0.99 ± 0.07	6–16	≥4 σ
PKS 0548−32	1983, 306, 16:51	306, 19:59	12.30 ± 1.00	6.47 ± 0.70	3.04 ± 0.05	3–22	≥4 σ
	1983, 334, 16:56	334, 19:40	12.30 ± 1.50	6.31 ± 0.77	2.76 ± 0.06	4–20	≥4 σ
	1986, 066, 04:39	066, 11:40	10.40 ± 0.40	...	2.01 ± 0.04	4–23	≥4 σ
	1986, 066, 11:45	066, 18:05	10.40 ± 0.40	...	2.08 ± 0.04	4–21	≥4 σ
	1986, 066, 23:55	067, 04:00	10.40 ± 0.40	...	2.12 ± 0.05	4–21	≥4 σ
PKS 0754+10	1984, 043, 06:07	043, 13:36	0.70 ± 0.10	0.29 ± 0.08	0.51 ± 0.04	5–23	≥4 σ
OJ 287	1983, 281, 14:39	281, 21:05	4.00 ± 0.38	...	0.83 ± 0.07	4–11	≥4 σ
	1984, 040, 07:49	040, 11:00	4.75 ± 0.65	...	0.49 ± 0.05	5–14	≥4 σ
Mrk 421	1984, 035, 12:32	035, 15:36	48.70 ± 2.50	18.10 ± 1.00	1.25 ± 0.10	6–16	≥4 σ
	1984, 337, 17:04	337, 20:18	100.00 ± 4.0	42.20 ± 1.70	11.08 ± 0.06	2–32	≥4 σ
	1984, 338, 19:12	339, 02:08	126.60 ± 2.40	54.70 ± 2.00	13.95 ± 0.06	2–33	≥4 σ
	1984, 340, 19:12	340, 22:30	128.60 ± 5.00	57.50 ± 2.00	14.10 ± 0.10	3–27	≥4 σ
	1985, 004, 14:26	004, 18:03	56.30 ± 3.00	20.50 ± 4.00	1.76 ± 0.06	4–18	≥4 σ
	1985, 112, 05:19	112, 10:35	63.60 ± 2.20	26.90 ± 1.20	3.05 ± 0.04	3–24	≥4 σ
	1985, 118, 19:18	119, 01:04	49.00 ± 1.70	20.10 ± 0.90	2.99 ± 0.04	3–26	≥4 σ
	1985, 126, 22:24	127, 04:56	48.60 ± 1.70	19.90 ± 0.80	1.84 ± 0.04	4–23	≥4 σ
	1985, 131, 20:51	132, 03:16	56.50 ± 2.00	21.60 ± 1.00	2.66 ± 0.04	3–24	≥4 σ
	1985, 132, 15:34	132, 16:59	54.10 ± 2.00	...	1.92 ± 0.08	4–18	≥4 σ
	1985, 141, 13:00	141, 19:00	44.40 ± 1.60	17.70 ± 0.90	2.09 ± 0.05	4–21	≥4 σ
Mrk 180	1984, 333, 04:43	333, 09:20	11.30 ± 0.80	5.04 ± 0.52	0.44 ± 0.04	5–10	≥4 σ
	1985, 093, 16:35	093, 19:30	21.30 ± 1.60	...	1.01 ± 0.07	5–16	≥4 σ
B2 1147+245	1984, 016, 06:44	016, 15:35	0.41 ± 0.06	...	0.30 ± 0.04	6–11	≥4 σ
3C 273	1984, 005, 23:00	006, 13:17	21.80 ± 0.10	...	7.49 ± 0.07	4–30	≥4 σ
	1985, 032, 13:34	032, 19:00	21.17 ± 0.12	...	6.46 ± 0.06	2–34	≥4 σ
	1985, 138, 11:49	138, 17:37	29.90 ± 0.10	...	6.79 ± 0.04	3–35	≥4 σ
	1986, 017, 18:19	017, 05:51	35.40 ± 0.11	...	9.36 ± 0.03	2–41	≥4 σ
	1986, 018, 06:07	019, 06:08	36.10 ± 0.10	...	9.06 ± 0.03	2–41	≥4 σ
1E 1402+04	1985, 031, 16:05	032, 10:19	1.26 ± 0.11	...	0.21 ± 0.02	7–11	≥4 σ
1E 1415+259	1986, 063, 19:24	064, 06:02	6.94 ± 0.20	...	0.49 ± 0.03	4–16	≥4 σ
1H 1427+42	1985, 012, 21:14	012, 23:25	37.60 ± 0.90	...	4.78 ± 0.07	3–26	≥4 σ
PKS 1510−089	1984, 216, 12:56	218, 00:20	0.47 ± 0.07	0.41 ± 0.06	0.59 ± 0.03	6–19	≥4 σ
	1985, 212, 23:59	213, 11:11	0.52 ± 0.08	...	0.46 ± 0.03	6–19	≥4 σ
Mrk 501	1984, 034, 12:02	034, 14:26	48.30 ± 2.00	22.90 ± 2.00	4.62 ± 0.05	3–24	≥4 σ
	1984, 086, 12:00	086, 14:30	42.50 ± 2.00	18.50 ± 2.00	4.14 ± 0.07	4–24	≥4 σ
	1984, 183, 20:25	183, 23:47	46.50 ± 2.00	19.00 ± 1.00	2.47 ± 0.05	3–20	≥4 σ
	1984, 191, 06:09	191, 08:44	42.00 ± 2.00	18.20 ± 1.00	2.69 ± 0.07	3–19	≥4 σ
	1984, 201, 06:44	201, 09:45	41.00 ± 2.00	16.80 ± 1.00	2.78 ± 0.05	3–24	≥4 σ
	1984, 207, 00:24	207, 03:37	44.50 ± 2.00	21.50 ± 1.00	3.05 ± 0.06	3–22	≥4 σ

TABLE 2—*Continued*

Source	Start Time[a]	End Time[b]	LE Count Rate (10^{-4} cm^{-2} s^{-1}) LX3	LE Count Rate (10^{-4} cm^{-2} s^{-1}) Al/P	ME[c] Count Rate (10^{-3} cm^{-2} s^{-1})	ME Signal Significance Channel Range	ME Signal Significance Signal
	1984, 209, 20:14	209, 23:50	41.70 ± 2.00	19.20 ± 1.00	3.36 ± 0.05	3–25	≥4 σ
	1985, 099, 09:43	099, 14:26	41.20 ± 2.00	18.90 ± 0.90	2.54 ± 0.06	4–21	≥4 σ
	1986, 074, 13:44	075, 14:28	44.50 ± 1.00	...	4.29 ± 0.03	4–21	≥4 σ
4U 1722+119	1985, 246, 11:45	246, 16:59	2.89 ± 0.30	2.00 ± 0.30	0.84 ± 0.04	5–16	≥4 σ
I Zw 186	1984, 181, 15:20	181, 23:09	9.16 ± 0.60	4.71 ± 0.50	0.85 ± 0.04	5–17	≥4 σ
3C 371	1984, 255, 20:14	256, 08:25	5.18 ± 0.23	...	0.42 ± 0.04	7–17	≥4 σ
3C 390.3	1985, 033, 06:39	033, 09:14	...	1.51 ± 0.17	2.48 ± 0.07	4–24	≥4 σ
	1985, 033, 09:31	033, 22:09	1.84 ± 0.34	1.51 ± 0.17	2.60 ± 0.06	4–26	≥4 σ
	1986, 076, 12:00	076, 22:59	2.30 ± 0.23	1.44 ± 0.17	1.84 ± 0.04	4–25	≥4 σ
OV 236	1984, 287, 06:49	287, 14:01	0.54 ± 0.11	...	0.36 ± 0.04	6–14	≥4 σ
1928+73 (4C 73.18)	1983, 283, 03:52	283, 11:59	1.00 ± 0.39	...	0.37 ± 0.06	6–13	≥4 σ
	1983, 344, 04:07	344, 11:29	0.68 ± 0.08	...	0.45 ± 0.05	6–12	≥4 σ
PKS 2005−489	1984, 254, 07:30	254, 13:05	50.10 ± 2.00	28.60 ± 1.00	3.16 ± 0.04	3–23	≥4 σ
	1984, 287, 16:09	287, 21:49	68.60 ± 3.00	36.70 ± 1.70	6.96 ± 0.06	2–24	≥4 σ
	1985, 289, 07:30	289, 13:20	17.30 ± 0.90	9.54 ± 0.50	0.65 ± 0.04	4–10	≥4 σ
PKS 2155−304	1983, 304, 00:44	304, 16:11	90.70 ± 3.00	...	2.16 ± 0.03	3–24	≥4 σ
	1984, 311, 13:42	311, 17:47	230.00 ± 8.00	...	9.37 ± 0.06	2–29	≥4 σ
	1984, 312, 09:47	312, 13:47	280.00 ± 9.00	...	12.80 ± 0.06	2–31	≥4 σ
	1984, 316, 11:24	316, 14:43	274.00 ± 9.00	...	8.34 ± 0.06	2–27	≥4 σ
	1985, 297, 10:59	298, 00:56	438.00 ± 13.0	...	17.80 ± 0.06	2–32	≥4 σ
	1985, 305, 20:45	305, 22:40	218.00 ± 6.00	...	5.80 ± 0.15	3–21	≥4 σ
	1985, 306, 07:57	307, 00:56	211.00 ± 8.00	...	6.22 ± 0.03	4–29	≥4 σ
	1985, 316, 12:05	317, 06:10	274.00 ± 9.00	...	8.34 ± 0.06	2–22	≥4 σ

[a] Format: year, day, hour:minutes.
[b] Format: day, hour:minutes.
[c] ME count rates are for PHA channels 4–23 corresponding to the energy range 1.3–7 keV with the best signal-to-noise ratio.

ken power-law plus fixed absorption model, or the double power-law plus fixed absorption model ($\Delta\chi^2 > 10$; for details see Tables 4C and 4D). Similarly, we find that the best fits to the spectra of 3C 273 were obtained with the power-law plus fixed absorption plus blackbody model or the power-law plus fixed absorption plus thermal bremsstrahlung model, and these two models resulted in significant improvements ($\Delta\chi^2 > 10$) over other models (for comparison see Tables 3, 4D, and 4E). Spectra of PKS 2155−304 can be best described by the power-law plus fixed absorption plus absorption-edge model or by the broken power-law with fixed absorption model (see Tables 4F and 4G). Details of the spectral analysis will be discussed in § 4. The photon spectra of 28 blazars are presented in Figures 2*a*–2*ab* along with the power-law model convolved through the detector response. The residuals between the model and the spectra are shown in the lower panel of each figure.

3.2. *Multifrequency Spectra*

All the objects in the *EXOSAT* blazar sample are included in the list of Burbidge & Hewitt (1992) and in the catalog of Véron-Cetty & Véron (1993), where many references to radio, optical, and X-ray data are listed. We have also surveyed the literature, and from the published results we have selected the average flux value at each energy band (radio, millimeter, infrared, and optical), except for far-infrared, ultraviolet, and X-rays, for each blazar. Far-infrared, ultraviolet, and X-ray fluxes were obtained from the *IRAS* survey, the *IUE* Uniform Low Dispersion Archive (ULDA) database (installed on our computer), and the present analysis, respectively. To derive the average fluxes at each frequency, we have imposed a number of criteria to select the data, and they are as follows: (1) we have excluded the data during the flare states[1] of the blazars; (2) observations of certain objects were simultaneous with the *EXOSAT* data, and we have selected data only from those observations; (3) for objects for which simultaneous observations are not available, we have selected data from the literature for near-simultaneity observations;[2] (4) for objects with multiple *EXOSAT* observations, we have selected flattest and steepest X-ray spectra for multifrequency continuum energy distribution. Radio through X-ray continuum emission spectra of 28 blazars are plotted in Figures 3*a*–3*n* and 4*a*–4*n* for RBLs and XBLs, respectively. To compute the errors for fluxes plotted in Figures 3 and 4, we have followed the following steps. First, for simultaneous observations we have plotted the observational errors along with the fluxes at different frequencies. Then we found that the error bars are smaller than the sizes of different symbols used in the multifrequency plots (plotted on a logarithmic scale). Next we computed the rms deviation errors for nonsimultaneous observations (fluxes were collected from

[1] When the source brightness increased by a factor of 3 or more on timescales of weeks to months, we considered that the source was in flare state.
[2] When the observations were made within a week from the *EXOSAT* observations, those observations were considered as near-simultaneity observations.

TABLE 3

POWER LAW PLUS ABSORPTION

SOURCE	DATE (year, day)	Γ[a]	N[b]	N_H[c]	N_H[d]	FLUX[e] (keV) 0.1–2	FLUX[e] (keV) 2–10	χ^2_r/dof
3C 66A	1986, 006	$1.90^{+0.60}_{-0.50}$	$1.85^{+1.80}_{-0.80}$	14^{+20}_{-11}	7.5	0.34 ± 0.06	0.40 ± 0.04	0.55/17
	1986, 032	$1.96^{+0.33}_{-0.30}$	$2.80^{+2.00}_{-1.27}$	30^{+25}_{-16}		0.28 ± 0.05	0.45 ± 0.02	0.58/18
AO 0235+164	1984, 214	$1.75^{+0.80}_{-0.65}$	$2.17^{+7.00}_{-2.00}$	80^{+90}_{-70}	9.1	0.09 ± 0.02	0.24 ± 0.04	0.48/14
0317+18	1985, 013	$2.41^{+0.72}_{-0.60}$	$6.97^{+8.60}_{-3.70}$	32^{+33}_{-20}	9.8	0.62 ± 0.13	1.08 ± 0.09	0.99/14
	1985, 039	$2.11^{+0.30}_{-0.30}$	$3.62^{+1.80}_{-1.19}$	15^{+11}_{-7}		0.42 ± 0.07	0.82 ± 0.05	0.62/21
H0323+022	1984, 265	$2.84^{+0.35}_{-0.30}$	$10.45^{+8.2}_{-4.30}$	12^{+13}_{-10}	8.4	1.72 ± 0.20	0.79 ± 0.03	0.62/17
	1984, 267	$2.50^{+0.25}_{-0.24}$	$7.60^{+1.90}_{-1.60}$	10^{+7}_{-5}		1.36 ± 0.10	1.13 ± 0.10	0.79/17
NRAO 140	1985, 025	$1.36^{+0.26}_{-0.26}$	$1.54^{+0.67}_{-0.48}$	19^{+14}_{-10}	14.2	0.22 ± 0.03	1.08 ± 0.04	0.89/12
	1985, 025	$1.54^{+0.20}_{-0.20}$	$2.09^{+0.68}_{-0.50}$	29^{+14}_{-11}		0.26 ± 0.03	0.99 ± 0.04	0.65/18
1H 0414+009	1984, 253	$1.91^{+0.10}_{-0.13}$	$8.40^{+0.77}_{-0.74}$	$7.90^{+4.10}_{-2.50}$	8.6	1.71 ± 0.21	2.41 ± 0.05	0.66/21
	1984, 258	$1.88^{+0.08}_{-0.08}$	$9.70^{+0.62}_{-0.58}$	$8.10^{+2.20}_{-2.00}$		1.91 ± 0.18	2.86 ± 0.06	0.43/25
	1984, 266	$2.38^{+0.25}_{-0.27}$	$8.32^{+0.66}_{-0.60}$	$13.0^{+5.0}_{-5.0}$		1.66 ± 0.19	1.74 ± 0.05	0.95/20
	1984, 274	$2.44^{+0.09}_{-0.10}$	$8.48^{+0.90}_{-0.90}$	$10.8^{+6.1}_{-3.9}$		1.79 ± 0.19	1.24 ± 0.05	0.72/18
3C 120	1983, 228	$1.60^{+0.06}_{-0.05}$	$8.51^{+0.70}_{-0.63}$	$4.82^{+1.15}_{-0.96}$	10.0	1.95 ± 0.10	4.02 ± 0.05	1.12/22
	1983, 305	$1.94^{+0.08}_{-0.08}$	$14.85^{+1.79}_{-1.61}$	$13.30^{+3.07}_{-2.67}$		2.54 ± 0.18	3.41 ± 0.04	1.34/16
	1984, 249	$1.81^{+0.06}_{-0.06}$	$14.02^{+1.23}_{-1.11}$	$11.54^{+3.40}_{-2.67}$		2.48 ± 0.26	4.79 ± 0.04	0.67/19
	1984, 276	$1.72^{+0.05}_{-0.05}$	$13.20^{+0.97}_{-0.90}$	$12.32^{+2.40}_{-2.08}$		2.29 ± 0.13	5.19 ± 0.03	0.33/19
	1984, 277	$1.76^{+0.07}_{-0.07}$	$12.15^{+1.17}_{-1.06}$	$14.25^{+2.90}_{-2.55}$		1.98 ± 0.12	4.44 ± 0.09	1.32/20
	1984, 278	$1.67^{+0.06}_{-0.06}$	$11.31^{+1.03}_{-0.93}$	$10.81^{+3.19}_{-2.52}$		2.06 ± 0.25	4.81 ± 0.06	0.44/21
	1984, 280	$1.65^{+0.08}_{-0.07}$	$9.39^{+1.06}_{-0.95}$	$10.33^{+2.70}_{-2.29}$		1.74 ± 0.09	4.09 ± 0.06	0.71/18
	1984, 284	$1.90^{+0.08}_{-0.08}$	$12.45^{+1.31}_{-1.18}$	$16.30^{+3.50}_{-3.10}$		1.89 ± 0.13	3.67 ± 0.04	0.58/22
	1984, 286	$1.74^{+0.06}_{-0.07}$	$11.19^{+1.05}_{-0.96}$	$10.97^{+2.99}_{-2.43}$		2.02 ± 0.15	4.28 ± 0.05	0.37/19
	1985, 044	$1.72^{+0.10}_{-0.10}$	$9.11^{+1.29}_{-1.13}$	$9.41^{+3.21}_{-2.54}$		1.73 ± 0.11	3.57 ± 0.06	0.57/18
	1985, 283	$1.80^{+0.08}_{-0.08}$	$13.01^{+1.56}_{-1.38}$	$12.74^{+3.33}_{-2.83}$		2.22 ± 0.15	4.50 ± 0.05	1.02/15
	1986, 044	$1.86^{+0.10}_{-0.09}$	$8.88^{+1.25}_{-1.07}$	$13.21^{+6.00}_{-4.25}$		1.48 ± 0.23	2.77 ± 0.04	0.57/19
PKS 0521−36	1983, 306	$1.70^{+0.20}_{-0.20}$	$2.88^{+0.90}_{-0.60}$	$5.76^{+4.90}_{-2.88}$	3.5	0.64 ± 0.10	1.15 ± 0.04	0.70/19
	1983, 334	$1.81^{+0.30}_{-0.30}$	$3.50^{+1.80}_{-1.20}$	$8.60^{+10.40}_{-5.60}$		0.69 ± 0.15	1.17 ± 0.08	0.53/19
PKS 0548−32	1983, 306	$2.33^{+0.09}_{-0.09}$	$18.93^{+2.00}_{-2.00}$	$7.20^{+2.10}_{-1.70}$	2.49	4.10 ± 0.33	2.96 ± 0.05	0.83/18
	1983, 334	$2.14^{+0.12}_{-0.12}$	$13.90^{+2.10}_{-1.90}$	$4.40^{+2.10}_{-1.48}$		3.48 ± 0.42	2.90 ± 0.06	0.61/19
	1986, 066	$2.15^{+0.08}_{-0.08}$	$10.47^{+1.10}_{-1.00}$	$3.40^{+0.70}_{-0.68}$		2.80 ± 0.11	2.20 ± 0.04	0.98/21
	1986, 066	$2.24^{+0.11}_{-0.11}$	$11.27^{+1.53}_{-1.42}$	$4.01^{+1.15}_{-1.00}$		2.97 ± 0.11	2.04 ± 0.04	0.96/17
	1986, 066	$2.11^{+0.12}_{-0.12}$	$10.23^{+1.47}_{-1.37}$	$3.20^{+1.00}_{-0.90}$		2.80 ± 0.11	2.23 ± 0.05	0.65/18
PKS 0754+10	1984, 043	$1.70^{+0.20}_{-0.20}$	$0.87^{+0.10}_{-0.10}$	$3.40^{+2.00}_{-1.40}$	2.7	0.23 ± 0.03	0.54 ± 0.05	0.55/09
OJ 287	1983, 281	$3.15^{+1.05}_{-0.82}$	$9.97^{+17.80}_{-5.87}$	$15.73^{+23.50}_{-11.61}$	3.0	1.60 ± 0.15	0.52 ± 0.01	0.28/8
	1984, 040	$2.94^{+0.64}_{-0.56}$	$6.85^{+5.42}_{-3.08}$	$8.82^{+11.00}_{-5.60}$		1.55 ± 0.21	0.47 ± 0.01	0.30/10
Mrk 421	1984, 035	$2.70^{+0.12}_{-0.08}$	$11.48^{+1.90}_{-1.47}$	$1.80^{+0.75}_{-0.50}$		5.57 ± 0.28	0.98 ± 0.08	0.47/13
	1984, 337	$2.16^{+0.06}_{-0.05}$	$53.50^{+0.25}_{-0.20}$	$2.30^{+0.85}_{-0.40}$		17.80 ± 0.71	11.20 ± 0.06	1.62/20
	1984, 338	$2.17^{+0.05}_{-0.05}$	$67.00^{+0.90}_{-0.84}$	$2.25^{+0.87}_{-0.15}$		22.60 ± 0.43	14.20 ± 0.06	2.68/25
	1984, 340	$2.31^{+0.04}_{-0.04}$	$82.40^{+3.80}_{-3.81}$	$2.61^{+0.31}_{-0.33}$		23.90 ± 0.93	13.80 ± 0.10	1.89/23
	1985, 004	$2.73^{+0.20}_{-0.07}$	$15.80^{+1.10}_{-0.80}$	$1.88^{+0.70}_{-0.50}$		6.77 ± 0.36	1.49 ± 0.05	0.48/15
	1985, 112	$2.55^{+0.09}_{-0.02}$	$23.49^{+0.67}_{-0.58}$	$2.20^{+0.54}_{-0.45}$		9.10 ± 0.31	2.75 ± 0.04	0.71/20
	1985, 118	$2.42^{+0.09}_{-0.05}$	$19.93^{+0.67}_{-0.50}$	$1.85^{+0.52}_{-0.35}$		7.21 ± 0.25	2.80 ± 0.04	0.67/24
	1985, 126	$2.64^{+0.09}_{-0.06}$	$15.80^{+0.53}_{-0.47}$	$1.95^{+0.39}_{-0.37}$		6.45 ± 0.22	1.63 ± 0.03	0.71/20
	1985, 131	$2.34^{+0.08}_{-0.06}$	$20.00^{+0.66}_{-0.59}$	$1.55^{+0.51}_{-0.34}$		7.08 ± 0.25	2.51 ± 0.04	0.80/24
	1985, 132	$2.66^{+0.60}_{-0.50}$	$17.10^{+2.15}_{-1.10}$	$2.38^{+2.86}_{-1.96}$		7.14 ± 0.26	1.70 ± 0.07	0.64/15
	1985, 141	$2.44^{+0.15}_{-0.06}$	$15.87^{+0.88}_{-0.50}$	$1.94^{+0.88}_{-0.55}$		6.12 ± 0.22	1.86 ± 0.04	0.58/19
Mrk 180	1984, 333	$2.49^{+0.42}_{-0.40}$	$3.19^{+0.35}_{-0.28}$	$2.25^{+2.38}_{-1.65}$	1.4	1.39 ± 0.09	0.38 ± 0.03	0.65/15
	1985, 093	$2.53^{+0.36}_{-0.36}$	$8.50^{+3.70}_{-2.70}$	$1.92^{+2.00}_{-1.20}$		3.18 ± 0.24	1.02 ± 0.07	0.35/16
B2 1147+245	1984, 016	$1.96^{+0.84}_{-0.40}$	$1.07^{+1.23}_{-0.50}$	$8.76^{+16.90}_{-4.00}$	2.0	0.21 ± 0.03	0.56 ± 0.07	0.57/12
3C 273	1984, 005	$1.58^{+0.02}_{-0.03}$	$19.55^{+0.50}_{-0.75}$	1.8	1.8	5.34 ± 0.02	9.66 ± 0.09	1.98/16
	1985, 032	$1.71^{+0.02}_{-0.02}$	$18.97^{+0.21}_{-0.22}$	1.8		5.31 ± 0.02	7.65 ± 0.08	11.84/16
	1985, 138	$1.85^{+0.01}_{-0.01}$	$23.68^{+0.25}_{-0.25}$	1.8		6.88 ± 0.02	7.58 ± 0.05	13.22/18
	1986, 017	1.61	24.72	1.8		6.79 ± 0.02	11.62 ± 0.04	7.56/20
	1986, 018	1.63	24.69	1.8		6.81 ± 0.02	11.16 ± 0.04	7.94/19

TABLE 3—*Continued*

SOURCE	DATE (year, day)	Γ^a	N^b	$N_H{}^c$	$N_H{}^d$	FLUX[e] (keV) 0.1–2	FLUX[e] (keV) 2–10	χ_r^2/dof
1E 1402+04	1985, 031	$2.42^{+0.10}_{-0.10}$	$1.66^{+0.18}_{-0.18}$	2.2	2.2	0.50 ± 0.05	0.19 ± 0.04	1.40/18
1E 1415+259	1986, 063	$2.91^{+0.30}_{-0.30}$	$6.06^{+2.20}_{-2.20}$	$5.60^{+2.30}_{-2.30}$	1.6	1.92 ± 0.05	0.39 ± 0.02	0.19/13
1H 1427+42	1985, 012	$2.06^{+0.07}_{-0.07}$	$21.30^{+1.90}_{-1.90}$	$1.55^{+0.38}_{-0.38}$	1.4	6.81 ± 0.16	5.00 ± 0.07	0.61/18
PKS 1510−089	1984, 216	$1.46^{+0.27}_{-0.24}$	$1.33^{+0.42}_{-0.35}$	$5.30^{+11.8}_{-4.30}$	7.6	0.27 ± 0.04	0.79 ± 0.04	0.82/16
	1985, 212	$1.60^{+0.39}_{-0.35}$	$1.32^{+0.53}_{-0.47}$	$8.70^{+15.4}_{-7.90}$		0.27 ± 0.04	0.61 ± 0.04	0.44/12
Mrk 501	1984, 034	$2.44^{+0.06}_{-0.06}$	$32.33^{+2.00}_{-2.00}$	$3.00^{+0.40}_{-0.40}$	...	10.00 ± 0.41	4.41 ± 0.05	1.01/19
	1984, 086	$2.29^{+0.09}_{-0.09}$	$24.30^{+2.30}_{-2.30}$	$2.14^{+0.48}_{-0.48}$		7.64 ± 0.36	4.17 ± 0.07	0.79/16
	1984, 183	$2.58^{+0.09}_{-0.09}$	$20.02^{+1.80}_{-1.80}$	$2.31^{+0.48}_{-0.48}$		7.23 ± 0.31	2.24 ± 0.04	1.15/18
	1984, 191	$2.39^{+12.0}_{-0.06}$	$17.60^{+2.10}_{-1.60}$	$1.75^{+0.80}_{-0.50}$		6.36 ± 0.30	2.53 ± 0.06	0.55/17
	1984, 201	$2.43^{+0.08}_{-0.08}$	$18.64^{+1.40}_{-1.40}$	$2.00^{+0.40}_{-0.40}$		6.50 ± 0.32	2.59 ± 0.05	0.92/16
	1984, 207	$2.63^{+0.09}_{-0.09}$	$25.70^{+2.50}_{-2.50}$	$3.11^{+0.63}_{-0.63}$		8.57 ± 0.38	2.68 ± 0.05	0.72/18
	1984, 209	$2.38^{+0.07}_{-0.07}$	$21.90^{+1.70}_{-1.70}$	$2.20^{+0.40}_{-0.40}$		7.55 ± 0.36	3.14 ± 0.05	0.63/17
	1985, 099	$2.58^{+0.10}_{-0.05}$	$20.15^{+1.79}_{-1.45}$	$2.47^{+0.80}_{-0.50}$		6.35 ± 0.31	2.35 ± 0.06	0.99/15
	1986, 074	$2.39^{+0.06}_{-0.03}$	$28.59^{+1.07}_{-1.04}$	$2.65^{+0.24}_{-0.23}$		9.01 ± 0.20	4.15 ± 0.03	1.40/16
4U 1722+119	1985, 245	$2.66^{+0.30}_{-0.30}$	$8.00^{+2.20}_{-2.20}$	15^{+7}_{-6}	8.6	1.26 ± 0.13	0.76 ± 0.04	0.63/16
I Zw 186	1984, 181	$2.52^{+0.13}_{-0.18}$	$4.90^{+0.85}_{-0.90}$	$3.90^{+0.50}_{-1.40}$	2.7	1.88 ± 0.12	0.79 ± 0.37	0.96/16
3C 371	1984, 255	$2.80^{+0.09}_{-0.09}$	$4.28^{+0.36}_{-0.36}$	4.90	4.9	1.25 ± 0.06	0.35 ± 0.03	1.10/15
3C 390.3	1985, 033	$1.42^{+0.14}_{-0.13}$	$4.39^{+0.94}_{-0.79}$	$1.04^{+0.88}_{-0.57}$	4.1	1.25 ± 0.20	2.78 ± 0.08	1.18/26
	1985, 033	$1.60^{+0.11}_{-0.12}$	$6.03^{+0.96}_{-0.84}$	$2.34^{+1.23}_{-0.89}$		1.18 ± 0.22	2.90 ± 0.07	0.71/26
	1986, 076	$1.53^{+0.10}_{-0.09}$	$4.09^{+0.53}_{-0.48}$	$1.13^{+0.60}_{-0.42}$		1.60 ± 0.16	2.15 ± 0.05	1.04/29
OV 236	1984, 287	$1.67^{+0.23}_{-0.30}$	$1.03^{+0.27}_{-0.31}$	4.00	...	0.22 ± 0.04	0.46 ± 0.05	1.31/11
1928+73 (4C 73.18)	1983, 283	$2.25^{+0.50}_{-0.45}$	$2.84^{+2.30}_{-1.24}$	13.00^{+75}_{-10}	...	0.47 ± 0.18	0.50 ± 0.08	0.97/29
	1983, 344	$2.11^{+0.40}_{-0.41}$	$2.38^{+1.70}_{-1.00}$	15.00^{+14}_{-10}		0.37 ± 0.04	0.15 ± 0.02	0.53/31
PKS 2005−489	1984, 254	$3.04^{+0.07}_{-0.07}$	$42.00^{+3.00}_{-3.00}$	$6.15^{+0.70}_{-0.70}$	4.6	12.10 ± 0.48	2.50 ± 0.03	1.00/18
	1984, 287	$2.70^{+0.06}_{-0.05}$	$64.22^{+2.98}_{-2.77}$	$5.06^{+0.41}_{-0.39}$		16.70 ± 0.73	6.07 ± 0.05	0.52/11
	1985, 289	$3.18^{+0.06}_{-0.06}$	$9.30^{+0.59}_{-0.61}$	$6.12^{+0.61}_{-0.50}$		3.38 ± 0.17	0.49 ± 0.03	0.68/15
PKS 2155−304	1983, 304	$2.77^{+0.02}_{-0.02}$	$21.37^{+0.45}_{-0.45}$	1.8	1.8	9.44 ± 0.34	1.85 ± 0.02	2.81/16
	1984, 311	$2.60^{+0.02}_{-0.02}$	$78.32^{+0.50}_{-0.52}$	1.8		27.00 ± 0.93	8.58 ± 0.05	4.6/19
	1984, 312	$2.52^{+0.03}_{-0.02}$	$96.48^{+2.45}_{-2.50}$	1.8		36.80 ± 1.18	11.70 ± 0.05	2.7/19
	1984, 316	$2.73^{+0.03}_{-0.02}$	$79.10^{+0.20}_{-0.16}$	1.8		34.10 ± 1.12	7.22 ± 0.05	1.26/19
	1985, 297	$2.65^{+0.03}_{-0.02}$	$155.00^{+3.20}_{-3.11}$	1.8		63.50 ± 1.88	15.80 ± 0.05	3.6/19
	1985, 305	$2.81^{+0.03}_{-0.03}$	$56.80^{+1.70}_{-1.69}$	1.8		25.80 ± 0.71	4.63 ± 0.12	0.60/19
	1985, 306	$2.74^{+0.03}_{-0.03}$	$60.50^{+1.23}_{-1.18}$	1.8		26.30 ± 0.99	5.42 ± 0.03	3.35/19
	1985, 316	$2.90^{+0.05}_{-0.06}$	$36.50^{+2.88}_{-2.72}$	1.8		17.60 ± 0.58	2.67 ± 0.02	2.20/19

[a] Photon index.
[b] Normalization in 10^{-3} photons cm^{-2} s^{-1} keV^{-1} at 1 keV.
[c] Observed hydrogen column density in 10^{20} cm^{-2}.
[d] Galactic column density in 10^{20} cm^{-2}.
[e] Flux in 10^{-11} ergs cm^{-2} s^{-1}.
[f] Fixed with corresponding Galactic column density value.

TABLE 4A

PARAMETERS OF BROKEN POWER-LAW MODEL FOR PKS 0548−322

Date (year, day)	$\Gamma_1{}^a$	$\Gamma_2{}^a$	$N_H{}^b$	$E_B{}^c$	χ_r^2/dof
1983, 306	$1.66^{+0.42}_{-0.61}$	$2.33^{+0.40}_{-0.21}$	$2.60^{+2.10}_{-1.50}$	$2.20^{+0.96}_{-0.58}$	0.67/16
1986, 066	$1.61^{+0.41}_{-0.46}$	$2.41^{+0.54}_{-0.33}$	$2.10^{+2.00}_{-1.30}$	$2.00^{+0.95}_{-0.61}$	0.71/19

[a] Photon index.
[b] Hydrogen column density in 10^{20} cm^{-2}.
[c] Break energy in keV.

TABLE 4B

PARAMETERS OF HIGH-ENERGY CUTOFF MODEL FOR MARKARIAN 421

Date (year, day)	Γ^a	$N_H{}^b$	$E_c{}^c$	$E_r{}^d$	χ_r^2/dof
1984, 337	$2.10^{+0.10}_{-0.22}$	$1.73^{+0.74}_{-0.58}$	$2.98^{+1.88}_{-2.41}$	$24.90^{+30.20}_{-16.40}$	1.29/18
1984, 338	$1.94^{+0.18}_{-0.20}$	$1.41^{+0.81}_{-0.64}$	$2.58^{+0.90}_{-1.21}$	$12.40^{+4.80}_{-5.60}$	1.22/23
1984, 340	$2.04^{+0.23}_{-0.13}$	$1.33^{+0.96}_{-0.91}$	$2.81^{+0.91}_{-1.08}$	$7.90^{+2.80}_{-2.94}$	1.27/18

[a] Photon index.
[b] Hydrogen column density in 10^{20} cm^{-2}.
[c] Cutoff energy in keV.
[d] Rate in keV.

TABLE 4C

PARAMETERS OF POWER-LAW PLUS ABSORPTION-EDGE MODEL FOR MARKARIAN 421

Date (year, day)	Γ^a	N^b	$N_H{}^c$	E^d	τ^e	χ_r^2/dof
1984, 337	$2.27^{+0.06}_{-0.06}$	$65.60^{+6.90}_{-6.20}$	$2.01^{+0.36}_{-0.32}$	$0.52^{+0.10}_{-0.07}$	$4.62^{+5.11}_{-3.02}$	1.06/22
1984, 338	$2.29^{+0.05}_{-0.04}$	$86.20^{+6.00}_{-6.00}$	$2.14^{+0.24}_{-0.22}$	$0.55^{+0.08}_{-0.06}$	$5.98^{+4.02}_{-2.80}$	0.85/21
1984, 340	$2.38^{+0.05}_{-0.04}$	$91.97^{+6.10}_{-4.80}$	$2.57^{+0.50}_{-0.41}$	$0.51^{+0.11}_{-0.10}$	$2.90^{+2.11}_{-1.39}$	1.34/21

[a] Photon index.
[b] Normalization in 10^{-3} photons cm^{-2} s^{-1} keV^{-1} at 1 keV.
[c] Hydrogen column density in 10^{20} cm^{-2}.
[d] Edge energy in keV.
[e] Optical depth.

TABLE 4D

POWER-LAW PLUS THERMAL BREMSSTRAHLUNG PLUS FIXED ABSORPTION FITS TO THE SPECTRA OF 3C 273

Date (year, day)	Γ^a	N^b	kT^c	$N_B{}^d$	χ_r^2/dof
1984, 005	$1.48^{+0.05}_{-0.05}$	$17.30^{+1.12}_{-1.07}$	$0.10^{+0.32}_{-0.00}$	$218.6^{+82.0}_{-85.1}$	0.88/17
1985, 032	$1.39^{+0.08}_{-0.09}$	$12.72^{+1.45}_{-1.37}$	$0.13^{+0.13}_{-0.03}$	$187.4^{+83.6}_{-86.1}$	0.62/15
1985, 138	$1.52^{+0.05}_{-0.04}$	$15.57^{+0.85}_{-0.85}$	$0.40^{+0.04}_{-0.04}$	$54.69^{+5.60}_{-5.11}$	0.65/17
1986, 017	$1.53^{+0.02}_{-0.02}$	$22.44^{+0.59}_{-0.57}$	$0.10^{+0.05}_{-0.05}$	$482.1^{+66.0}_{-65.0}$	0.65/19
1986, 018	$1.56^{+0.02}_{-0.03}$	$22.40^{+0.58}_{-0.55}$	$0.12^{+0.04}_{-0.05}$	$491.8^{+68.0}_{-68.2}$	0.79/19

[a] Photon index.
[b] Normalization in 10^{-3} photons cm^{-2} s^{-1} keV^{-1} at 1 keV.
[c] Plasma temperature in keV.
[d] Bremsstrahlung normalization in 10^{-3} photons cm^{-2} s^{-1} keV^{-1} at 1 keV.

TABLE 4E

POWER-LAW PLUS BLACKBODY PLUS FIXED ABSORPTION FITS TO THE SPECTRA OF 3C 273

Date (year, day)	Γ^a	N^b	kT^c	$N_{BB}{}^d$	χ_r^2/dof
1984, 005	$1.48^{+0.05}_{-0.05}$	$17.29^{+1.17}_{-1.10}$	$0.05^{+0.05}_{-0.04}$	$0.23^{+0.20}_{-0.12}$	0.88/17
1985, 032	$1.39^{+0.08}_{-0.09}$	$12.69^{+1.46}_{-1.34}$	$0.06^{+0.05}_{-0.04}$	$0.29^{+0.12}_{-0.06}$	0.60/15
1985, 138	$1.55^{+0.04}_{-0.04}$	$16.28^{+0.71}_{-0.69}$	$0.08^{+0.03}_{-0.003}$	$0.39^{+0.03}_{-0.03}$	0.69/17
1986, 017	$1.54^{+0.02}_{-0.02}$	$22.45^{+0.59}_{-0.57}$	$0.04^{+0.02}_{-0.02}$	$0.57^{+0.21}_{-0.22}$	0.64/19
1986, 018	$1.56^{+0.02}_{-0.03}$	$22.41^{+0.58}_{-0.52}$	$0.04^{+0.02}_{-0.02}$	$0.56^{+0.20}_{-0.21}$	0.79/19

[a] Photon index.
[b] Normalization in 10^{-3} photons cm^{-2} s^{-1} keV^{-1} at 1 keV.
[c] Plasma temperature in keV.
[d] Blackbody normalization in 10^{-3} photons cm^{-2} s^{-1} keV^{-1} at 1 keV.

TABLE 4F

POWER-LAW PLUS ABSORPTION-EDGE FIT TO THE SPECTRA OF PKS 2155−304

Date (year, day)	Γ^a	$N_H{}^b$	E^c	τ^d	χ_r^2/dof
1983, 304	$2.81^{+0.10}_{-0.07}$	$1.92^{+0.20}_{-0.18}$	$0.65^{+0.07}_{-0.08}$	$3.20^{+1.30}_{-1.20}$	1.41/14
1984, 311	$2.61^{+0.08}_{-0.05}$	$1.63^{+0.14}_{-0.12}$	$0.88^{+0.13}_{-0.11}$	$1.30^{+0.44}_{-0.39}$	1.10/16
1984, 312	$2.59^{+0.07}_{-0.06}$	$1.69^{+0.11}_{-0.10}$	$0.60^{+0.07}_{-0.06}$	$1.85^{+0.46}_{-0.41}$	1.33/16
1984, 316	$2.89^{+0.07}_{-0.05}$	$3.41^{+0.47}_{-0.40}$	$0.70^{+0.08}_{-0.05}$	$2.96^{+0.56}_{-0.47}$	1.24/16
1985, 297	$2.71^{+0.05}_{-0.03}$	$2.85^{+0.17}_{-0.14}$	$0.57^{+0.23}_{-0.21}$	$1.88^{+0.47}_{-0.41}$	1.20/16
1985, 306	$2.81^{+0.08}_{-0.07}$	$2.41^{+0.24}_{-0.19}$	$0.59^{+0.25}_{-0.21}$	$1.94^{+0.52}_{-0.48}$	1.10/16
1985, 316	$2.94^{+0.08}_{-0.07}$	$2.32^{+0.29}_{-0.27}$	$0.62^{+0.25}_{-0.22}$	$1.39^{+0.91}_{-0.87}$	1.40/16

[a] Photon index.
[b] Hydrogen column density in 10^{20} cm^{-2}.
[c] Edge energy in keV.
[d] Optical depth.

TABLE 4G

BROKEN POWER-LAW FIT TO THE SPECTRA OF PKS 2155−304

Date (year, day)	$\Gamma_1{}^a$	$\Gamma_2{}^a$	$E_B{}^b$	$N_H{}^c$	χ_r^2/dof
1983, 304	$5.31^{+1.71}_{-1.59}$	$2.60^{+0.11}_{-0.09}$	$0.47^{+0.09}_{-0.08}$	$3.62^{+1.67}_{-1.52}$	1.43/14
1984, 311	$3.42^{+0.57}_{-0.55}$	$2.37^{+0.08}_{-0.08}$	$0.59^{+0.21}_{-0.28}$	$2.10^{+0.56}_{-0.50}$	2.77/16
1984, 312	$7.90^{+1.51}_{-1.44}$	$2.31^{+0.06}_{-0.06}$	$0.39^{+0.05}_{-0.05}$	$6.90^{+1.62}_{-1.50}$	1.90/16
1984, 316	$5.69^{+1.33}_{-1.10}$	$2.80^{+0.08}_{-0.07}$	$0.51^{+0.11}_{-0.09}$	$6.71^{+1.53}_{-1.47}$	1.21/16
1985, 297	$6.11^{+1.80}_{-1.20}$	$2.40^{+0.18}_{-0.14}$	$0.49^{+0.15}_{-0.11}$	$4.30^{+1.61}_{-1.22}$	2.81/16
1985, 306	$5.90^{+1.52}_{-1.33}$	$2.49^{+0.21}_{-0.17}$	$0.42^{+0.19}_{-0.14}$	$3.51^{+1.94}_{-1.09}$	2.69/16
1985, 316	$7.43^{+1.94}_{-1.81}$	$2.64^{+0.88}_{-0.21}$	$0.51^{+0.20}_{-0.15}$	$4.60^{+1.52}_{-1.22}$	1.80/16

[a] Photon index.
[b] Break energy in keV.
[c] Hydrogen column density in 10^{20} cm^{-2}.

near-simultaneity observations). The values of the rms deviation errors were different at different frequencies for different blazars, and in many cases the error bars were smaller than the sizes of different symbols used in the plots. From the computed values of the rms deviation errors, for all the 28 blazars at different frequencies, we have found that the highest value of the error was around 36% of the average flux value of 1928+73, which was observed nonsimultaneously and only on few epochs. Then we decided to plot 40% error bars for all the objects at all frequencies along with the flux values (see Figs. 3 and 4). Precise references for the multifrequency plots are given in § 4 and in the figure captions.

We have computed the two-point spectral indices, between the two adjacent energy bands, α_{12} defined by $\alpha_{12} = -[\log(F_1/F_2)/\log(\nu_1/\nu_2)]$, where F_1 and F_2 are the observed fluxes at the frequencies ν_1 and ν_2, respectively. Computed values of α_{12} between different energy bands are listed on each multifrequency plot. It can be seen from the values of α_{12} that the multifrequency spectra can be fitted with different values of spectral indices which gradually increase from radio to ultraviolet for RBLs and from radio to X-rays for XBLs. Multifrequency spectra of RBLs display spectral discontinuity between the UV and the X-ray region, and it is not present in XBLs. This result has been confirmed using the simultaneous observations at UV and X-rays of 12 blazars (six RBLs and six XBLs) of the present sample (see Figs. 3*d*–3*g*, 3*i*, 3*k*, 4*b*, 4*e* and 4*f*, 4*j*, 4*m*, and 4*n*). The multifrequency spectra of 28 blazars presented in this paper are well represented by functions with continuous curvature, such as parabolae. Two such parabolae are required to represent the multifrequency spectra of RBLs, and a single parabola is needed for XBLs. Rapid variability of blazars suggests that any multifrequency studies need simultaneous or quasi-simultaneous observations. The average continuum energy distribution of blazars presented in this paper is based on observations which are partly simultaneous/quasi-simultaneous and partly nonsimultaneous. However, from simultaneous observations, correlated flux variation from infrared to X-ray has been detected in blazars (Brown et al. 1989; Kawai, Bregman, & Matsuoka 1989; Makino et al. 1989, 1991 and references therein), and such parallel variations of fluxes at different bands of these objects suggest that the shape of the multifrequency spectrum will not be affected by the variability (see Fig. 1 of Kawai et al. 1989, which shows the multifrequency plots of BL Lac observed at different

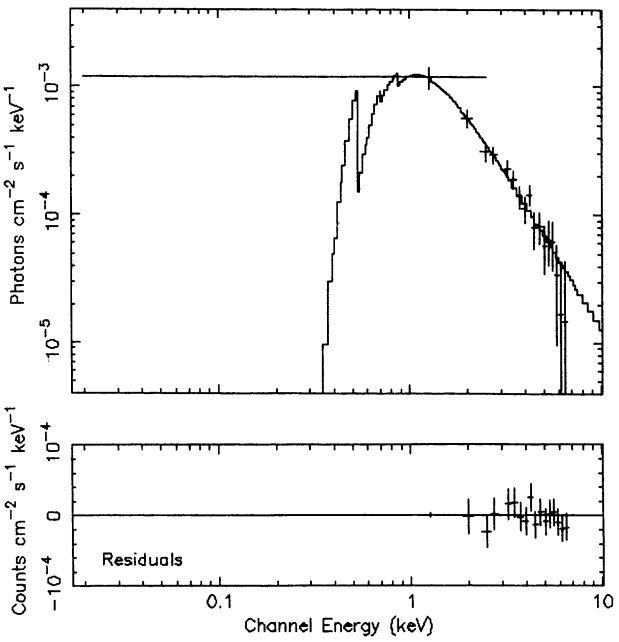

FIG. 2*a*

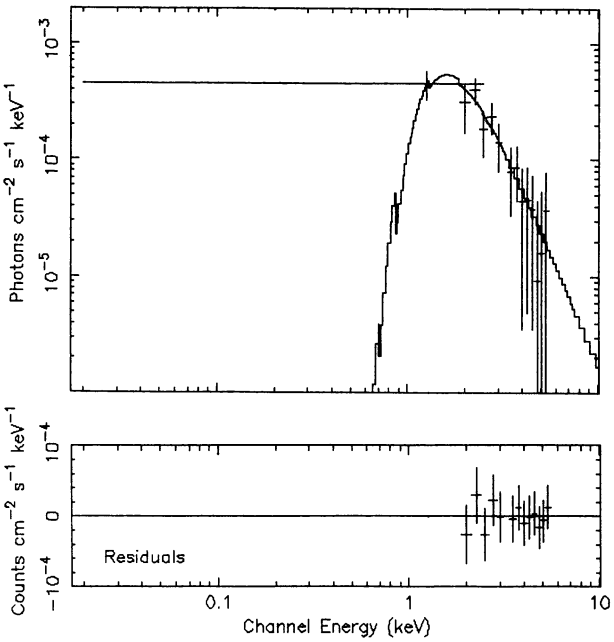

FIG. 2*b*

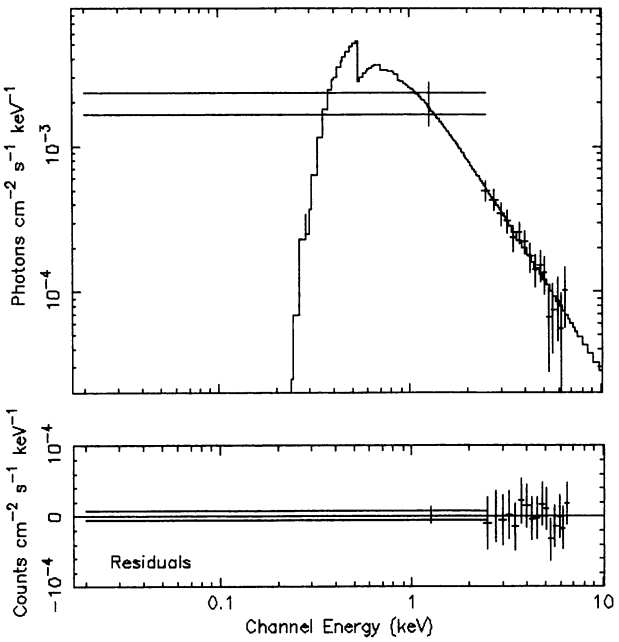

FIG. 2*c*

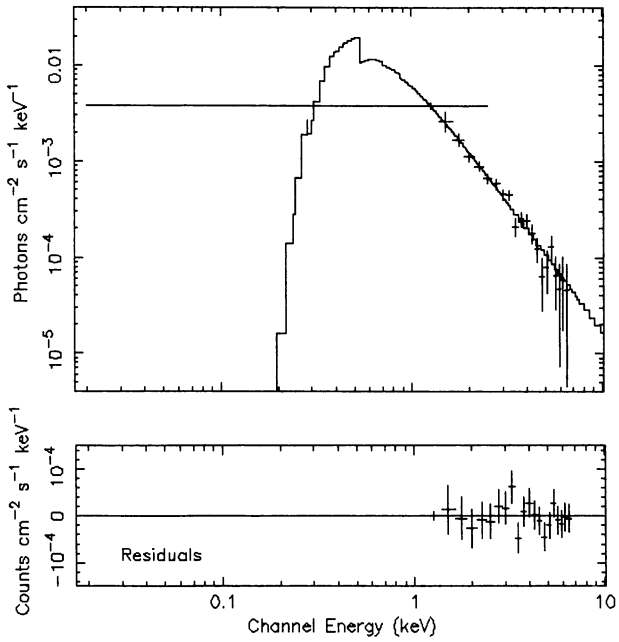

FIG. 2*d*

FIG. 2.—(*a*) Incident spectrum of the blazar 3C 66A. Solid line shows the fitted power-law model convolved through the detector response. The lower panel of the figure shows the residuals between the model and the spectrum, which was observed on 1986, day 032. (*b*) Same as (*a*), but for the blazar AO 0235+164, observed on 1984, day 214. (*c*) Same as (*a*), but for the blazar 0317+18, observed on 1985, day 039. (*d*) Same as (*a*), but for the blazar H0323+022, observed on 1984, day 267. (*e*) Same as (*a*), but for the blazar NRAO 140, observed on 1985, day 025. (*f*) Same as (*a*), but for the blazar 1H 0414+009, observed on 1984, day 258. (*g*) Same as (*a*), but for the blazar 3C 120, observed on 1984, day 278. (*h*) Same as (*a*), but for the blazar PKS 0521−365, observed on 1983, day 334. (*i*) Same as (*a*), but for the blazar PKS 0548−32, observed on 1983, day 306. (*j*) Same as (*a*), but for the blazar PKS 0754+100, observed on 1984, day 043. (*k*) Same as (*a*), but for the blazar OJ 287, observed on 1984, day 040. (*l*) Same as (*a*), but for the blazar Mrk 421, observed on 1985, day 112. (*m*) Same as (*a*), but for the blazar Mrk 180, observed on 1985, day 093. (*n*) Same as (*a*), but for the blazar B2 1147+245, observed on 1984, day 016. (*o*) Same as (*a*), but for the blazar 3C 273, observed on 1986, day 018. (*p*) Same as (*a*), but for the blazar 1E 1402+04, observed on 1985, day 187. (*q*) Same as (*a*), but for the blazar 1E 1415+259, observed on 1986, day 063. (*r*) Same as (*a*), but for the blazar 1H 1427+42, observed on 1985, day 012. (*s*) Same as (*a*), but for the blazar PKS 1510−089, observed on 1984, day 216. (*t*) Same as (*a*), but for the blazar Mrk 501, observed on 1984, day 207. (*u*) Same as (*a*), but for the blazar 4U 1722+119, observed on 1985, day 246. (*v*) Same as (*a*), but for the blazar I Zw 186, observed on 1984, day 181. (*w*) Same as (*a*), but for the blazar 3C 371, observed on 1984, day 273. (*x*) Same as (*a*), but for the blazar 3C 390.3, observed on 1986, day 076. (*y*) Same as (*a*), but for the blazar OV 236, observed on 1984, day 287. (*z*) Same as (*a*), but for the blazar 1928+73, observed on 1983, day 344. (*aa*) Same as (*a*), but for the blazar PKS 2005−489, observed on 1984, day 287. (*ab*) Same as (*a*), but for the blazar PKS 2155−304, observed on 1984, day 316.

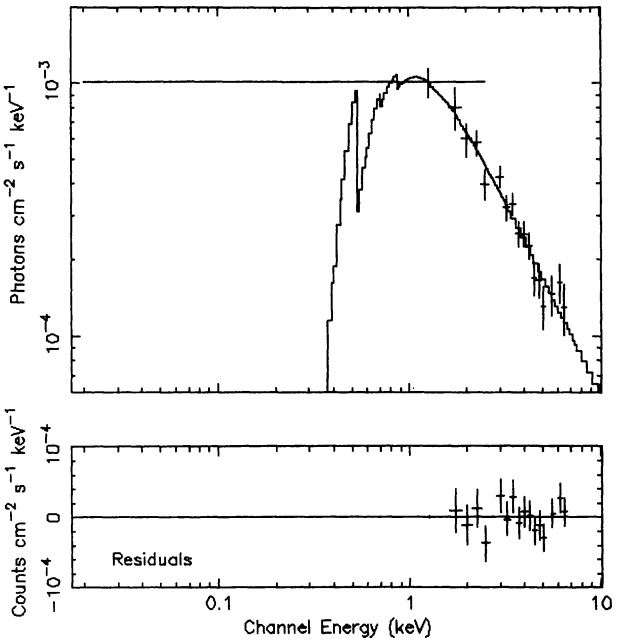

FIG. 2*e*

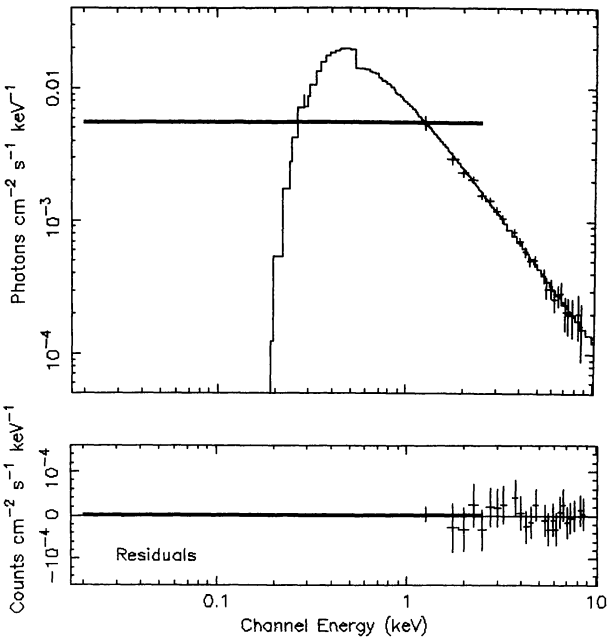

FIG. 2*f*

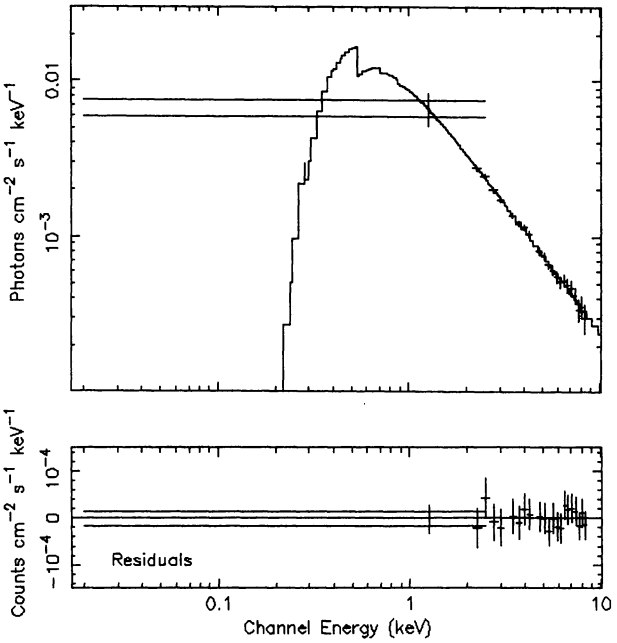

FIG. 2*g*

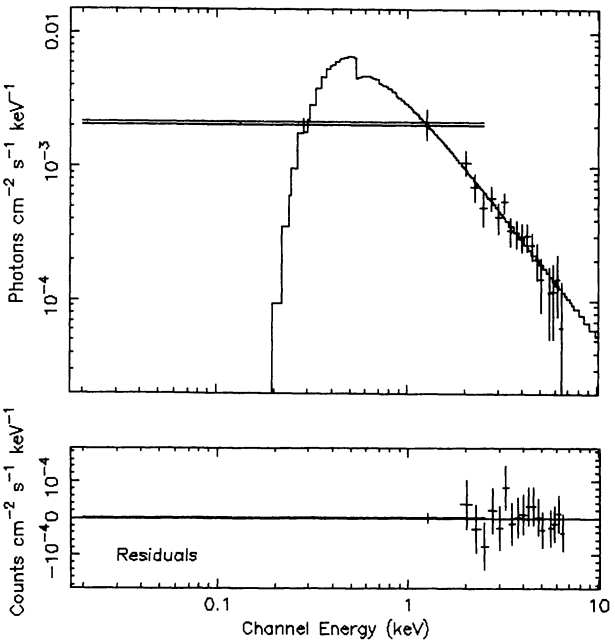

FIG. 2*h*

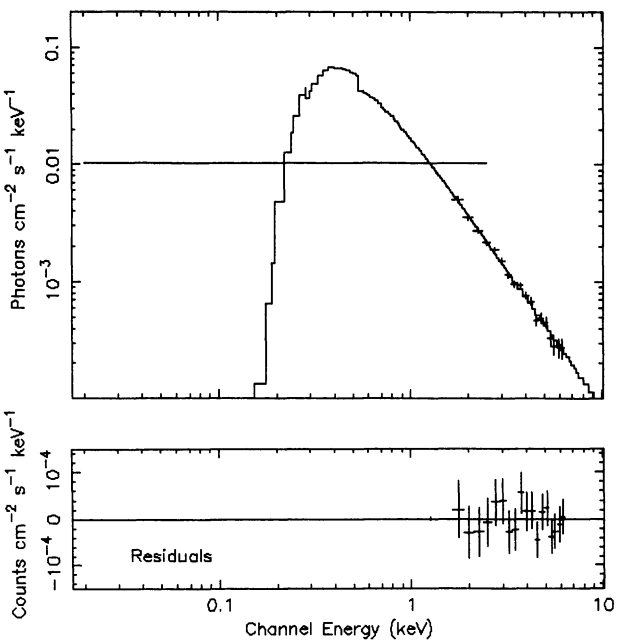

FIG. 2*i*

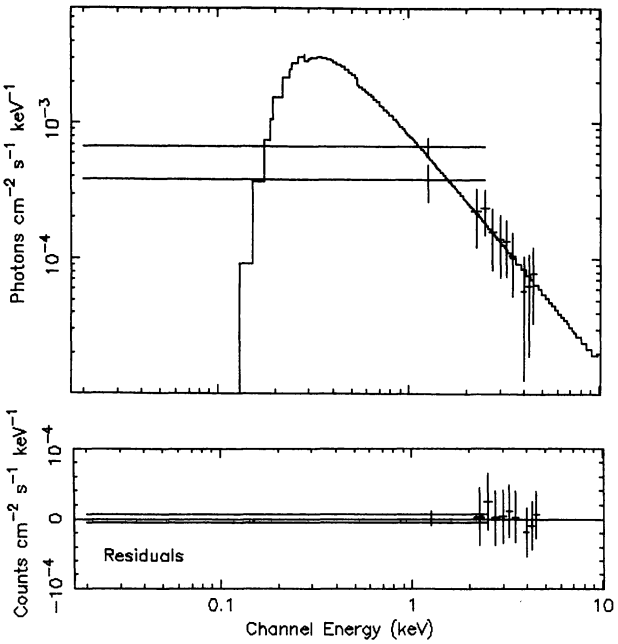

FIG. 2*j*

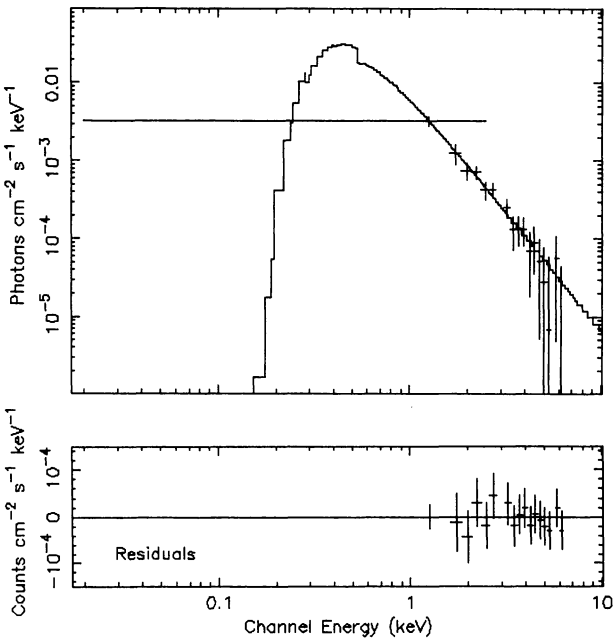

FIG. 2*k*

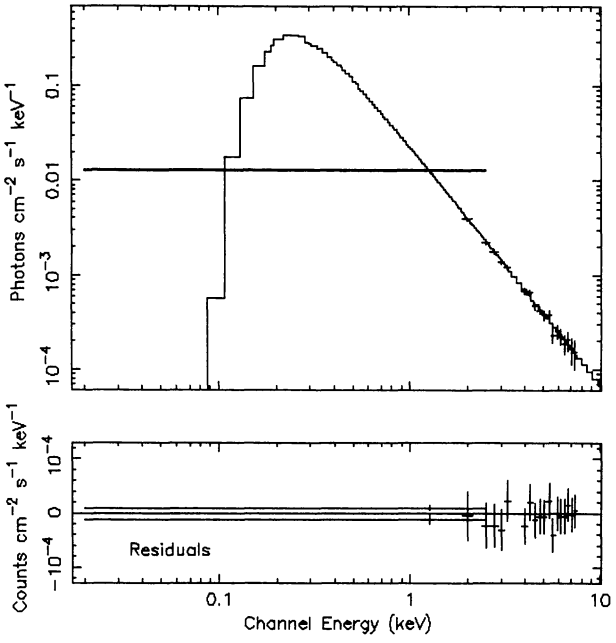

FIG. 2*l*

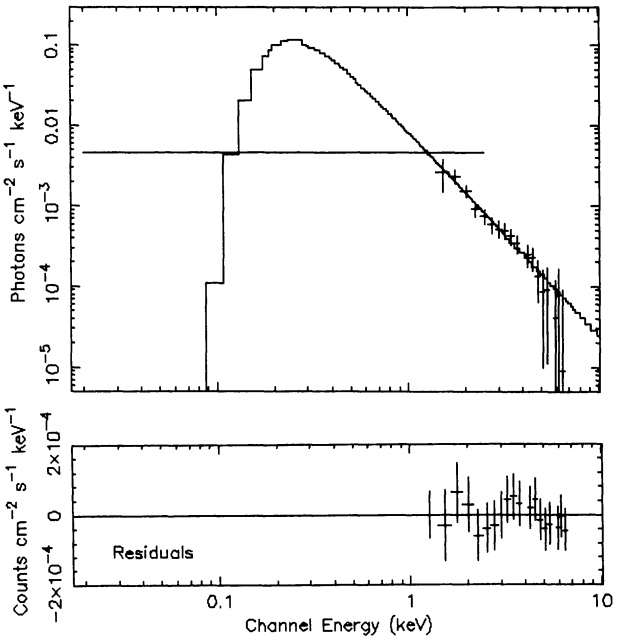

FIG. 2*m*

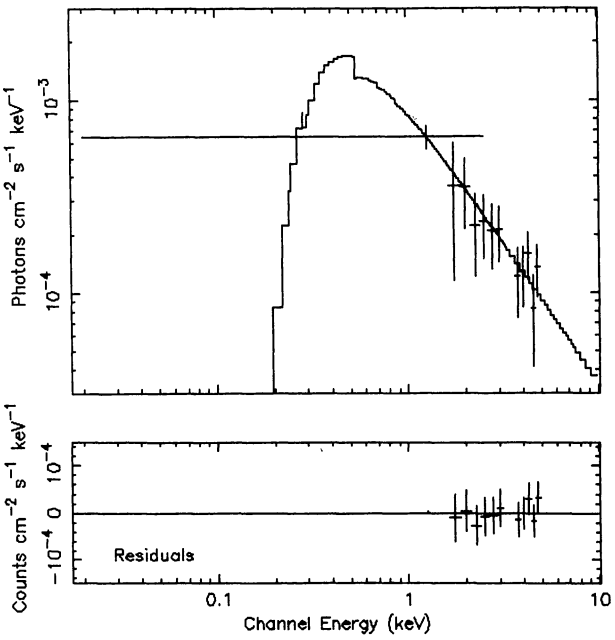

FIG. 2*n*

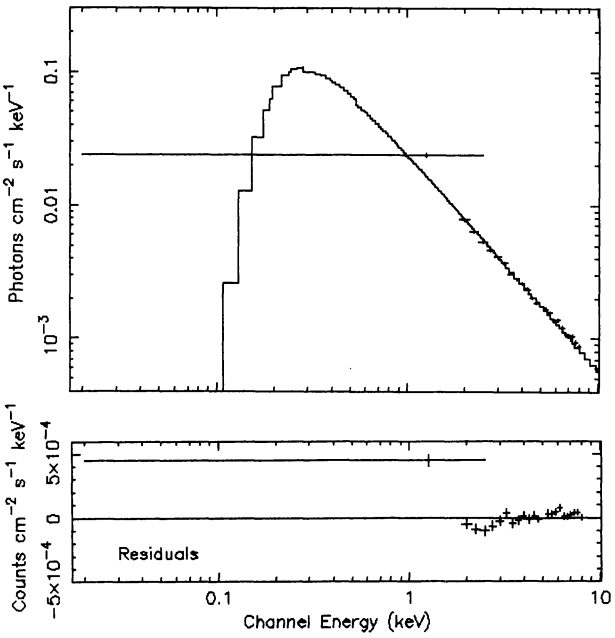

FIG. 2*o*

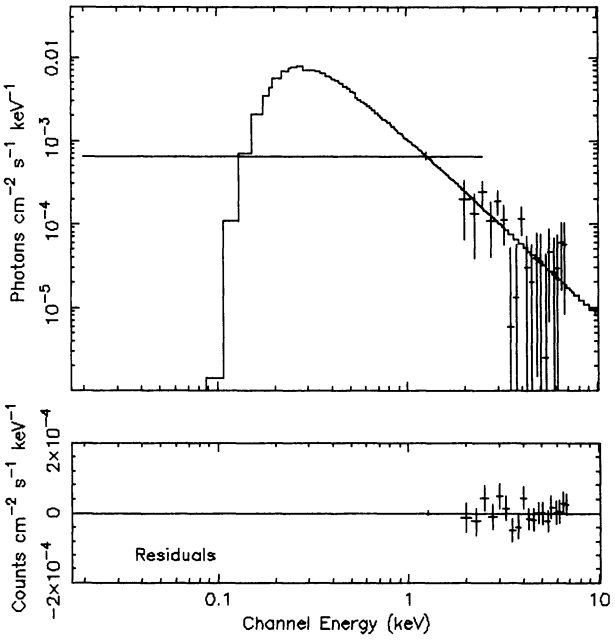

FIG. 2*p*

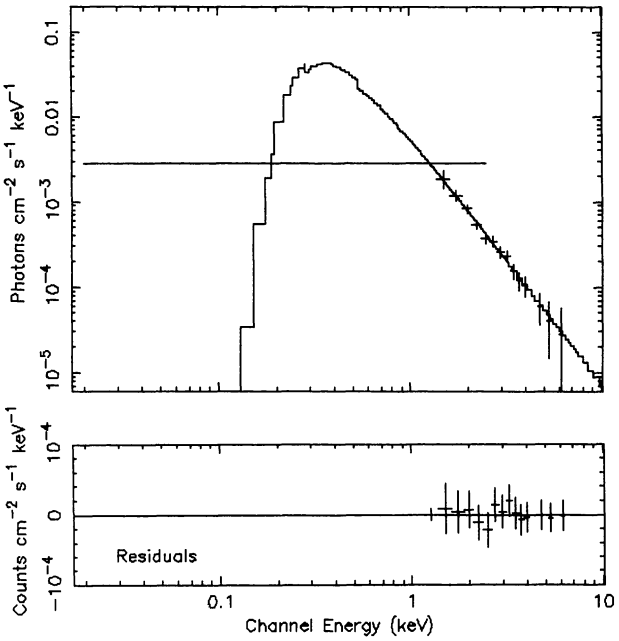

FIG. 2*q*

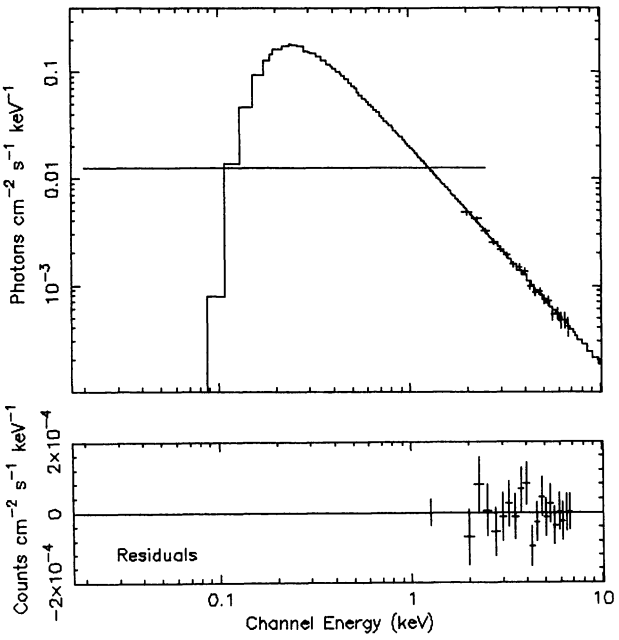

FIG. 2*r*

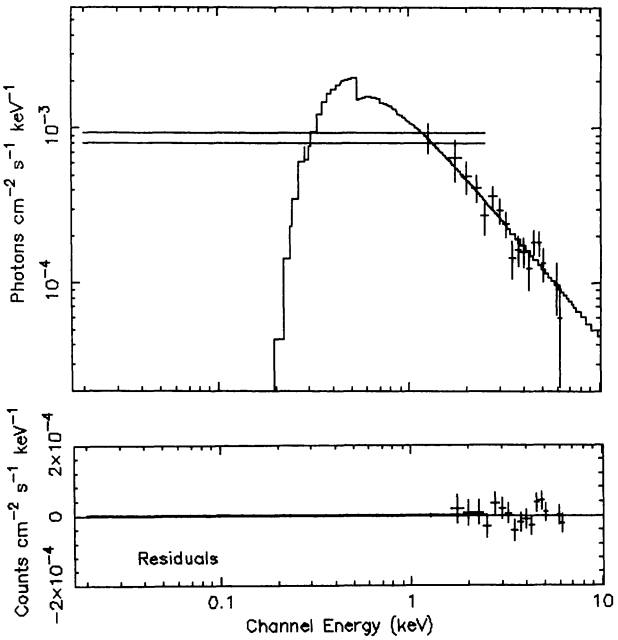

FIG. 2*s*

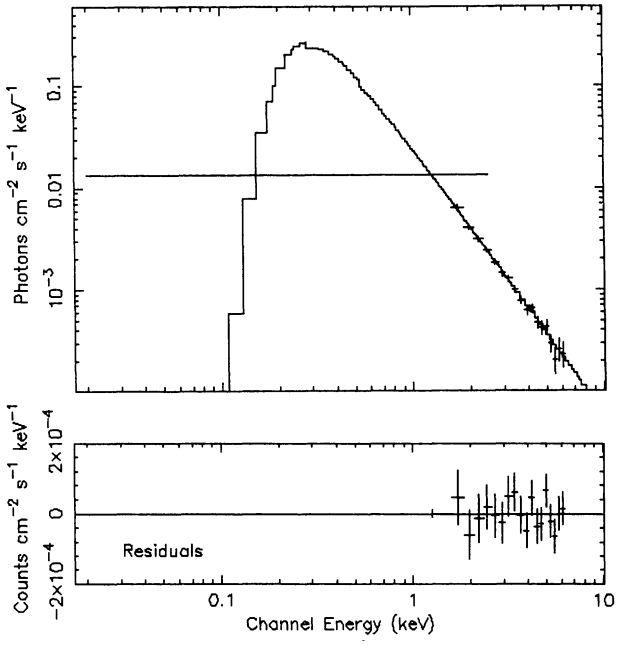

FIG. 2*t*

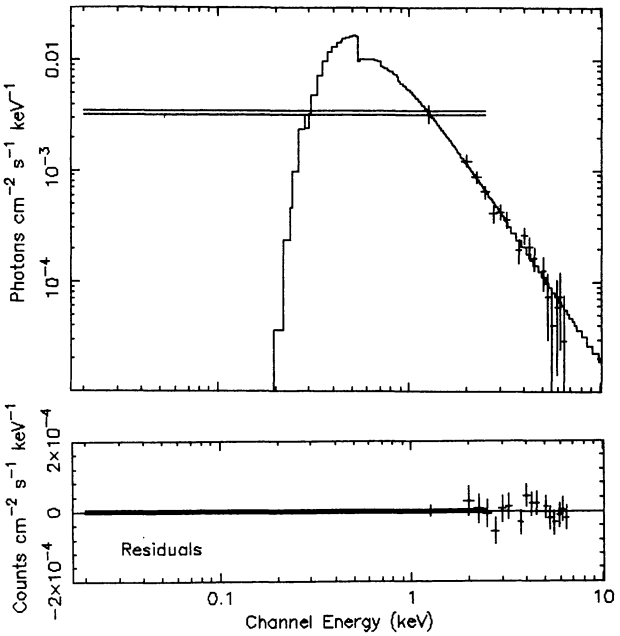

FIG. 2*u*

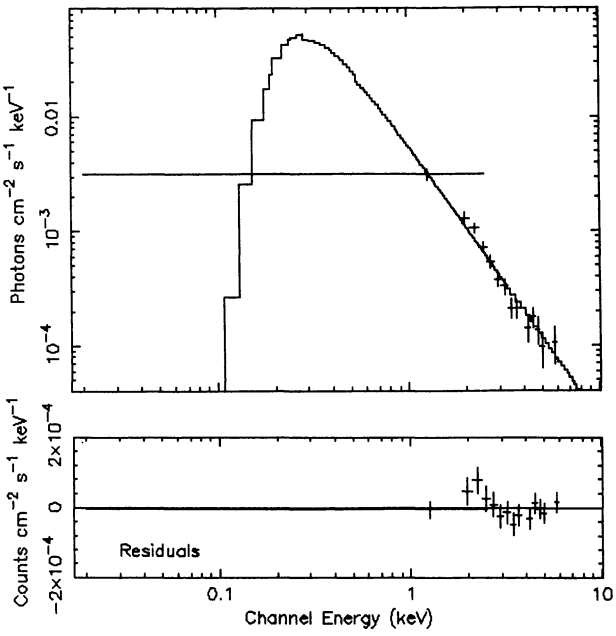

FIG. 2*v*

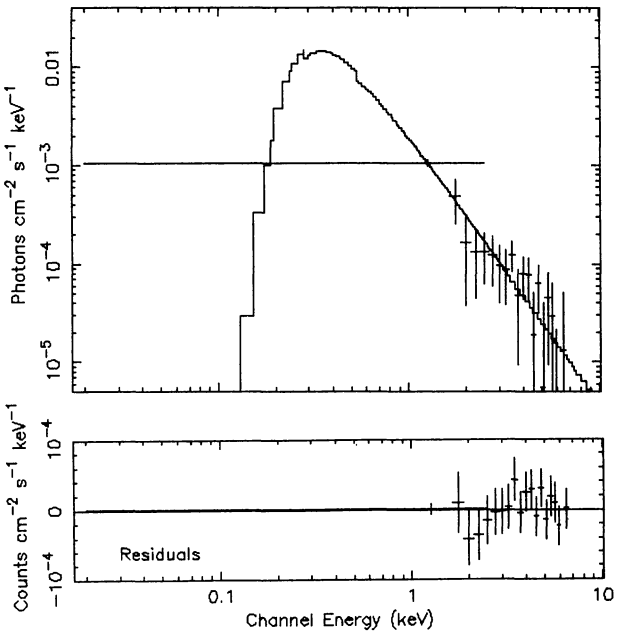

FIG. 2*w*

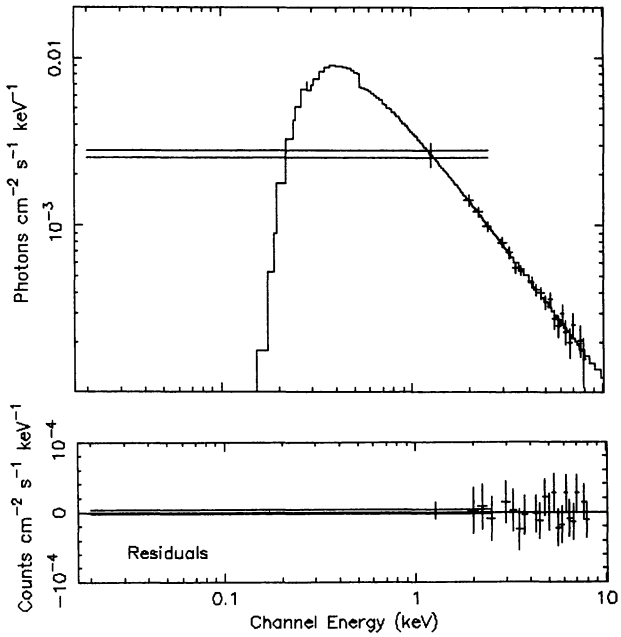

FIG. 2*x*

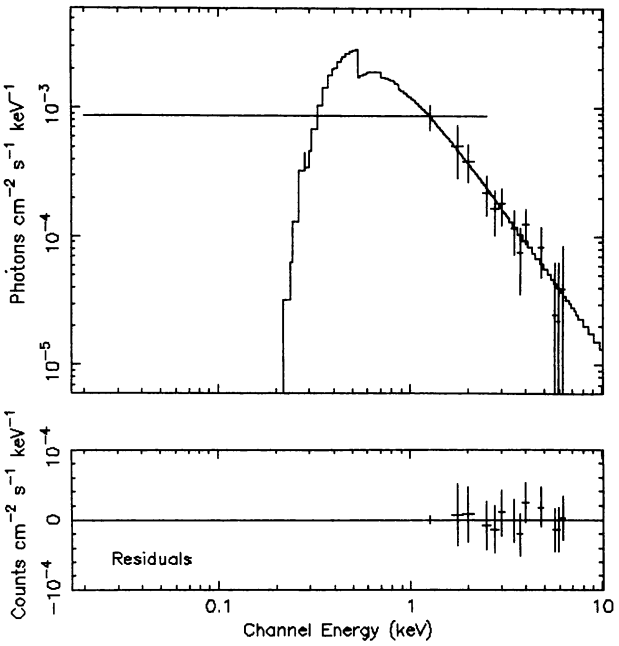

FIG. 2*y*

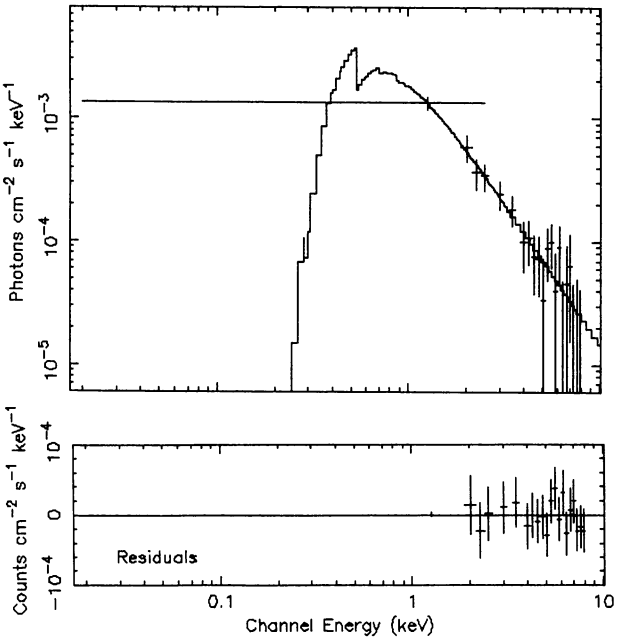

FIG. 2*z*

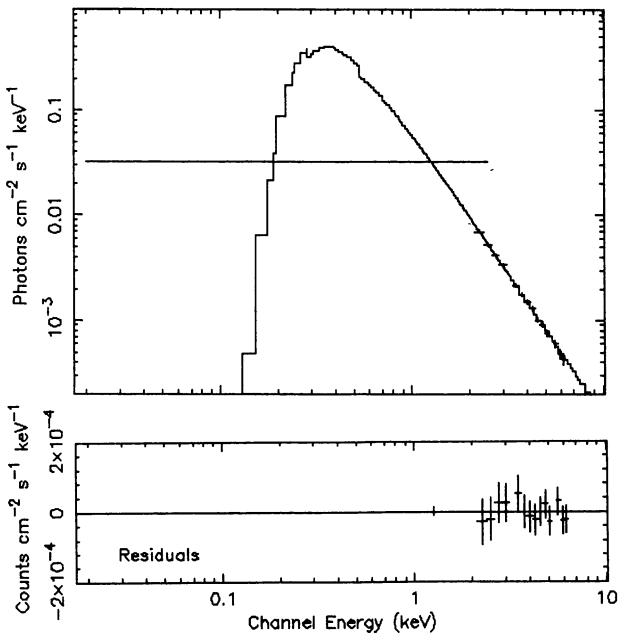

FIG. 2*aa*

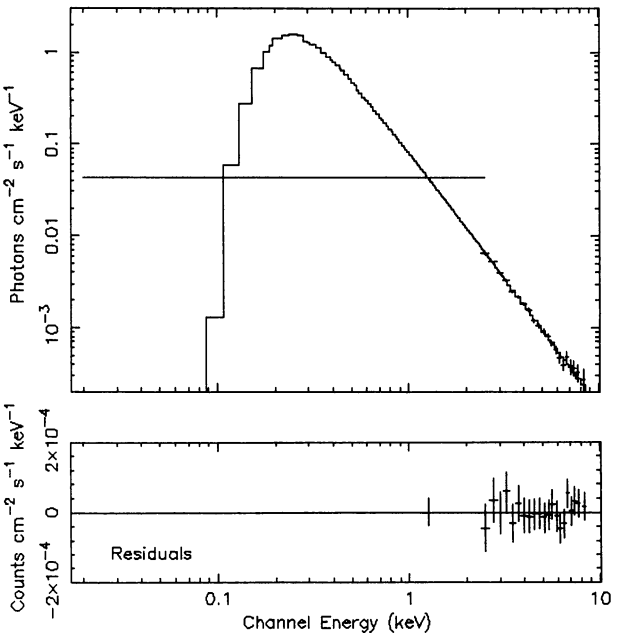

FIG. 2*ab*

epochs). Additional reasons for the above suggestion are as follows: (1) It may be noted from Figures 3 and 4 that the multifrequency spectra of RBLs and XBLs can be represented by two parabolic components and by a single parabolic component, respectively. These two types of multifrequency spectra for RBLs and XBLs have already been noted by other authors from simultaneous/quasi-simultaneous observations of blazars (Landau et al. 1986; Bregman et al. 1982; Brown et al. 1989; Kawai et al. 1989; Makino et al. 1987; Makino 1989; Mufson et al. 1984). (2) Blazars emit radio to X-ray continuum radiation over nearly 8–9 decades in flux (ergs cm^{-2} s^{-1} Hz^{-1}), and the variability of blazars, even by factors of 2–3 (except the flares), will not substantially affect the overall shape of the average multifrequency spectra of these objects, which have been plotted on a logarithmic scale (Impey & Neugebauer 1988).

4. RESULTS

The X-ray photon index Γ and the radio (5 GHz), far-infrared (FIR; 60 μm), near-infrared (NIR; 2.2 μm), optical (5560 Å), UV (2000 Å), and X-ray (2–10 keV) luminosities of 28 blazars are listed in Tables 5A (for RBLs) and 5B (for XBLs). Each luminosity was computed using $H_0 = 50$ km s^{-1} Mpc^{-1}, and $q_0 = 0$ and assuming isotropic emission. No correction for Galactic extinction was made to the computed luminosities. Measured fluxes at each frequency (except for FIR, UV, and X-ray fluxes) were taken from the literature. Brief results for these objects are given below:

4.1. *3C 66A*

3C 66A is a well-known blazar (Angel & Stockman 1980), and its optical image appears to be a stellar-like object ($\theta_{VLA} \sim 11''$). A broad emission line of Mg II is present in the optical spectrum of this object. It has displayed high optical polarization ($\sim$16%) (Mead et al. 1990) and large-amplitude ($\Delta B \sim 1.4$ mag) optical variations during the flare states (Cruz-Gonzalez & Huchra 1984). Also, from Figure 1, which plots α_{RO} against α_{OX}, we find that 3C 66A occupies the position in the upper part of the plot where all other RBLs are present. Also, this source has been classified as an RBL (Giommi et al. 1990; Hewitt & Burbidge 1993).

3C 66A was observed with *EXOSAT* on three occasions between 1986 January 6 and February 1. On one occasion (1986 January 15) the LE observation was contaminated by the other object in the field, and we have excluded this observation from our analysis. During *EXOSAT* observations, the LE count rate of this object did not vary, but the ME count rates varied on a timescale of weeks (see Table 2). Neither the LE nor the ME observations displayed any rapid variability (on timescales of hours) within each single observation. Spectral fits with N_H free to vary show that the Γ values of the LE + ME spectra are in the range 1.4–2.5, and the lower limit value of N_H (4 times higher than the Galactic N_H value) suggests that no significant absorption is present in the X-ray spectra of this source (Table 3). Our results are in agreement with the results of Maccagni et al. (1987). We have also used other models (power-law plus absorption plus blackbody, power-law plus absorption plus thermal bremsstrahlung, power-law plus absorption plus high-energy cutoff, power-law plus absorption plus absorption-edge, broken power-law plus absorption, and double power-law plus absorption) to fit the X-ray spectra of this RBL. However, we could not find any significant improvement over the power-law plus absorption model ($\Delta\chi^2 < 2$). Measured fluxes from simultaneous observations at radio, NIR, optical, and UV (Worrall et al. 1984b) and nonsimultaneous observations at FIR and X-ray frequencies have been used to construct the multifrequency spectrum of this blazar, which can be well represented by two parabolic components (see Fig. 3*a*).

4.2. *AO 0235+164*

AO 0235+164 is a strong emission-line object (the rest-frame equivalent width is more than 5 Å) (Cohen et al. 1987). It is a highly variable ($\Delta V \sim 5$ mag during the flare states) and highly polarized ($\sim$25%) (Rieke et al. 1976; MacLeod, Andrew, & Harvey 1976; Ledden, Aller, & Dent 1976; Angel & Stockman 1980; Stickel et al. 1991; Webb et al. 1988; Mead et al. 1990) superluminal source (Impey 1987). It is also known as an OVV blazar (Burbidge & Hewitt 1992), and it has been classified as an RBL (Giommi et al. 1990; Hewitt & Burbidge 1993). The X-ray spectrum of this source, which was observed on 1984 August 1 by I. McHardy, can be well represented by the power-law plus absorption model. Best-fit parameters of the spectrum (Table 3) suggest that no intrinsic absorption is present in this source. We have also used other models, mentioned in § 4.1, to fit the spectrum, but other models do not yield significant improvement over the power-law model. The multifrequency spectrum of this blazar was constructed using the measured fluxes from simultaneous observations at radio, millimeter, NIR, and optical wavelength. (Brown et al. 1989) and nonsimultaneous observations at FIR, UV, and X-ray frequencies (see Fig. 3*b*).

4.3. *1E 0317+18*

1E 0317+18 is a BL Lac object (Stocke et al. 1989, 1990; Burbidge & Hewitt 1992) which has also been classified as an XBL (Giommi et al. 1990; Hewitt & Burbidge 1993). X-ray spectra of this source can be best fitted with the power-law plus absorption model. It is a steep X-ray spectrum source ($\Gamma \sim 2.4+0.60$; Table 3 and Giommi et al. 1987), and it did not vary during *EXOSAT* observations (1985 January 14 and February 9). Derived values of N_H are consistent with the Galactic N_H value. No rapid X-ray variability on the timescales of hours was detected in this source. The radio to X-ray spectrum of this blazar can be represented by a single parabolic curve (Fig. 4*a*).

4.4. *1H 0323+022*

This blazar is an XBL (Giommi et al. 1990; Mead et al. 1990). *EXOSAT* spectra of this source have been described by the power-law plus absorption model (Sambruna et al. 1993). Results of our spectral analysis are consistent with the results of Sambruna et al. (1993). We have also tried to improve the fit statistics by using other models as mentioned in § 4.1, but no significant improvement was found. During the *EXOSAT* observations the LE flux did not vary but the ME flux varied with the spectral slope. The spectrum hardens when the source brightens, and the measured N_H is in agreement with the Galactic value. Neither the LE nor the ME fluxes varied on hourly

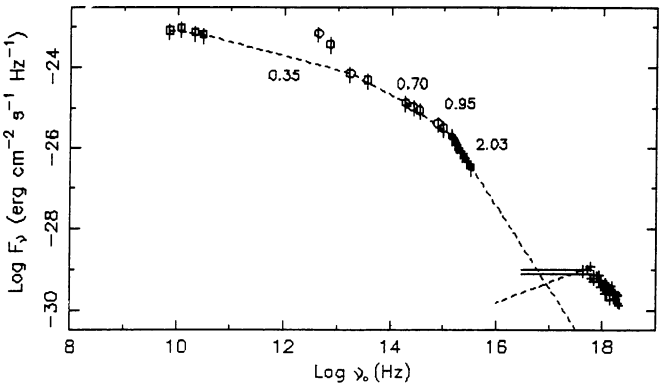

FIG. 3*a*

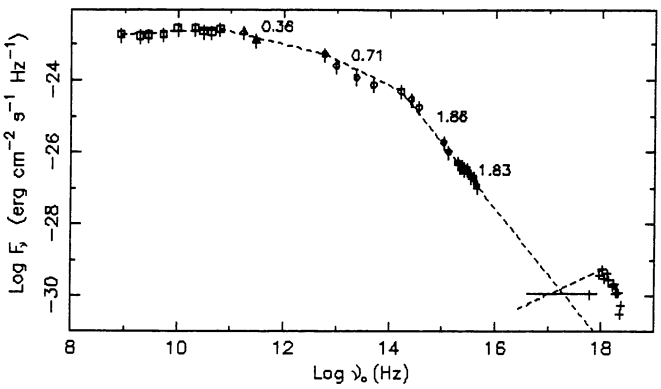

FIG. 3*b*

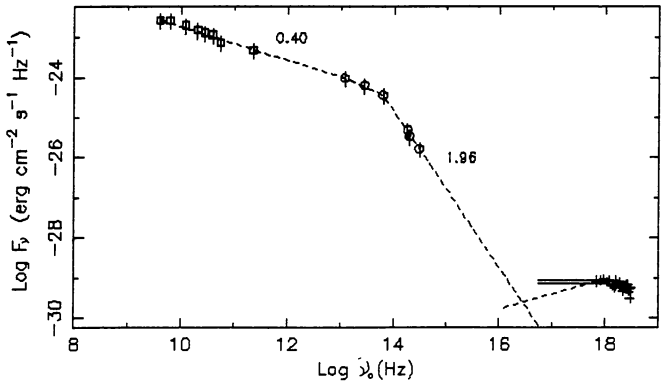

FIG. 3*c*

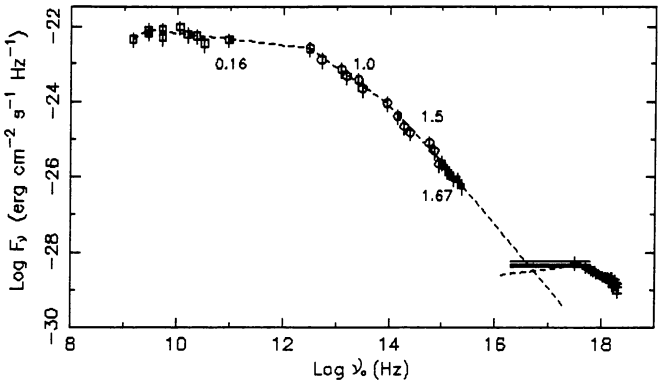

FIG. 3*d*

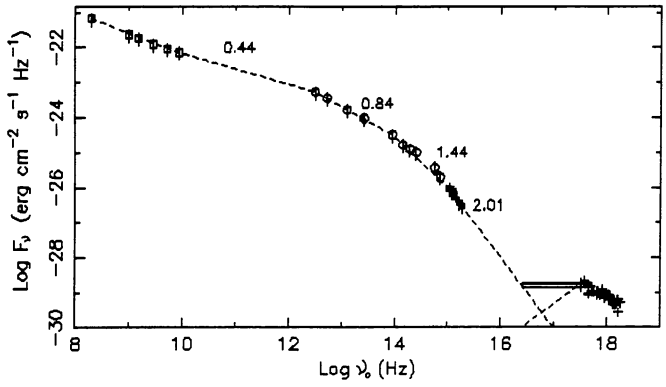

FIG. 3*e*

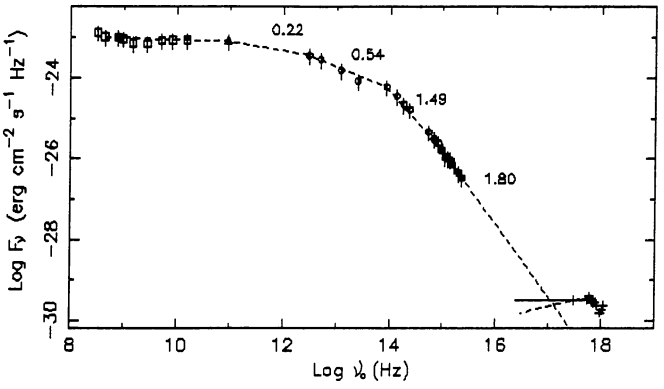

FIG. 3*f*

FIG. 3.—(*a*) Multifrequency spectrum of 3C 66A with two X-ray spectra. Error bars are 40% of the local fluxes. *Open squares:* Worrall et al. (1984b). *Circles:* Impey & Neugebauer (1988); Worrall et al. (1984b). *Filled squares: IUE*-ULDA database. *Plus signs:* present paper. (*b*) Same as (*a*), but for the blazar AO 0235+164 with one X-ray spectrum. *Open squares:* Kuhr et al. (1981b); Landau, Epstein, & Rather (1980); Brown et al. (1989). *Triangles:* Brown et al. (1989). *Circles:* Impey & Neugebauer (1988); Brown et al. (1989); Cruz-Gonzalez & Huchra (1984). *Filled squares: IUE*-ULDA database. *Plus signs:* present paper. (*c*) Same as (*a*), but for the blazar NRAO 140. *Squares:* Marscher (1988). *Circles:* Neugebauer et al. (1986); Courvoisier, Bell-Burnell, & Blecha (1986). *Plus signs:* present paper. (*d*) Same as (*a*), but for the blazar 3C 120. *Open squares:* Kuhr et al. (1981b). *Circles:* Ward et al. (1987); Maraschi et al. (1991). *Filled squares: IUE*-ULDA database. *Plus signs:* present paper. (*e*) Same as (*a*), but for the blazar PKS 0521−365. *Open squares:* Kuhr et al. (1981b). *Circles:* Impey & Neugebauer (1988); Cruz-Gonzalez & Huchra (1984). *Filled squares: IUE*-ULDA database. *Plus signs:* present paper. (*f*) Same as (*a*), but for the blazar PKS 0754+100 with one X-ray spectrum. *Open squares:* Worrall et al. (1984b); Owen, Spangler, & Cotton (1980). *Triangles:* Owen et al. (1980). *Circles:* Impey & Neugebauer (1988); Worrall et al. (1984b). *Filled squares: IUE*-ULDA database. *Plus signs:* present paper. (*g*) Same as (*a*), but for the blazar OJ 287. *Open squares:* Brown et al. (1989); Landau et al. (1980). *Triangles:* Brown et al. (1989). *Circles:* Impey & Neugebauer (1988); Brown et al. (1989); Landau et al. (1986). *Filled squares: IUE*-ULDA database. *Plus signs:* present paper. (*h*) Same as (*a*), but for the blazar B2 1147+245 with one X-ray spectrum. *Squares:* Owen et al. (1980). *Circles:* Impey & Neugebauer (1988); Impey et al. (1984); Ledden & O'Dell (1985). *Plus signs:* present paper. (*i*) Same as (*a*), but for the blazar 3C 273. *Open squares:* Kuhr et al. (1981b); Landau et al. (1986). *Circles:* Ward et al. (1987); Landau et al. (1986). *Filled squares: IUE*-ULDA database. *Plus signs:* present paper. (*j*) Same as (*a*), but for the blazar PKS 1510−089. *Open squares:* Steppe et al. (1988); O'Dea, Barvainis, & Challis (1988). *Circles:* Impey & Neugebauer (1988); Landau et al. (1986). *Filled squares: IUE*-ULDA database. *Plus signs:* present paper. (*k*) Same as (*a*), but for the blazar 3C 371 with one X-ray spectrum. *Open squares:* Landau et al. (1986); Kuhr et al. (1981b); Worrall et al. (1984a). *Circles:* Impey & Neugebauer (1988); Worrall et al. (1984a). *Filled squares: IUE*-ULDA database. *Plus signs;* present paper. (*l*) Same as (*a*), but for the blazar 3C 390.3. *Open squares:* Kuhr et al. (1981b). *Circles:* Impey & Neugebauer (1988); McAlary et al. (1983). *Filled squares: IUE*-ULDA database. *Plus signs:* present paper. (*m*) Same as (*a*), but for the blazar OV 236 with one X-ray spectrum. *Open squares:* Brown et al. (1989); Giacani & Colomb (1988). *Triangles:* Brown et al. (1989); Gear et al. (1986); Roelling et al. (1986). *Circles:* Brown et al. (1989); Impey & Neugebauer (1988); Gear et al. (1986). *Filled squares:* IUE-ULDA database. *Plus signs:* present paper. (*n*) Same as (*a*), but for the blazar 1928+73 with one X-ray spectrum. *Open squares:* Kuhr et al. (1981b); Edelson (1987). *Filled squares: IUE*-ULDA database. *Plus signs:* present paper.

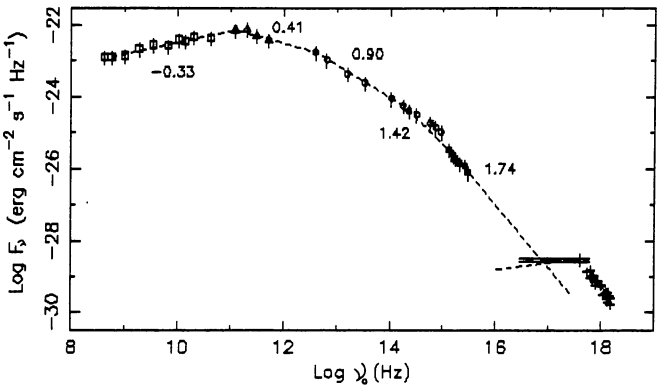

FIG. 3*g*

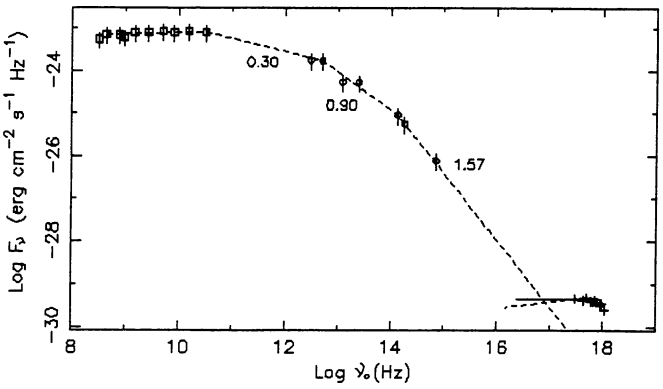

FIG. 3*h*

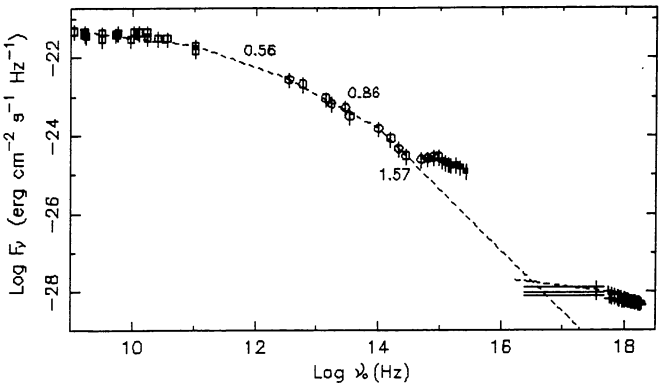

FIG. 3*i*

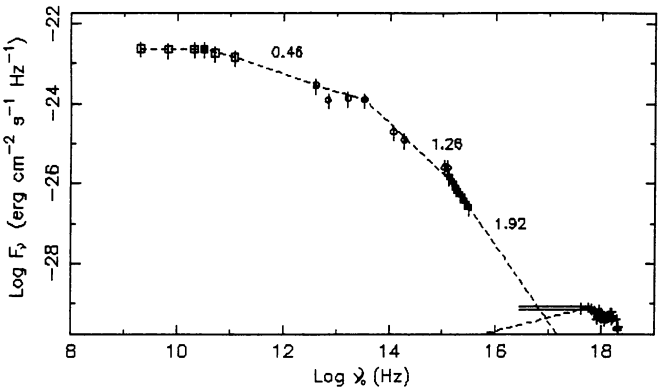

FIG. 3*j*

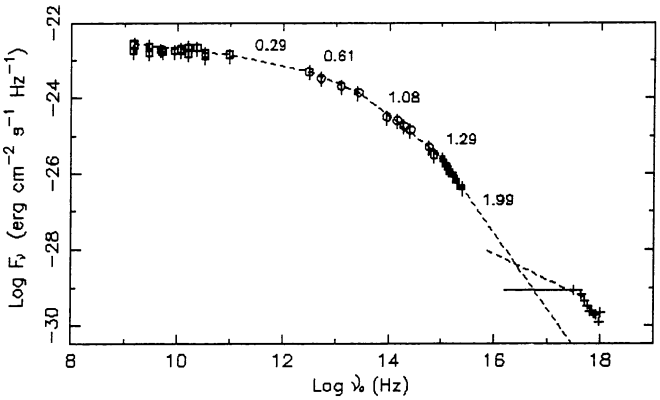

FIG. 3*k*

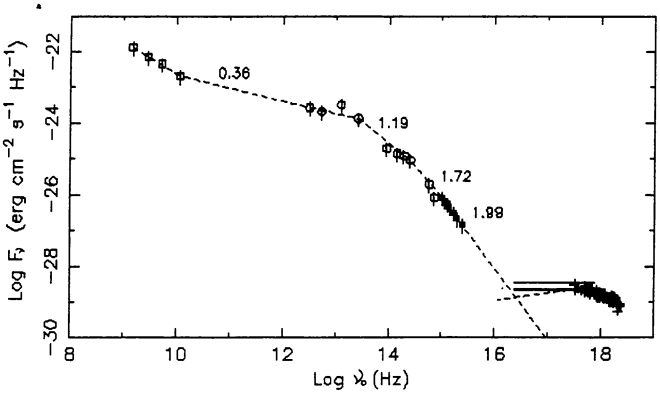

FIG. 3*l*

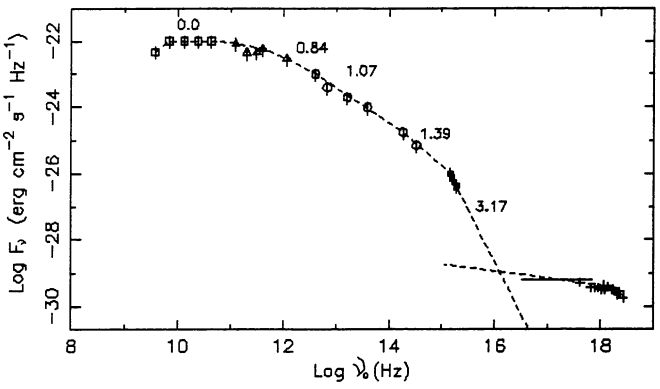

FIG. 3*m*

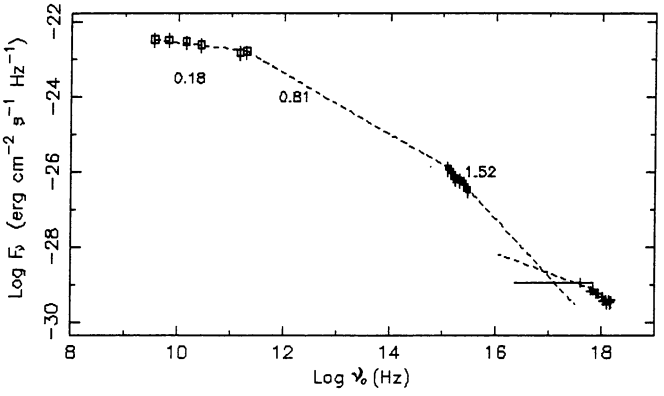

FIG. 3*n*

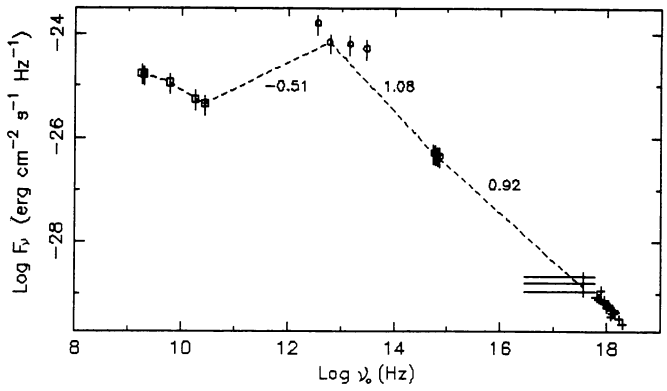

FIG. 4*a*

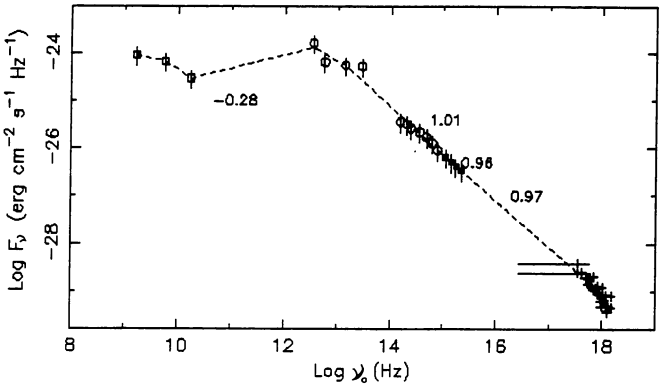

FIG. 4*b*

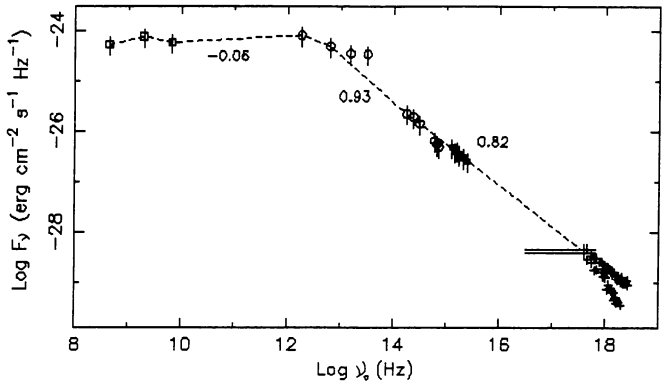

FIG. 4*c*

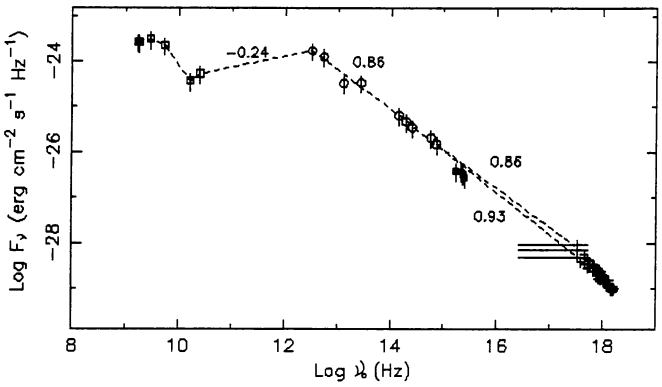

FIG. 4*d*

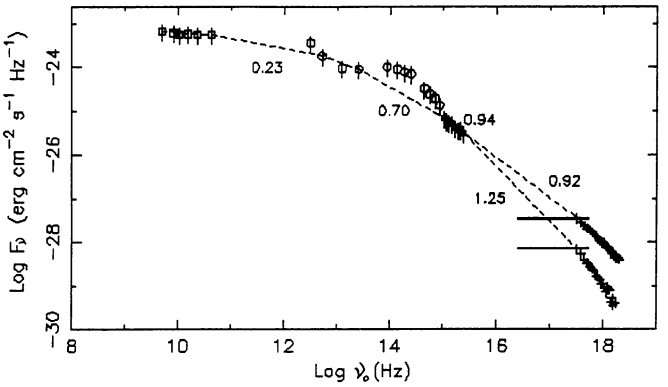

FIG. 4*e*

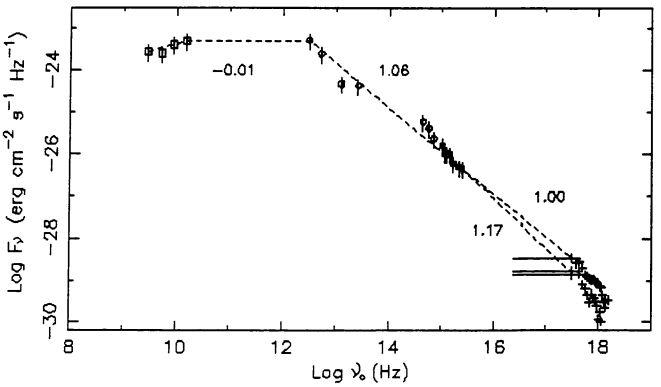

FIG. 4*f*

FIG. 4.—(*a*) Multifrequency spectrum of 1E 0317+18 with two X-ray spectra. *Squares:* Stocke et al. (1985). *Circles:* Impey & Neugebauer (1988); Stocke et al. (1985). *Plus signs:* present paper. (*b*) Same as (*a*), but for the blazar H0323+022. *Open squares:* Feigelson et al. (1986). *Circles:* Impey & Neugebauer (1988); Feigelson et al. (1986). *Filled squares: IUE*-ULDA database. *Plus signs:* present paper. (*c*) Same as (*a*), but for the blazar 1H 0414+009. *Open squares:* Ulmer et al. (1983). *Circles:* Impey & Neugebauer (1988); Halpern et al. (1991); Bersanelli et al. (1992). *Filled squares: IUE*-ULDA database. *Plus signs:* present paper. (*d*) Same as (*a*), but for the blazar PKS 0548−32. *Open squares:* Cruz-Gonzalez & Huchra (1984). *Circles:* Impey & Neugebauer (1988); Cruz-Gonzalez & Huchra (1984). *Filled squares: IUE*-ULDA database. *Plus signs:* present paper. (*e*) Same as (*a*), but for the blazar Mrk 421. *Open squares:* Makino et al. (1987). *Circles:* Impey & Neugebauer (1988); Makino et al. (1987). *Filled squares: IUE*-ULDA database. *Plus signs:* present paper. (*f*) Same as (*a*), but for the blazar Mrk 180. *Open squares:* Kuhr et al. (1981a); Mufson et al. (1984). *Circles:* Impey & Neugebauer (1988); Mufson et al. (1984). *Filled squares: IUE*-ULDA database. *Plus signs:* present paper. (*g*) Same as (*a*), but for the blazar 1E 1402+04 with one X-ray spectrum. *Squares:* Feigelson et al. (1982). *Circles:* Impey & Neugebauer (1988). *Plus signs:* present paper. (*h*) Same as (*a*), but for the blazar 1E 1415+259 with one X-ray spectrum. *Open squares:* Halpern et al. (1986). *Circles:* Impey & Neugebauer (1988); Halpern et al. (1986). *Filled squares: IUE*-ULDA database. *Plus signs:* present paper. (*i*) Same as (*a*), but for the blazar 1H 1427+42 with one X-ray spectrum. *Squares:* Remillard et al. (1989). *Circles:* Remillard et al. (1989). *Plus signs:* present paper. (*j*) Same as (*a*), but for the blazar Mrk 501. *Open squares:* Angel & Stockman (1980); Kuhr et al. (1981b); Landau et al. (1980); Sembay et al. (1985); Mufson et al. (1984). *Circles:* Sembay et al. (1985); Mufson et al. (1984); Cruz-Gonzalez & Huchra (1984). *Filled squares: IUE*-ULDA database. *Plus signs:* present paper. (*h*) Same as (*a*), but for the blazar 4U 1722+119 with one X-ray spectrum. *Squares:* Griffiths et al. (1989). *Circles:* Impey & Neugebauer (1988); Brissenden et al. (1990); Bersanelli et al. (1992). Plus signs present paper. (*l*) Same as (*a*), but for the blazar I Zw 186 with one X-ray spectrum. *Open squares:* Bregman et al. (1982). *Circles:* Impey & Neugebauer (1988); Bregman et al. (1982). *Filled squares: IUE*-ULDA database. *Plus signs:* present paper. (*m*) Same as (*a*), but for the blazar PKS 2005−489. *Open squares:* Large et al. (1981); Wall et al. (1975); *Circles:* Impey & Neugebauer (1988); Wall et al. (1986); Bersanelli et al. (1992). *Filled squares: IUE*-ULDA database; Wall et al. (1986). *Plus signs:* present paper. (*n*) Same as (*a*), but for the blazar PKS 2155−304. *Open squares:* Angel & Stockman (1980); Hjellming, Schnopper, & Moran (1978). *Circles:* Impey & Neugebauer (1988); Treves et al. (1989). *Filled squares: IUE*-ULDA database. *Plus signs:* present paper.

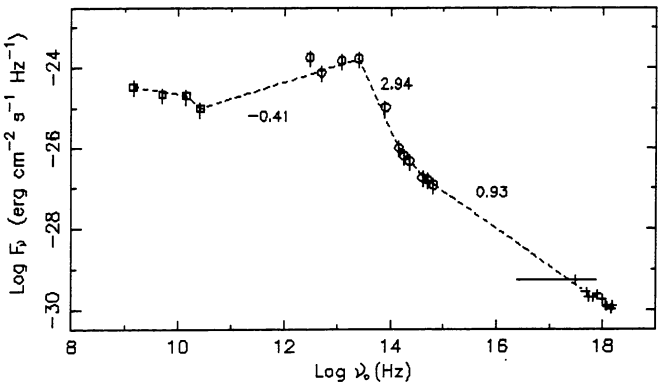

FIG. 4*g*

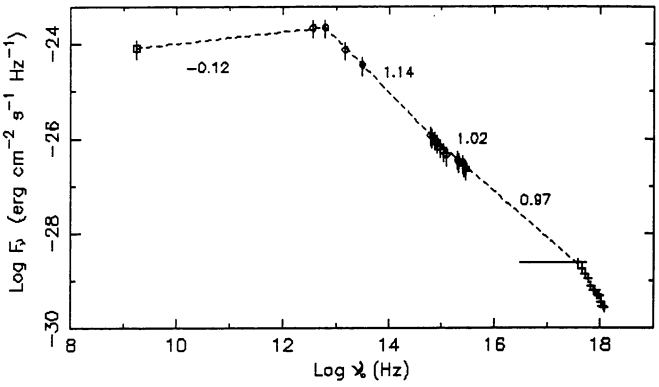

FIG. 4*h*

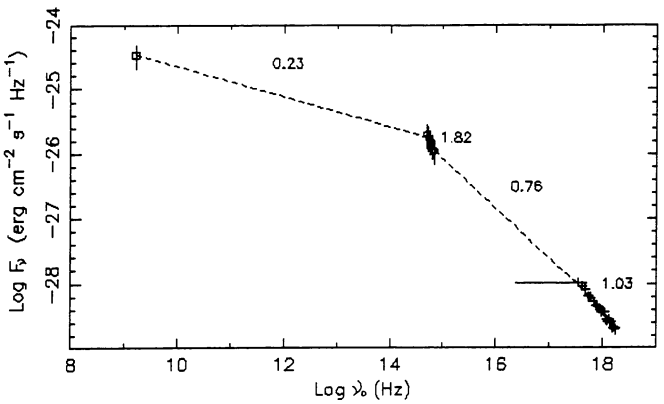

FIG. 4*i*

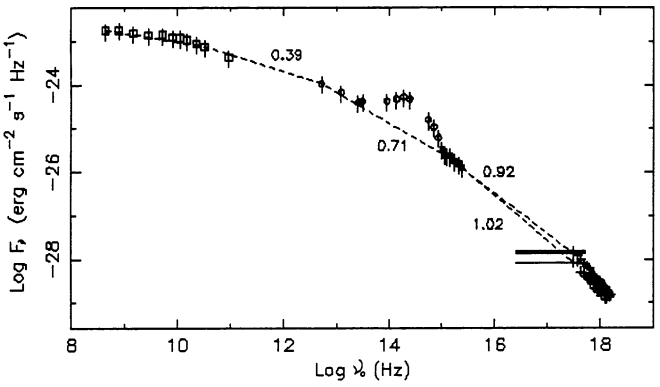

FIG. 4*j*

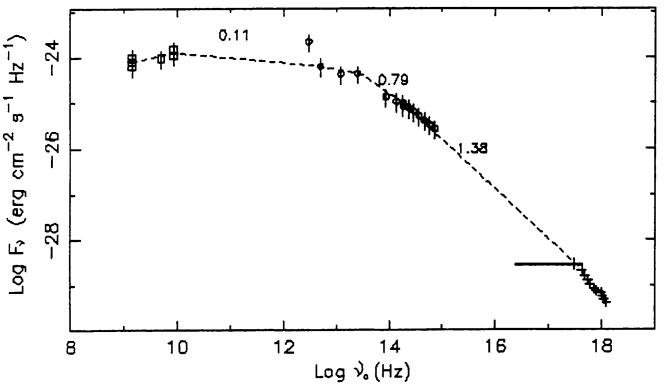

FIG. 4*k*

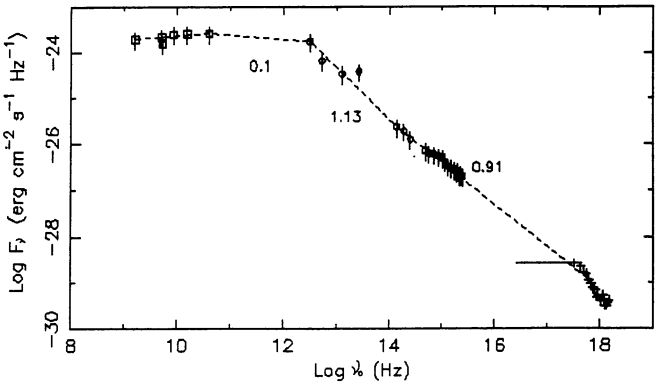

FIG. 4*l*

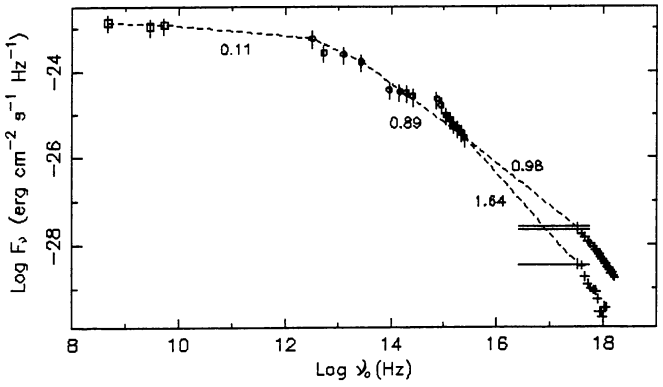

FIG. 4*m*

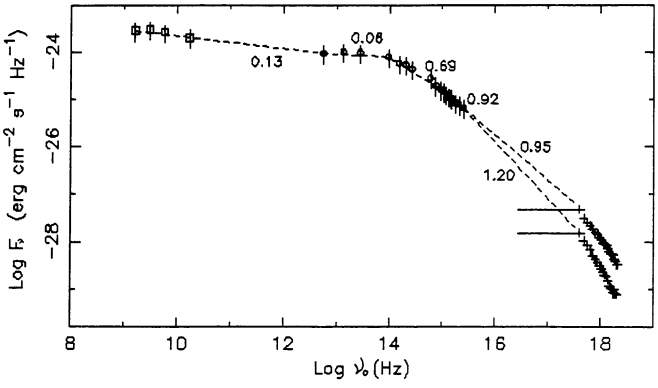

FIG. 4*n*

FIG. 4.—*Continued*

TABLE 5A

HARDNESS RATIO, PHOTON INDEX, AND LUMINOSITIES OF RBLs

Object Name	Γ^a	$L_5{}^b$	$L_{60}{}^c$	$L_{2.2}{}^d$	$L_O{}^e$	$L_{UV}{}^f$	$L_{2-10}{}^g$
3C 66A	1.39	0.66	6.53	28.80	33.50	21.80	7.21
AO 0235+164	1.80	11.40	225.80	648.00	250.40	93.40	27.90
NRAO 140	1.62	22.80	121.50	164.10	45.90	16.80	199.00
3C 120	1.75	0.02	0.33	0.28	0.22	0.09	0.21
PKS 0521−36	1.56	0.06	0.25	0.32	0.17	0.10	0.17
PKS 0754+10	1.70	...	...	...	...	...	...
OJ 287	2.94	0.96	38.40	54.10	33.80	20.10	2.62
B2 1147+245	1.90	...	...	...	...	...	...
3C 273	1.71	2.73	12.55	14.80	6.78	4.02	14.27
PKS 1510−089	1.46	1.69	9.56	16.99	14.90	12.80	6.13
3C 371	2.80	0.01	0.20	0.33	0.30	0.21	0.02
3C 390.3	1.42	0.03	0.17	0.37	0.20	0.07	0.41
OV 236	1.41	3.68	29.40	23.90	1.59	1.85	4.35
1928+73 (4C 73.18)	2.25	1.09	52.80	23.10	11.10	7.50	1.40

[a] X-ray (0.1–10 keV) photon index.
[b] 5 GH radio luminosity in 10^{44} ergs s^{-1}.
[c] Far-IR (60 μm) luminosity in 10^{45} ergs s^{-1}.
[d] Near-IR (2.2 μm) luminosity in 10^{45} ergs s^{-1}.
[e] Optical (5560 Å) luminosity in 10^{45} ergs s^{-1}.
[f] UV (2000 Å) luminosity in 10^{45} ergs s^{-1}.
[g] X-ray (2–10 keV) luminosity in 10^{45} ergs s^{-1}.

TABLE 5B

HARDNESS RATIO, PHOTON INDEX, AND LUMINOSITIES OF XBLs

Object Name	Γ^a	$L_5{}^b$	$L_{60}{}^c$	$L_{2.2}{}^d$	$L_O{}^e$	$L_{UV}{}^f$	$L_{2-10}{}^g$
0317+18	1.92	1.02	0.11	1.10	2.60	3.13	1.49
H0323+022	2.41	2.10	0.45	5.32	7.32	7.79	1.33
1H 0414+009	2.40	19.20	10.10	17.80	19.20	27.80	8.06
PKS 0548−32	2.02	2.52	1.29	2.06	2.28	2.44	0.67
Mrk 421	2.87	1.48	0.40	1.60	2.41	3.05	0.47
Mrk 180	2.59	1.40	1.48	1.22	1.13	1.06	0.11
1E 1402+04	2.30						
1E 1415+259	2.13	8.16	36.50	26.60	22.70	21.50	1.48
1H 1427+42	2.03	1.54	0.23	2.76	8.16	9.81	4.46
Mrk 501	2.47	3.37	0.28	0.73	1.09	1.39	0.17
4U 1722+119	2.38						
I Zw 186	2.42	1.17	0.43	0.46	0.55	0.51	0.11
PKS 2005−489	3.21	13.80	5.08	12.00	14.10	15.60	0.61
PKS 2155−304	2.82	11.20	3.30	56.10	85.80	105.00	3.57

[a] X-ray (0.1–10 keV) photon index.
[b] 5 GH radio luminosity in 10^{41} ergs s^{-1}.
[c] Far-IR (60 μ) luminosity in 10^{44} ergs s^{-1}.
[d] Near-IR (2.2 μ) luminosity in 10^{44} ergs s^{-1}.
[e] Optical (5560 Å) luminosity in 10^{44} ergs s^{-1}.
[f] UV (2000 Å) luminosity in 10^{44} ergs s^{-1}.
[g] X-ray (2–10 keV) luminosity in 10^{45} ergs s^{-1}.

timescales. Measured fluxes from simultaneous observations of UV and X-ray and from nonsimultaneous observations between radio and optical frequencies have been plotted in Figure 4*b* which can be represented by a single parabolic curve.

4.5. *NRAO 140*

NRAO 140 is a broad and strong emission-line quasar (Kristian & Sandage 1970; Burbidge & Strittmatter 1972) with superluminal motion in it (Zensus 1989). It has been classified as an RBL (Hewitt & Burbidge 1993). Details of X-ray observations of this source using *HEAO 1*, the *Einstein Observatory*, and *EXOSAT* are given in Marscher (1988). Here we present only the results of *EXOSAT* observations. NRAO 140 was observed with *EXOSAT* on 1985 January 25 and 26, and no rapid or long-term flux (LE and ME) and spectral index variations were noted in this source. The power-law plus absorption model results in the best fit with the spectra of this source. It is a flat-spectrum ($\Gamma \sim 1.5 \pm 0.2$) source, and it displayed correlated variability of compact radio and X-ray fluxes between 1979 and 1985 (Marscher 1988). Using the simultaneously measured radio and X-ray fluxes and nonsimultaneously mea-

sured FIR and optical fluxes, we have constructed the multifrequency spectrum (Fig. 3*c*) of this RBL, which can be fitted with two parabolic components.

4.6. *1H 0414+009*

1H 0414+009 is a BL Lac object (Impey & Tapia 1988; Mead et al. 1990; Maccagni et al. 1989; Halpern et al. 1991) and has been classified as an XBL (Giommi et al. 1990; Hewitt & Burbidge 1993). It was observed with *EXOSAT* on four occasions during 1984 September 9–30 (Sambruna et al. 1993). No variations of the LE flux were noticed in this source, but the ME flux varied by a factor of 2 within 16 days (1984 days 258–274). Rapid (on the timescales of hours) variability of the ME flux of this blazar was found on 1984 September 9, which was also noted by Giommi et al. 1990. We have used the power-law plus absorption model and other models mentioned in § 4.1 to fit the spectra of this XBL. We find that the power-law plus absorption model fits the spectra best, and other models do not differ significantly (i.e., with significance at less than the 5% level) from the power-law model. The best-fit parameters of the spectral analysis are given in Table 3. From the results of the spectral analysis of 1H 0414+009, we find that the spectral slope steepened when the source intensity (2–10 keV) decreased (see Table 3). The multifrequency spectrum of this source can be represented by a single parabolic component, except for the infrared fluxes, which are much stronger than the radio and optical fluxes (Fig. 4*c*).

4.7. *3C 120*

3C 120 is a superluminal source (Zensus 1989), and the optical continuum is highly variable (Wlerick, Westerlund, & Garnier 1979; French & Miller 1980; Oke, Readhead, & Sargent 1980). It is an OVV-type blazar (Webb et al. 1988; Burbidge & Hewitt 1992). This source was observed on 14 occasions with *EXOSAT* between 1983 August and 1986 February. Signal significances of the two spectra are less than 4 σ, and those of the remaining 12 spectra are above 4 σ (Table 2). Results of simultaneous/quasi-simultaneous observations of this blazar in the optical, ultraviolet, and X-ray bands have been described by Maraschi et al. (1991).

Best-fit parameters of the LE and ME spectra with the power-law plus absorption model are listed in Table 3. Results of our analysis are consistent with the results of Turner & Pounds (1989) and Maraschi et al. (1991). It may be noted from Table 3 that the spectral slope ($\Gamma \sim 1.6$–1.94) is correlated with the LE flux and anticorrelated with the ME flux. This result suggests a pivoting of the spectrum around 2 keV. Derived values of N_H from the power-law fits suggest that no intrinsic absorption is present in this source. Variability in the LE and ME bands with timescales shorter than a day is not found. Using the simultaneous observations of optical, ultraviolet, and X-ray bands (Maraschi et al. 1991) and nonsimultaneous observations between radio and IR bands, we have constructed the multifrequency spectrum of this blazar (Fig. 3*d*), which shows the spectral discontinuity between UV and X-ray region, and two parabolic components can represent the multifrequency spectrum.

4.8. *PKS 0521−36*

The optical spectrum of this blazar (Angel & Stockman 1980) is dominated by the permitted and forbidden emission lines (Danziger et al. 1979), very similar to the optical spectrum of the OVV object, 3C 371 (Angel & Stockman 1980). PKS 0521−36 is an optically variable ($\Delta V > 1$ mag during the flare states) and highly polarized quasar (Angel & Stockman 1980). Angel & Stockman (1980) have classified PKS 0521−36 and 3C 371 (an OVV object) as the same type of blazar. Also, this source has been classified as an RBL (Giommi et al. 1990; Hewitt & Burbidge 1993).

This RBL was observed on 1983 November 2 and 30 with *EXOSAT* (Garilli & Maccagni 1990). No rapid or long-term variations of the LE and ME count rates of PKS 0521−36 were found during *EXOSAT* observations. The power-law plus absorption model and other models, which were mentioned in § 4.1, were used to fit the spectra of this source. *F*-test analysis shows that the power-law plus absorption model fits best with the spectra of PKS 0521−36. Best-fitting parameters of the spectra are given in Table 3, and it can be seen from this table that PKS 0521−36 is a flat-spectrum ($\Gamma = 1.7 \pm 0.2$) source with no intrinsic absorption. Results of our spectral analysis are in agreement with the results of Garilli & Maccagni (1990). Fluxes from simultaneous observations of UV and X-rays and nonsimultaneous observations of radio to optical frequencies were used to draw the multifrequency spectrum of this blazar (Fig. 3*e*). Two spectral components are required to represent this spectrum.

4.9. *PKS 0548−32*

PKS 0548−32 is a BL Lac object (Angel & Stockman 1980; Maccagni et al. 1989; Burbidge & Hewitt 1992), and it is also an XBL blazar (Giommi et al. 1990; Hewitt & Burbidge 1993). It was observed at five epochs with *EXOSAT* between 1983 and 1986 (Barr, Giommi, & Maccagni 1988; Garilli & Maccagni 1990). This source did not display long-term variability of the LE and the ME count rates, but significant rapid variability of the ME count rate was found on 1983 November 2 and 1986 March 7 and 8, which was also noted by Giommi et al. (1990). The parameters of the power-law fit are listed in Table 3, and they are consistent with the results of Barr et al. (1988) and Garilli & Maccagni (1990). No intrinsic absorption is present in this source. Also we have used different models described in § 4.1 and found that the broken power-law model also fits the spectra well but not significantly better than the power-law model (see Table 4A). However, there is a trend of spectral steepening around 2–3 keV (Table 4A). A single parabola can represent the multifrequency spectrum of this blazar (Fig. 4*d*).

4.10. *PKS 0754+10*

The optical image of this source appears to be a stellar-like object, and it is a compact radio source of $\theta_{VLA} \sim 1''.8$. Optically it is a highly variable ($\Delta B > 2$ mag during the flare states) and highly polarized ($P \sim 26\%$) object (Angel & Stockman 1980; Mead et al. 1990). It has been classified as an RBL (Giommi et al. 1990; Hewitt & Burbidge 1993). This blazar was observed on 1984 February 12 with *EXOSAT*, and the

spectrum has not been published. The power-law plus absorption model fits the spectrum of this blazar best. It is a flat-spectrum ($\Gamma = 1.7 \pm 0.2$) source (Table 3). The derived value of N_H is consistent with the Galactic value. No rapid variability was found within the single observation of this source. Using the fluxes from simultaneous/quasi-simultaneous multifrequency observations (Worrall et al. 1984b), we have constructed the multifrequency spectrum (Fig. 3*f*) of this blazar. Two spectral components are required to represent this multifrequency spectrum.

4.11. *OJ 287*

OJ 287, which is a superluminal source (Porcas 1987), has displayed both sharp and broad emission lines in its optical spectrum (Miller, French, & Hawley 1978; Sitko & Junkkarinan 1985; Stickel et al. 1991). It is an optically variable ($\Delta V >$ 3 mag during the flare states) and highly polarized ($\sim$32%) blazar (Angel & Stockman 1980; Mead et al. 1990). It has been classified as an RBL (Giommi et al. 1990; Hewitt & Burbidge 1993). This blazar was observed on many occasions with *EXOSAT*, but only two spectra have signal significances above 4 σ (see Table 2). The power-law plus absorption model and other models that were mentioned in § 4.1 were used to fit the spectra of this RBL. From *F*-test analysis we find that the power-law model fits the spectra best. Results of the spectral analysis are given in Table 3. Photon index values of the two spectra, in the 0.1–5 keV range, are slightly steeper than those usually found in RBLs. However, from *Ginga* observations it has been inferred that this RBL is a flat X-ray spectrum source (Makino 1989). Values of N_H are very close to the Galactic value. Fluxes from simultaneous radio through X-ray observations (Brown et al. 1989) were used to construct the multifrequency spectrum of this RBL, and it has been plotted in Figure 3*g*.

4.12. *Mrk 421*

This blazar (Angel & Stockman 1980; Maccagni et al. 1989; Burbidge & Hewitt 1992) has been classified as an XBL object (Giommi et al. 1990; Hewitt & Burbidge 1993). It was observed on many epochs with *EXOSAT* and *IUE* between 1984 and 1985 (George, Warwick, & Bromage 1988a; Edelson et al. 1992). X-ray spectra of this blazar were fitted using a power-law plus absorption model, and the fitting parameters are listed in Table 3. This model fitted all the spectra well, except for three spectra of this source when it was in a brighter state (1984 days 337, 338, and 340). Next, we have used other models, mentioned in § 4.1, to fit the three spectra. From *F*-test analysis we find that, among all these models, the power-law plus absorption plus high-energy cutoff and the power-law plus absorption plus absorption-edge models fit best with the three spectra, and these two models are highly significant compared with the simple power-law model ($\Delta\chi^2 > 15$, which is significant at better than the 99.9% level. Results of the fit parameters are listed in Tables 4B and 4C, respectively. Values of N_H listed in Tables 3, 4B, and 4C suggest that no intrinsic absorption is present in Mrk 421. It has displayed rapid and correlated variability of the ME count rate with the hardness ratio, which was also noted by Giommi et al. (1990). Derived values of Γ and ME fluxes (Table 3) are also correlated (George et al. 1988a). Simultaneous observations of radio through X-rays were used to construct the multifrequency spectrum of Mrk 421 (Makino et al. 1987), and it can be fitted by a single parabolic curve (Fig. 4*e*). The presence of the blue emission bump can also be seen in this figure.

4.13. *Mrk 180*

Mrk 180 is a BL Lac object (Angel & Stockman 1980; Maccagni et al. 1989; Burbidge & Hewitt 1992). It has been classified as an XBL (Giommi et al. 1990; Hewitt & Burbidge 1993). X-ray spectra of this source were obtained with *EXOSAT* on 1984 November 28 and 1985 April 3 (George, Warwick, & McHardy 1988b). Both the LE and ME fluxes increased by a factor of 2 between the *EXOSAT* observations. Correlated variability of the ME count rate and the hardness ratio of the source was also noted in this blazar (Giommi et al. 1990). X-ray spectra of Mrk 180 (Fig. 2*m*) are best fitted with the power-law plus absorption model (Table 3), and our results are in good agreement with that of George et al. (1988b). Mrk 180 is a steep-spectrum source with no intrinsic absorption. Radio to X-ray fluxes were obtained from simultaneous and quasi-simultaneous (Mufson et al. 1984) observations of Mrk 180 and were used to construct the multifrequency spectrum (Fig. 4*f*), which can be fitted with a single parabola.

4.14. *B2 1147+245*

This blazar (Angel & Stockman 1980; Ledden & O'Dell 1985; Stickel et al. 1991; Burbidge & Hewitt 1992) has been classified as an RBL (Giommi et al. 1990; Hewitt & Burbidge 1993). It was observed with *EXOSAT* on 1984 January by A. P. Willmore, but the results have not been published. We have carried out detailed spectral analysis and have found that the power-law plus absorption model fits best with the spectrum of this source. Results of the analysis are listed in Table 3. The value of N_H is consistent with the Galactic value. Radio through X-ray continuum emission fluxes can be well represented by two parabolic curves (Fig. 3*h*).

4.15. *3C 273*

3C 273 is a superluminal source (Zensus 1989), and it has been classified as an RBL object (Giommi et al. 1990; Hewitt & Burbidge 1993). This blazar was observed with *EXOSAT* on six occasions between 1984 and 1986. Both *EXOSAT* and *Ginga* observations of this source have been described by Turner et al. (1990 and references therein). We used the power-law plus absorption model to fit the *EXOSAT* spectra of 3C 273, but the derived values of N_H are smaller than the Galactic value. Next we fitted the spectra using the power-law plus fixed absorption model, and the results are listed in Table 3. It can be seen from this table that the reduced χ^2 values are very large, which suggests that the fits to the spectra are not acceptable. Then we tried to fit the spectra using all the models mentioned in § 4.1. From the *F*-test analysis (using Tables 3, 4D, and 4E), we find that the power-law plus blackbody and thermal bremsstrahlung plus fixed absorption models fit the spectra best, and also these two models are highly significant (>99.99%) over the power-law model. Simultaneous multifrequency observations of this source were carried out at different

epochs (Landau et al. 1986; Courvoisier et al. 1990 and references therein), and the results of such observations were used to construct the multifrequency spectrum of this RBL (Fig. 3*i*), which can be represented by two parabolic curves.

4.16. *1E 1402+04*

1E 1402+04 is a BL Lac object (Ledden & O'Dell 1985; Stocke et al. 1990; Burbidge & Hewitt 1992) and is also known as an XBL (Giommi et al. 1990; Hewitt & Burbidge 1993). It was observed at three epochs with *EXOSAT* (Giommi et al. 1986, 1987), but only one spectrum has signal significance above 4 σ. This spectrum can be best modeled by a power-law plus fixed absorption model (see Table 3). Rapid X-ray variability, on timescales of hours, was detected in this blazar, which was also noted by Giommi et al. (1990). Radio, far-infrared, infrared, optical, and X-ray fluxes of this XBL are plotted in Figure 4*g*. Optical to X-ray fluxes can be fitted by a smooth curve. However, because of the steep radio spectrum and nonavailability of measured millimeter fluxes, we are not sure about the nature of the multifrequency spectrum between radio and infrared frequencies.

4.17. *1E 1415+259*

1E 1415+259 is an XBL (Impey & Tapia 1988; Maccagni et al. 1989; Burbidge & Hewitt 1992; Hewitt & Burbidge 1993), and it was observed on 1986 March 7 with *EXOSAT* (Giommi et al. 1987). The X-ray spectrum of this blazar can be best described by a power-law plus absorption model (Fig. 2*u*). No rapid variability of this source was noted within the single observation. The multifrequency spectrum of this source, which was constructed using nonsimultaneous observations, can be represented by a single parabolic curve (Fig. 4*h*).

4.18. *1H 1427+42*

1H 1427+42 is an XBL (Maccagni et al. 1989; Remillard et al. 1989; Burbidge & Hewitt 1992; Giommi et al. 1990; Hewitt & Burbidge 1993). It was observed with *EXOSAT* on 1985 January 12. The power-law plus absorption model fits this spectrum best (Table 3). This blazar is a steep-spectrum ($\Gamma = 2.10 \pm 0.07$) source with no intrinsic absorption (Remillard et al. 1989). The radio through X-ray spectrum of this blazar is shown in Figure 4*i*, and it can be represented by a single parabolic spectral component.

4.19. *PKS 1510−089*

PKS 1510−089 was confirmed as a blazar by Moore & Stockman (1984) and Smith et al. (1987). It is one of the most violently variable ($\Delta V \sim 5.4$ during the flare states) and highly polarized quasar (Moore & Stockman 1981; Ledden & O'Dell 1985; Mead et al. 1990; Burbidge & Hewitt 1992). This blazar has been classified as an RBL (Hewitt & Burbidge 1993). Two spectra of this source, obtained with *EXOSAT*, have signal significances above 4 σ, and these two spectra can be best fitted with the power-law plus absorption model; the parameters are listed in Table 3. Variations of the LE and ME fluxes, on timescales of hours, are absent in this source. There is no detection of any significant low-energy absorption within this flat spectrum. Results of our spectral analysis are consistent with the results of Singh, Rao, & Vahia (1990). Radio through X-ray continuum fluxes of this object are shown in Figure 3*j*, and the spectrum can be well represented by two parabolic components.

4.20. *Mrk 501*

Mrk 501 is a well-known BL Lac object (Angel & Stockman 1980; Maccagni et al. 1989; Stickel et al. 1991; Burbidge & Hewitt 1992). It has been classified as an XBL (Giommi et al. 1990; Hewitt & Burbidge 1993). Mrk 501 was observed on many occasions with *EXOSAT*. In Table 2 we have listed only those observations which have signal significance above 4 σ. Details of X-ray observations of this source with *uhuru, ariel 5, HEAD 1* and *2,* and *EXOSAT* are given in Staubert et al. (1986a), and *EXOSAT* and *IUE* observations are given in George et al. (1988b) and Edelson et al. (1992). Correlated variability of the ME count rates with the hardness ratio of this source was detected from *EXOSAT* observations (Giommi et al. 1990). This blazar also displayed rapid variability of the ME flux on timescales of hours. To fit the spectra of Mrk 501, we have used different models, mentioned in § 4.1. We have found that the power-law plus absorption model fits these spectra best. Results of the fit parameters show that Mrk 501 is a steep-spectrum (Fig. 2*x*) source with no intrinsic absorption (Table 3). The multifrequency spectrum of this XBL was constructed using simultaneous/quasi-simultaneous multifrequency observations (Mufson et al. 1984; Sembay et al. 1985). This spectrum (Fig. 4*j*) can be represented by a single spectral component.

4.21. *4U 1722+119*

4U 1722+119 is an X-ray–selected BL Lac object (Griffiths et al. 1989; Brissenden et al. 1990; Burbidge & Hewitt 1992; Hewitt & Burbidge 1993; Giommi et al. 1990). The X-ray spectrum of this blazar, observed with *EXOSAT,* can be best fitted with the power-law plus absorption model. The fit parameters are listed in Table 3, and it can be seen from this table that 4U 1722+119 is a steep-spectrum source with no intrinsic absorption. Using the fluxes from nonsimultaneous observations, we have constructed the multifrequency spectrum of this blazar, which can be fitted with a single parabolic curve (Fig. 4*k*).

4.22. *I Zw 186*

I Zw 186 is a BL Lac object (Angel & Stockman 1980; Maccagni et al. 1989; Burbidge & Hewitt 1992), and it has been classified as an XBL (Giommi et al. 1990; Hewitt & Burbidge 1993). The *EXOSAT* spectrum of this blazar can be best described by a power-law plus absorption model. The best-fitting spectral parameters are listed in Table 3, and our results are in agreement with the results of Garilli & Maccagni (1990). Simultaneous observations at radio, NIR, and optical frequencies (Bregman et al. 1982) and nonsimultaneous observations at FIR, UV, and X-rays were used to construct the multifrequency continuum energy distribution of this blazar, which can be fitted with a single parabolic spectral component (Fig. 4).

4.23. *3C 371*

3C 371 is an optically violent variable object (Angel & Stockman 1980; Webb et al. 1988; Stickel et al. 1991; Burbidge & Hewitt 1992) and is also a superluminal source (Mutel 1989) which has been classified as a RBL (Giommi et al. 1990; Hewitt & Burbidge 1993). *EXOSAT* observations of this blazar were carried out on 1984 September 11 and 29 (Staubert, Brunner, & Worrall 1986b), but only the spectrum of September 11 has signal significance above 4 σ. In the present analysis we have used only this spectrum, which can be best fitted with a power-law plus fixed absorption model. Best-fitting parameters are listed in Table 3. Results of our analysis are in agreement with that of Staubert et al. (1986b). Using the simultaneous observations at radio, NIR, optical, and UV wavelengths during 1981 May (Worrall et al. 1984a), radio and millimeter wavelengths during 1983 March–April (Landau et al. 1986), and UV and X-rays during September 29 and 30 1984, we have constructed the multifrequency spectrum of this blazar (Fig. 3*k*), and it can be well represented by two parabolic spectral components.

4.24. *3C 390.3*

3C 390.3 is a radio galaxy and is also called a highly polarized quasar (Angel & Stockman 1980; Ledden & O'Dell 1985; Burbidge & Hewitt 1992). It is also known as a superluminal source (Porcas 1987), and we have classified this blazar as an RBL. This source was observed with *EXOSAT* on many epochs between 1984 and 1986, but only three spectra have signal significances above 4 σ. Detailed results of the X-ray spectral analysis of this blazar, based on *EXOSAT* observations, have been described by Ghosh & Soundararajaperumal (1991). We have used different models to fit the spectra and have found that only the broken power-law plus fixed absorption and the power-law plus fixed absorption plus emission-line models fit slightly better than the power-law plus fixed absorption model, but these two models are not statistically significant ($\Delta\chi^2 \sim 2$–4) over the power-law plus absorption model. Radio through X-ray continuum fluxes of this RBL can be fitted with two parabolic components (Fig. 3*l*).

4.25. *OV 236*

OV 236 is a highly polarized quasar as well as an optically violent variable blazar (Ledden & O'Dell 1985; Pica et al. 1988; Mead et al. 1990; Burbidge & Hewitt 1992). It is also known as an RBL object (Hewitt & Burbidge 1993). The X-ray spectrum of this blazar can be best described by a power-law plus absorption model (Table 3). The multifrequency spectrum (Fig. 3*m*) of this luminous source has been constructed using the fluxes from simultaneous observations at radio, millimeter, NIR, and optical wavelengths (Brown et al. 1989) and nonsimultaneous observations at UV and X-rays.

4.26. *1928+73*

The object 1928+73 is a superluminal source (Zensus 1989), and it is known as a HPQ/OVV-type blazar (Burbidge & Hewitt 1992; Ghosh & Soundararajaperumal 1992), and it has also been classified as an RBL (Hewitt & Burbidge 1993). It was observed with *EXOSAT* at four epochs between 1983 and 1984, but only two spectra have signal significances above 4 σ. Detailed spectral analysis of this source has been described by Ghosh & Soundararajaperumal (1992). Best-fitting parameters of the power-law plus absorption model are listed in Table 3. This source displayed uncorrelated variability of the LE and ME fluxes. Variations of this type indicate that the LE and ME fluxes have different origins (Ghosh & Soundararajaperumal 1992; Turner et al. 1990). A soft excess for such sources may not be significant above the extrapolation of the ME power law, but the distribution of their fluxes indicates a separate component. The multifrequency spectrum of this blazar is shown in Figure 3*n*, and it can be represented by two parabolic curves.

4.27. *PKS 2005−489*

PKS 2005−489 is an X-ray–selected BL Lac object (Stickel et al. 1991; Burbidge & Hewitt 1992; Giommi et al. 1990). It was observed on five occasions with *EXOSAT* in 1984 and 1985. Out of five observations, only three have signal significance above 4 σ. These three spectra were best fitted with the power-law plus absorption model (Table 3). It can be seen from Tables 2 and 3 that the spectral slope flattened as the ME count rate of the source increased. Also, rapid variability of the ME count rate was observed in this source (Giommi et al. 1990). Using the simultaneous observations at UV and X-rays and nonsimultaneous observations at radio, FIR, NIR, and optical frequencies, we have constructed the multifrequency spectrum of this source, which can be fitted with a single parabolic curve. A weak emission bump around the near-infrared and optical bands is present, and there is no discontinuity in the UV–X-ray region (Fig. 4*m*).

4.28. *PKS 2155−304*

PKS 2155−304 is a well-studied XBL (Angel & Stockman 1980; Mead et al. 1990; Maccagni et al. 1989; Burbidge & Hewitt 1992; Giommi et al. 1990; Hewitt & Burbidge 1993). Simultaneous multifrequency observations of this blazar were carried out during *EXOSAT* observations, and correlated flux variability at different frequencies was observed in this source (Treves et al. 1989). The power-law plus absorption model was used to fit the LE and ME spectra, but this model did not fit well with the spectra of this blazar ($\chi_r^2 > 2$). Next we have used all the other models, mentioned in § 4.1, to fit the spectra, and from *F*-test analysis we find that the spectra of PKS 2155−304 can be best described by the power-law plus fixed absorption plus absorption-edge model (Table 4F) or by the broken power-law with fixed absorption model (Table 4G). The derived values of N_H are consistent with the Galactic value. Results of our spectral analysis are consistent with the results of Treves et al. (1989). PKS 2155−304 has displayed the same type of spectral variability in X-rays as was seen in PKS 2005−489 (Morini et al. 1986; Giommi et al. 1990; also see Tables 2 and 3). The multifrequency spectrum of this source, which has been constructed using fluxes at different frequencies from simultaneous observations, is also similar to that of the XBL PKS 2005−489 (Fig. 4*n*).

5. DISCUSSION

Results of the X-ray spectral analysis and the multifrequency spectra of 28 blazars have been described in the previ-

ous section. In this section we will first summarize the results and then discuss the results in the framework of a unified model of blazars. In Tables 5A and 5B we have listed the values of X-ray photon indices and luminosities at different frequencies between radio and X-rays for RBLs and XBLs, respectively. It may be noted from these tables that the X-ray spectral indices of RBLs are in general flatter than those of XBLs. Also, it can be seen from Tables 5A and 5B that the RBLs are much more luminous in radio than the XBLs (by two or three orders of magnitude). However, the RBLs, which are in general higher redshift objects than the XBLs, are slightly more luminous in X-rays (by factors of 4–7) than the XBLs. Luminosities in different bands (radio, FIR, IR, optical, UV, and X-ray) for RBLs and XBLs are given in Tables 5A and 5B, respectively. Radio luminosity versus FIR (60 μm), IR (2.2 μm), optical (5560 Å), UV (2000 Å), and X-ray (2–10 keV) luminosities of RBLs and XBLs are plotted in Figures 5*a*–5*e*. These figures clearly show the bimodal nature of the distribution of blazars. Also it may be noted from the comparison of the above figures that the separation between RBLs and XBLs gradually increases as we move from Figure 5*a* to Figure 5*e*, and the largest separation and the best correlations are present in the X-ray versus radio luminosity plot (Fig. 5*e*).

Most of the objects of our sample have not been observed in the millimeter-wavelength region, and the lack of such observations did not allow us to plot radio luminosity versus millimeter-wave luminosity and millimeter-wave luminosity versus FIR luminosity. FIR luminosity versus IR, optical, UV, and X-ray luminosities are plotted in Figures 5*f*–5*i*. Similarly, IR luminosity versus optical, UV, and X-ray luminosities; optical luminosity versus UV and X-ray luminosities; and UV versus X-ray luminosities are plotted in Figures 5*j*–5*l*, Figures 5*m*–5*n*, and Figure 5*o*, respectively. It can be seen from these luminosity-luminosity plots that the best correlations are present between FIR versus IR (Fig. 5*f*), IR versus optical (Fig. 5*j*) and optical versus UV (Fig. 5*m*) luminosities. A weak correlation is also present in Fig. 5*o*, which displays UV versus X-ray luminosities of blazars. Careful inspection of this figure shows that the UV and X-ray luminosities are better correlated if we consider only the XBLs rather than all the blazars (XBLs plus RBLs). This can be clearly seen from Figures 6*a* and 6*b*, which show the plots of two-point spectral indices between UV and X-ray ($\alpha_{\rm UV\text{-}X}$) versus the UV spectral index ($\alpha_{\rm UV}$) for XBLs and RBLs, respectively. It may be noted from these figures (Figs. 5*o* and 6*a*) that the UV and X-ray fluxes from XBLs are correlated and that those from RBLs are not correlated, and because of these results we find the spectral continuity and discontinuity in the UV–X-ray region for XBLs and RBLs, respectively. Also we have obtained the same results using only simultaneous UV and X-ray observations of 12 blazars of our sample which were carried out with *IUE* and *EXOSAT* (six RBLs: 3C 120, PKS 0521−36, PKS 0754+10, OJ 287, 3C 273 and 3C 371; six XBLs: H0323+022, Mrk 421, Mrk 180, Mrk 501, PKS 2005−489, and PKS 2155−304).

Multifrequency spectra (radio through X-ray) of 28 blazars are plotted in Figures 3 and 4. These spectra have been constructed using simultaneous/nonsimultaneous observations. Almost 50% of the sources of our sample were observed simultaneously at UV and X-rays. Such simultaneous observations are very important for multifrequency studies, because these observations will display how the X-ray spectrum gets connected with the continuum at the lower frequencies. In general, the radio through X-ray continuum emission spectra of XBLs can be represented by a single parabola (see § 3.2). Such a smooth change of the continuum spectra of XBLs from radio to X-ray (from flat to steep spectral indices) indicates that they are produced via synchrotron radiation (Königl 1981; Ghisellini, Maraschi, & Treves 1985; Urry, Mushotzky, & Holt 1986 and references therein). However, two parabolae (one for radio through UV and the other one for X-rays) are required to represent the multifrequency spectra of RBLs with spectral discontinuity in the UV–X-ray region (see Fig. 3). Also, the detected X-ray fluxes from RBLs are much higher than expected from IR through UV extrapolation. Such excess of X-rays indicates that IR through UV and X-rays are produced from different physical processes. It has been suggested that the radio through UV emissions are from synchrotron radiation and the X-ray emissions are from the inverse Compton mechanism (Ghisellini et al. 1985 and references therein).

A large number of observational results such as superluminal motion (Zensus 1989), high brightness temperature, rapid variability, paucity of X-ray self-Compton radiation (Blandford 1987), and radio jets (Liang 1988; Garington et al. 1988) have been interpreted in the framework of relativistic beaming models, which was first suggested by Blandford & Rees (1978). At present there are two such beaming models: (1) the "accelerating jet" model (Ghisellini & Maraschi 1989 and references therein) and (2) the "wide-jet" model (Celotti et al. 1993 and references therein). In the accelerating jet model it has been suggested that the flow velocity of the relativistic beam increases with radial distance so that relativistic beaming is weak in the inner, X-ray–emitting region of the jet, but strong in the outer, radio-emitting region of the jet (Ghisellini & Maraschi 1989). This model explains most of the observed results of blazars including the observed energy distributions, but it is difficult in this model to explain the rapid and large-amplitude X-ray variability (Treves et al. 1989). In the "wide-jet" model (Celotti et al. 1993) it is assumed that the flow velocity is constant but the degree of beaming increases with decreasing frequency, that is, the opening angle of the X-ray–emitting region at the inner part of the jet is much wider than that of the radio-emitting region at the outer part (collimation of the jet increases with distance). We will discuss the results for 28 blazars, presented in this paper, using the wide-jet model with the assumption that the XBLs are observed at intermediate angles and the RBLs are observed at small angles with the jet axis (Urry, Maraschi, & Phinney 1991a). If the beaming cone at the inner region of the jet is wider than at the outer region, an observer at intermediate angles will receive, relatively, more X-rays than radio emission. The X-rays produced via synchrotron radiation will have a steep spectrum because of the short radiative lifetimes and because of high-energy cutoffs in the particle spectra. The X-ray emission of XBLs (observed at intermediate angles) could thus be interpreted as synchrotron emission from the inner part of the jet, and the X-ray luminosity of these objects will be greater than the radio luminosity of the RBLs (see Table 5B) because the degree of beaming increases with decreasing frequency. Farther out of the X-ray–emitting region, the jet becomes more collimated and emits synchrotron radiation from the UV to the radio band.

An observer at small angles with the jet axis will receive do-

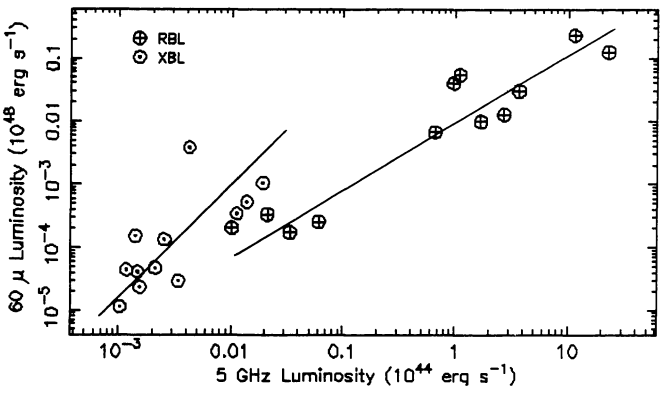

FIG. 5*a*

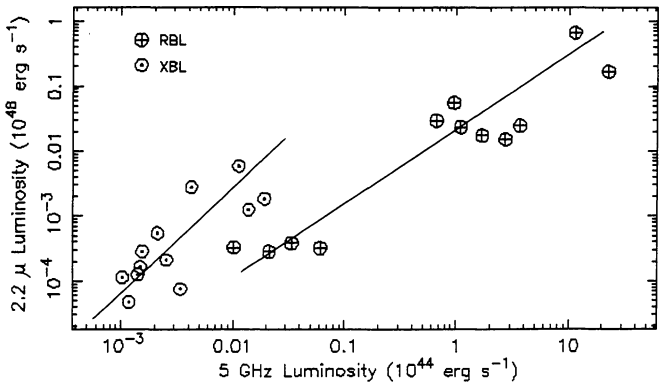

FIG. 5*b*

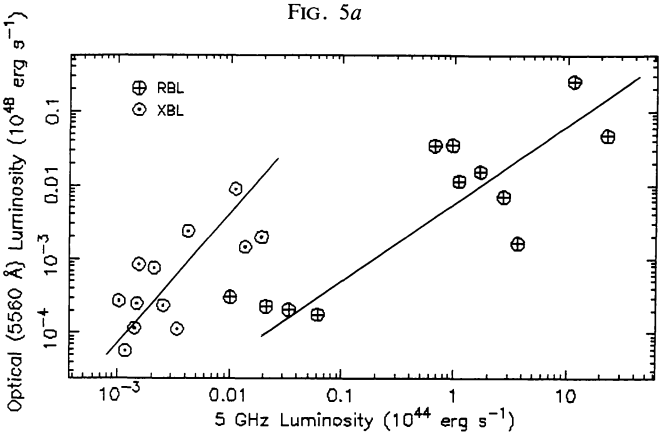

FIG. 5*c*

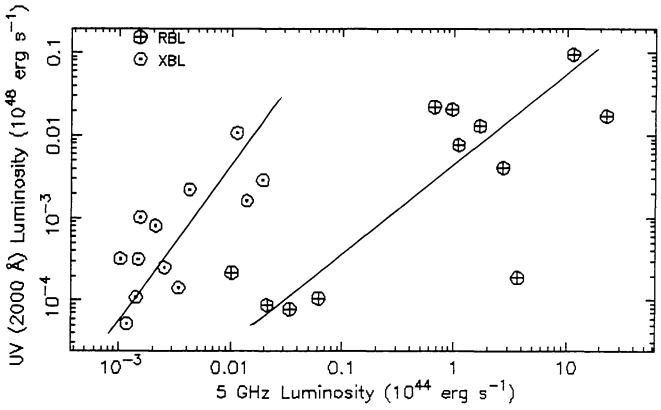

FIG. 5*d*

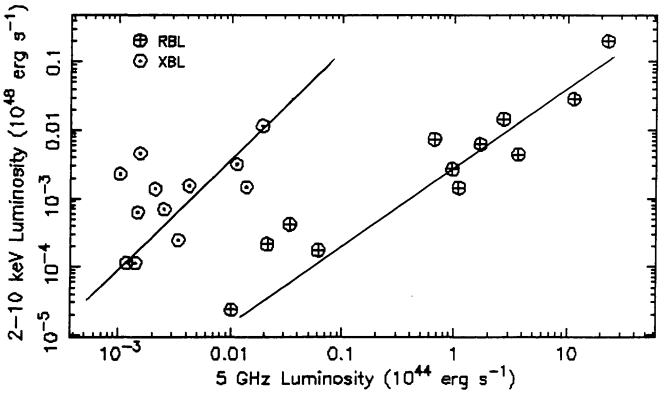

FIG. 5*e*

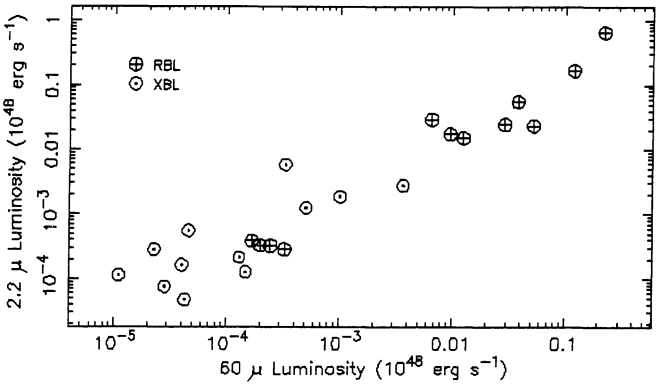

FIG. 5*f*

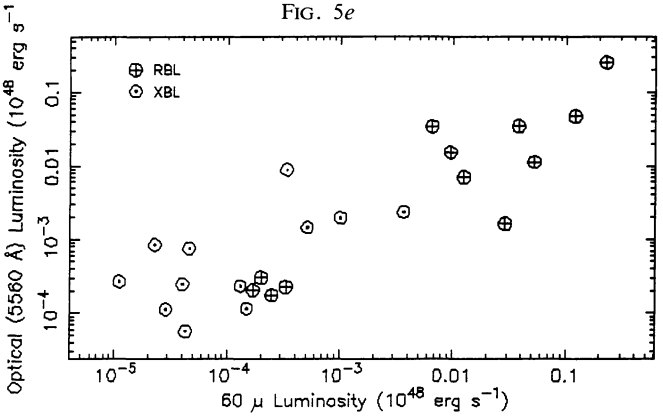

FIG. 5*g*

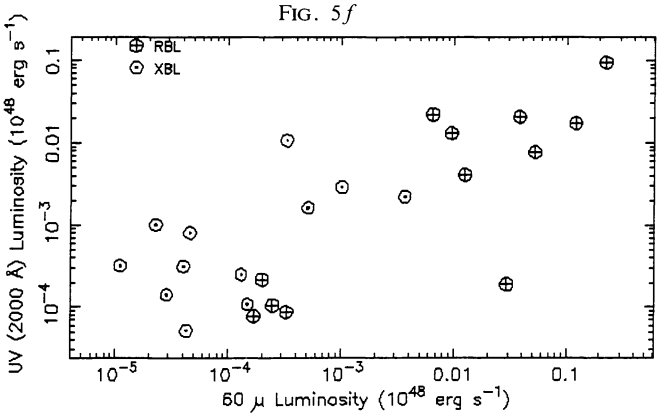

FIG. 5*h*

FIG. 5.—(*a*) Radio (5 GHz) luminosity vs. FIR (60 μm) luminosity of blazars. (*b*) Same as (*a*), but for radio vs. NIR (2.2 μm). (*c*) Same as (*a*), but for radio vs. optical (5560 Å). (*d*) Same as (*a*), but for radio vs. UV (2000 Å). (*e*) Same as (*a*), but for radio vs. X-ray (2–10 keV). (*f*) Same as (*a*), but for FIR vs. NIR. (*g*) Same as (*a*), but for FIR vs. optical. (*h*) Same as (*a*), but for FIR vs. UV. (*i*) Same as (*a*), but for FIR vs. X-ray. (*j*) Same as (*a*), but for NIR vs. optical. (*k*) Same as (*a*), but for NIR vs. UV. (*l*) Same as (*a*), but for NIR vs. X-ray. (*m*) Same as (*a*), but for optical vs. UV. (*n*) Same as (*a*), but for optical vs. X-ray. (*o*) Same as (*a*), but for UV vs. X-ray.

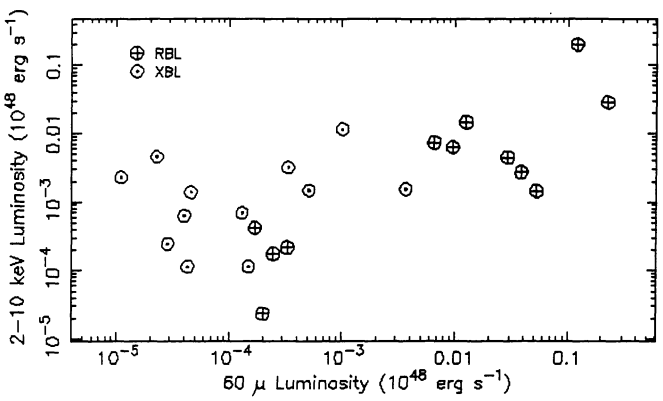

FIG. 5*i*

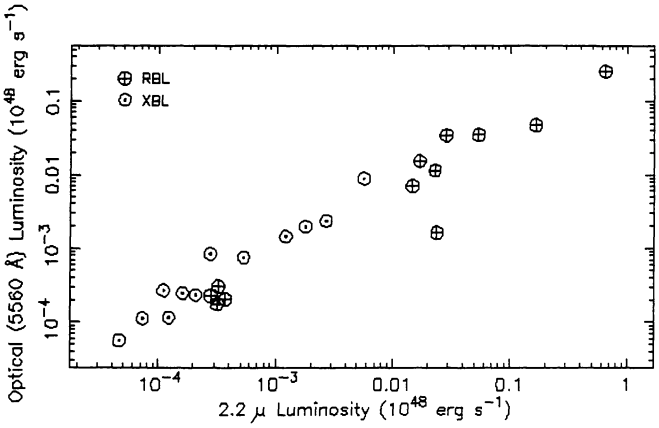

FIG. 5*j*

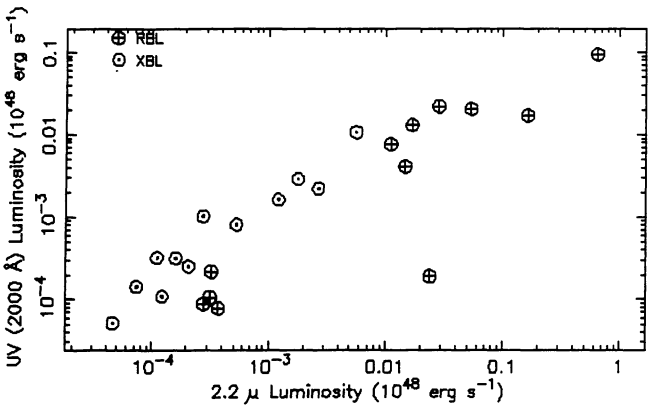

FIG. 5*k*

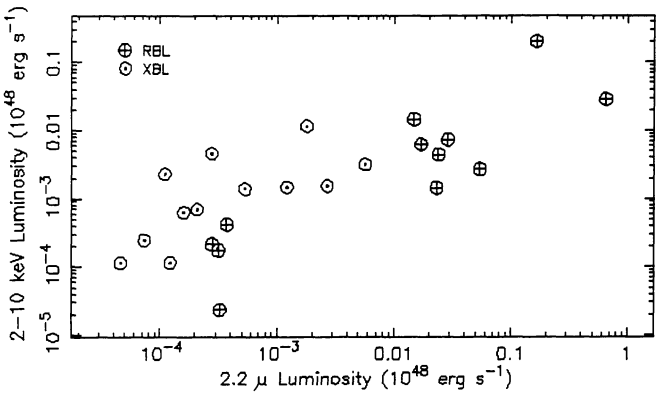

FIG. 5*l*

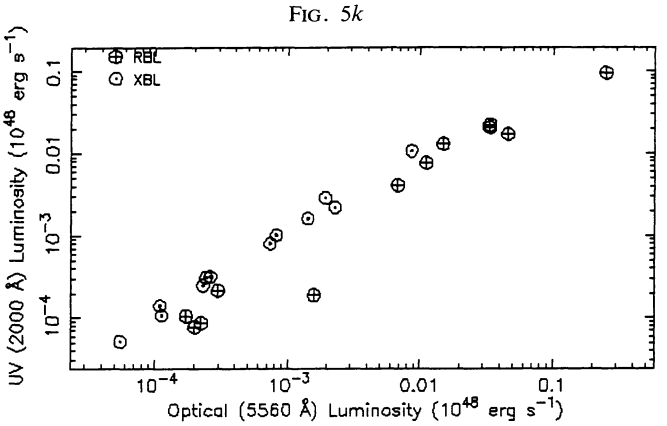

FIG. 5*m*

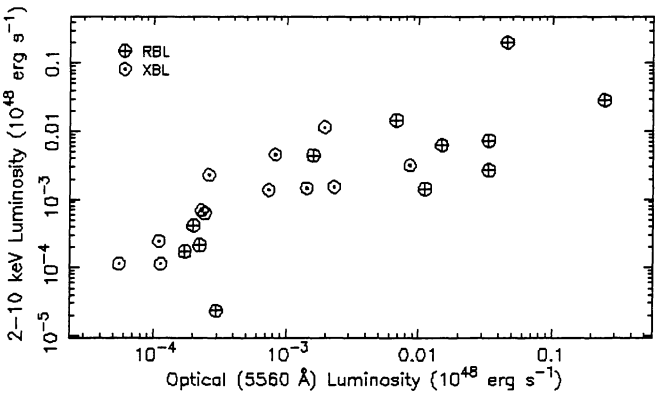

FIG. 5*n*

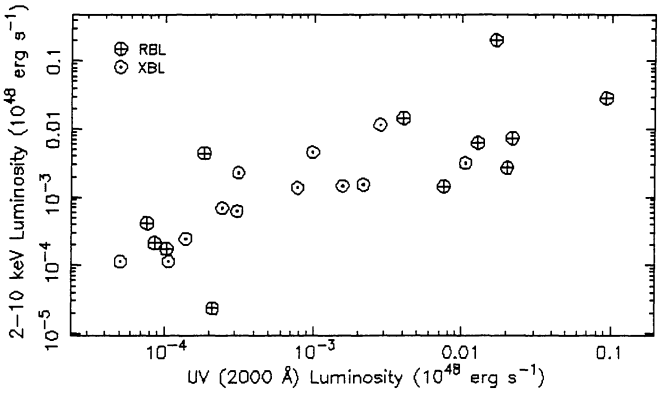

FIG. 5*o*

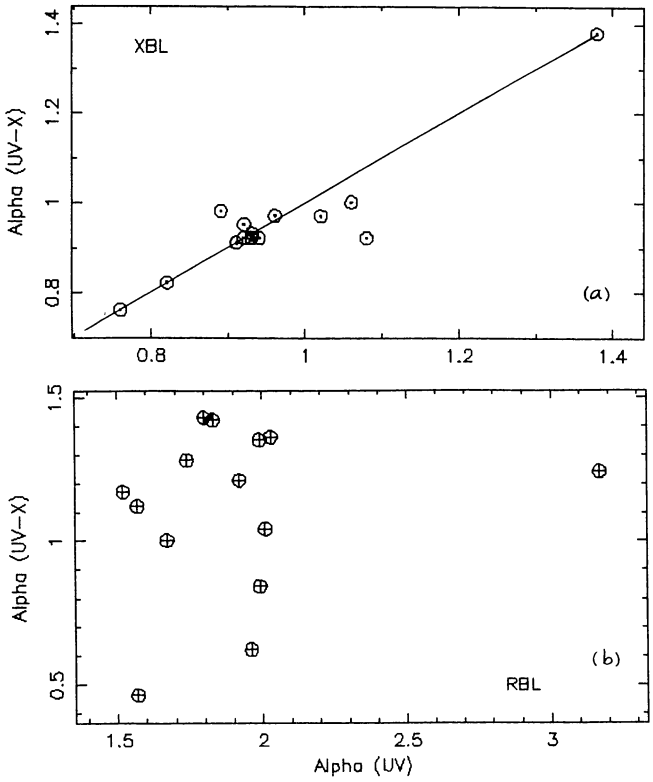

FIG. 6.—(*a*) Plot of $\alpha_{UV\text{-}X}$ vs. α_{UV} for XBLs. (*b*) Same as (*a*), but for RBLs.

minant fluxes from the outer part rather than the inner part. If the X-rays are produced from the inverse Compton mechanism in the outer region of the jet in a narrower cone, the emitted X-rays will have a flat spectrum and a large excess with respect to the UV emission. In RBLs, the X-rays could thus be interpreted as due to the inverse Compton mechanism from the outer region of the jet with spectral discontinuity between the UV and the X-ray bands.

The bimodal distribution of blazars in the luminosity-luminosity plane (see Figs. 5*a*–5*e*) and the increase in separation between XBLs and RBLs may be due to the increasing collimation of the jet with distance and the effect of the viewing angles of the two groups of blazars. Also, the bimodal spectral and spatial distribution of XBLs and RBLs (see Fig. 1) may be interpreted if the X-rays are beamed in a wider cone than the radio emissions (Celotti et al. 1993). Even though the wide-jet model can explain the observed properties of blazars, including the rapid and large-amplitude X-ray variability, it will be interesting to test this model with a larger and unbiased complete sample of blazars.

We are grateful to Professor J. C. Bhattacharyya for his support and encouragement in all respects. Our thanks to the *EXOSAT* Observatory staff, especially to N. E. White, A. N. Parmar, F. Habrel, P. Giommi, P. Barr, and A. M. T. Pollock, at ESTEC, who helped us to get the data from the archives and provided us with the XSPEC software package. One of us, K. K. G., wants to express his sincere thanks to the *EXOSAT* staff for their help in data analysis during his stay at ESTEC. Our sincere thanks to the anonymous referee for valuable comments and suggestions that improved the paper considerably.

REFERENCES

Angel, J. R. P., & Stockman, H. S. 1980, ARA&A, 18, 321
Barr, P., Giommi, P., & Maccagni, D. 1988, ApJ, 324, L11
Bersanelli, M., Bouchet, P., Falomo, R., & Tanzi, E. G. 1992, AJ, 104, 28
Blandford, R. D. 1987, in Superluminal Radio Sources, ed. A. Zensus & T. Pearson (Cambridge: Cambridge Univ. Press), 310
Blandford, R. D., & Rees, M. J. 1978, in Pittsburgh Conf. on BL Lac Objects, ed. A. M. Wolfe (Pittsburgh: Univ. Pittsburgh Press), 328
Boksenberg, A., et al. 1978, Nature, 275, 404
Bregman, J. N., et al. 1982, ApJ, 253, 19
Brissenden, R. J. V., Remillard, R. A., Tuohy, I. R., Schwartz, D. A., & Hertz, P. L. 1990, ApJ, 350, 578
Brown, L. M. J., et al. 1989, ApJ, 340, 129
Burbidge, E. M., & Strittmatter, P. A. 1972, ApJ, 172, L37
Burbidge, G., & Hewitt, A. 1992, in Variability of Blazars, ed. E. Valtaoja & M. Valtonen (Cambridge: Cambridge Univ. Press), 4
Celotti, A., Maraschi, L., Ghisellini, G., Caccianiga, A., & Maccacaro, T. 1993, ApJ, 416, 118
Cohen, R. D., Smith, H. E., Junkkarinen, V. T., & Burbidge, E. M. 1987, ApJ, 318, 577
Courvoisier, T. J. L., Bell-Burnell, J., & Blecha, A. 1986, A&A, 169, 43
Courvoisier, T. J. L., et al. 1990, A&A, 234, 73
Cruz-Gonzalez, I., & Huchra, J. P. 1984, AJ, 89, 441
Danziger, I. J., Fosbury, R. A. E., Goss, W. M., & Ekers, R. D. 1979, MNRAS, 188, 415
de Korte, P. A. J., Bleeker, J. A. M., den Boggende, A. J. F., Branduardi-Raymont, G., Culhane, J. L., Gronenschild, E. H. B. M., Mason, I., & McKechnie, S. P. 1981, Space Sci. Rev., 30, 495
Edelson, R. A. 1987, AJ, 94, 1150
Edelson, R., Pike, G. F., Saken, J. M., Kinney, A., & Shull, J. M. 1992, ApJS, 83, 1
Elvis, M., Lockman, F. J., & Wilkes, B. 1989, AJ, 97, 777
Feigelson, E. D., Maccacaro, T., & Zamorani, G. 1982, ApJ, 255, 392
Feigelson, E., et al. 1986, ApJ, 302, 337
French, H. B., & Miller, J. S. 1980, PASP, 92, 753
Garilli, B., & Maccagni, D. 1990, A&A, 229, 88
Garington, S. T., Leahy, J. P., Conway, R. G., & Liang, R. A. 1988, Nature 331, 147
Gear, W. K., et al. 1986, 304, 295
George, I. M., Warwick, R. S., & Bromage, G. E. 1988a, MNRAS, 232, 793
George, I. M., Warwick, R. S., & McHardy, I. M. 1988b, MNRAS, 235, 787
Ghisellini, G., & Maraschi, L. 1989, ApJ, 340, 181
Ghisellini, G., Maraschi, L., & Treves, A. 1985, A&A, 146, 204
Ghosh, K. K., & Soundararajaperumal, S. 1991, AJ, 102, 1298
———. 1992, MNRAS, 254, 563
Giacani, E. B., & Colomb, F. R. 1988, A&AS, 76, 15
Giommi, P., Barr, P., Garrilli, B., Gioia, I. M., Maccacaro, T., Maccagni, D., & Schild, R. E. 1987, ApJ, 322, 662
Giommi, P., Barr, P., Garrilli, B., Maccagni, D., & Pollock, A. M. T. 1990, ApJ, 356, 432
Giommi, P., Barr, P., Gioia, I. M., Maccacaro, T., Schild, R. E. Garrilli, B., & Maccagni, D. 1986, ApJ, 303, 596
Griffiths, R. E., Wilson, A. S., Ward, M. J., Tapia, S., & Ulvestad, J. S. 1989, MNRAS, 240, 33
Halpern, J. P., Chen, V. S., Madejski, G. M., & Chanan, G. A. 1991, AJ, 101, 818
Halpern, J. P., Impey, C. D., Bothun, G. D., Tapia, S., Schillman, E. D., Wilson, A. S., & Meurs, E. J. A. 1986, ApJ, 302, 711
Hewitt, A., & Burbidge, G. 1993, ApJS, 87, 451

Hjellming, R. M., Schnopper, H. W., & Moran, J. M. 1978, IAU Circ. 3309
Impey, C. D. 1987, in Superluminal Radio Sources, ed. J. A. Zensus & T. J. Pearson (Cambridge: Cambridge Univ. Press), 231
———. 1992, in Variability of Blazars, ed. E. Valtaoja & M. Valtonen (Cambridge: Cambridge Univ. Press), 55
Impey, C. D., & Neugebauer, G. 1988, AJ, 95, 307
Impey, C. D., & Tapia, S. 1988, ApJ, 333, 666
Impey, C. D., et al. 1984
Jannuzi, B. T., Smith, P. S., & Elston, R. 1994, ApJ, 428, 130
Jones, T. W., & O'Dell, S. L. 1977, ApJ, 215, 236
Kawai, N., Bregman, J. N., & Matsuoka, M. 1989, in Proc. 23d ESLAB Symp. on Two Topics in X-Ray Astronomy, ed. J. Hunt & B. Battrick (ESA SP-296; Noordwijk: ESA), 957
Kinman, T. D. 1975, in Variable Stars and Stellar Evolution, ed. E. Sherwood & L. Plaut (Boston: Reidel), 573
Königl, A. 1981, ApJ, 243, 700
Kristian, J., & Sandage, A. 1970, ApJ, 162, 391
Kuhr, H., Pauliny-Toth, I. I. K., Witzel, A., & Schmidt, J. 1981a, AJ, 86, 854
Kuhr, H., Witzel, A., Pauliny-Toth, I. I. K., & Nauber, U. 1981b, A&AS, 45, 367
Lampton, M., Margon, B., & Bowyer, S. 1976, ApJ, 208, 177
Landau, R., Epstein, E. E., & Rather, J. D. G. 1980, AJ, 85, 363
Landau, R., Jones, J. W., Epstein, E. E., Neugebauer, G., Soifer, B. J., Werner, M. W., Puschell, J. J., & Balonek, J. J. 1983, ApJ, 268, 68
Landau, R., et al. 1986, ApJ, 308, 78
Large, M. I., Mills, B. Y., Little, A. G., Crawford, D. F., & Sutton, J. M. 1981, MNRAS, 194, 1013
Ledden, I. E., Aller, H. D., & Dent, W. A. 1976, Nature, 260, 752
Ledden, J. E., & O'Dell, S. L. 1985, ApJ, 298, 630
Liang, R. A. 1988, Nature, 331, 149
Maccagni, D., Garilli, B., Barr, P., Giommi, P., & Pollack, A. 1989, in BL Lac Objects, ed. L. Maraschi, T. Maccacaro, & M.-H. Ulrich (Berlin: Springer), 281
Maccagni, D., Garilli, B., Schild, R., & Tarenghi, M. 1987, A&A, 178, 21
MacLeod, J. M., Andrew, B. H., & Harvey, G. A. 1976, Nature, 260, 751
Makino, F. 1989, in Proc. 23d ESLAB Symp. on Two Topics in X-Ray Astronomy ed. J. Hunt & B. Battrick (ESA SP-296; Noordwijk: ESA), 803
Makino, F., et al. 1987, ApJ, 313, 662
———. 1989, ApJ, 347, L9
———. 1991, in Variability of Active Galactic Nuclei, ed. H. Richard Miller & Paul J. Wiita (Cambridge: Cambridge Univ. Press), 13
Maraschi, L., Chiappetti, L., Falomo, R., Garilli, B., Malkan, M., Tagliaferri, G., Tanzi, E. G., & Treves, A. 1991, ApJ, 368, 138
Marscher, A. P. 1988, ApJ, 334, 552
McAlary, C. W., McLaren, R. A., McGonegal, R. J., & Maza, J. 1983, ApJS, 52, 341
Mead, A. R. G., Ballard, K. R., Brand, P. W. J. L., Hough, G. H., Brindle, C., & Bailey, J. A. 1990, A&AS, 83, 183
Miller, J. S., French, H. B., & Hawley, S. A. 1978, in Pittsburgh Conf. on BL Lac Objects, ed. A. M. Wolfe (Pittsburgh: Univ. Pittsburgh Press), 176
Moore, R. L., & Stockman, H. S. 1981, ApJ, 243, 60
———. 1984, ApJ, 279, 465
Morini, M., Chiappetti, L., Maccagni, D., Maraschi, D., Tanzi, E. G., Treves, A., & Wolter, A. 1986, ApJ, 306, L71
Morris, S. L., Stocke, J. T., Gioia, I. M., Schild, R. E., Wolter, A., Maccacaro, T., & Della Ceca, R. 1991, ApJ, 380, 49
Morrison, R., & McCammon, D. 1983, ApJ, 270, 119
Mufson, S. L., et al. 1984, ApJ, 285, 571
Mushotzky, R. F., Marshall, F. E., Boldt, E. A., Holt, S. S., Pravdo, S. H., Serlemitsos, P. J., Swank, J. H., & Rothschild, R. H. 1978, ApJ, 226, 65
Mutel, R. L. 1989, in NRAO Parsec-Scale Radio Jet Workshop (Socorro)
Neugebauer, G., Miley, G. K., Soifer, B. T., & Clegg, P. E. 1986, ApJ, 308, 815
O'Dea, C. P., Barvainis, R., & Challis, P. M. 1988, AJ, 96, 435
Oke, J. B., Readhead, A. C. S., & Sargent, W. L. W. 1980, PASP, 92, 758
Owen, F. N., Spangler, R., & Cotton, W. D. 1980, AJ, 85, 351
Padovani, P., & Urry, C. M. 1992, ApJ, 387, 449
Pauliny-Toth, I. I. K., & Kellermann, K. I. 1968, AJ, 73, 953
———. 1972, AJ, 77, 797
Pauliny-Toth, I. I. K., Kellermann, K. I., Davis, M. M., Fomalont, E. B., & Shaffer, D. B. 1972, AJ, 77, 265
Perley, R. A. 1982, AJ, 87, 859
Perlman, E. S., & Stocke, J. T. 1993, ApJ, 406, 430
Pica, A. J., Smith, A. G., Webb, J. R., Leacock, R. J., Clements, S., & Gombola, P. P. 1988, AJ, 96, 1215
Porcas, R. W. 1987, in Superluminal Radio Sources, ed. J. A. Zensus & T. J. Pearson (Cambridge: Cambridge Univ. Press), 12
Remillard, R. A., Tuohy, I. R., Brissenden, R. J. V., Buckley, D. A. H., Schwartz, D. A., Feigelson, E. D., & Tapia, S. 1989, ApJ, 345, 140
Rieke, G. H., Grasdalen, G. L., Kinman, T. D., Hintzen, P., Wills, B. J., & Wills, D. 1976, Nature, 260, 754
Roelling, T. L., Becklin, E. E., Impey, C. D., & Werner, M. W. 1986, ApJ, 304, 646
Sambruna, R. M., Barr, P., Maraschi, L., Togliaferri, G., & Treves, A. 1993, ApJ, 408, 452
Schmitt, J. L., 1968, Nature, 218, 663
Sembay, S., et al. 1985, MNRAS, 216, 121
Shafer, R. A., Haberl, F., & Arnaud, K. A. 1991, XSPEC User's Guide (Noordwijk: ESA)
Shimmins, A. J., & Bolton, J. G., 1972, Australian J. Phys. Astrophys. Suppl. 23, 1
———. 1974, Australian J. Phys. Astrophys. Suppl. 32, 1
Singh, K. P., Rao, A. R., & Vahia, M. N. 1990, ApJ, 365, 455
Sitko, L. M. 1989, in BL Lac Objects, ed. L. Maraschi, T. Maccacaro, & M.-H. Ulrich (Berlin: Springer), 119
Sitko, L. M., & Junkkarinen, V. T. 1985, PASP, 97, 1158
Smith, P. S., Balonek, T. J., Elston, R., & Heckert, P. A. 1987, ApJS, 64, 459
Stark, A. A., Gammie, C. F., Wilson, R. W., Bally, J., Linke, R. A., Heiles C., & Hurwitz, M. 1992, ApJS, 79, 77
Staubert, R., Bazzano, A., Ubertini, P., Brunner, H., Collmar, W., & Kendziorra, E. 1986a, A&A, 162, 16
Staubert, R., Brunner, H., & Worrall, D. M. 1986b, ApJ, 310, 694
Stein, W. A. 1978, in Pittsburgh Conf. on BL Lac Objects, ed. A. M. Wolfe (Pittsburgh: Univ. Pittsburgh Press), 328
Stein, W. A., O'Dell, S. L., & Strittmatter, P. A. 1976, ARA&A, 14, 173
Steppe, H., Salter, C. J., Chini, R., Kreysa, A., Brunswig, W., & Lobata Perez, J. 1988, A&AS, 75, 317
Stickel, M., Padovani, P., Urry, C. M., Fried, J. W., & Kuhr, H. 1991, ApJ, 374, 431
Stocke, J. T., Liebert, J., Schmidt, G., Gioia, I. M., Maccacaro, T., Schild, R. E., Maccagni, D., & Arp, H. 1985, ApJ, 298, 619
Stocke, J. T., Morris, S. L., Gioia, I. M., Maccacaro, T., Schild, R. E., & Wolter, A. 1988, in Optical Surveys for Quasars, ed. P. Osmer, A. C. Porter, R. Green, & C. Foltz (San Francisco: ASP), 311
———. 1989, in BL Lac Objects, ed. L. Maraschi, T. Maccacaro, & M.-H. Ulrich (Berlin: Springer), 209
———. 1990, ApJ, 348, 141
Strittmatter, P. A., Carswell, R. F., Gilbert, G., & Burbidge, E. M. 1974, ApJ, 190, 509
Treves, A., et al. 1989, ApJ, 341, 733
Turner, M. J. L., Smith, A., & Zimmerman, H. U. 1981, Space Sci. Rev., 30, 513
Turner, M. J. L., et al. 1990, MNRAS, 244, 310
Turner, T. J., & Pounds, K. A. 1989, MNRAS, 240, 833
Ulmer, M. P., Brown, R. L., Schwartz, D. A., Patterson, J., & Cruddace, R. G. 1983, ApJ, 270, L1
Ulrich, M.-H., Kinman, T. D., Lynds, C. R., Rieke, G. H., & Ekers, R. D. 1975, ApJ, 198, 261
Ulvestad, J. S., Johnston, K. J., & Weiler, K. W. 1983, ApJ, 266, 18
Urry, C. M., Maraschi, L., & Phinney, S. E. 1991a, Comm. Ap., 15, 111
Urry, C. M., Mushotzky, R. F., & Holt, S. S. 1986, ApJ, 305, 369
Urry, C. M., Padovani, P., & Stickel, M. 1991b, ApJ, 382, 501
Valtaoja, L., Valtaoja, E., Shakhovskoy, N. M., & Efimov, Yu. S. 1991, AJ, 101, 78
Véron-Cetty, M.-P., & Véron, P. 1993, A Catalogue of Quasars and Active Nuclei (6th ed.); ESO Sci. Rep. 5; Garching: ESO)
Wall, J. V., Danziger, I. J., Pettini, M., Warwick, R. S., & Wamsteker, W. 1986, MNRAS, 219, 23P
Wall, J. V., Shimmins, A. J., & Bolton, J. G. 1975, Australian J. Phys. Astrophys. Suppl., 34, 55

Ward, M., Elvis, M., Fabbiano, G., Carleton, N. P., Willner, S. P., & Lawrence, A. 1987, ApJ, 315, 74
Webb, J. R., Smith, A. G., Leacock, R. J., Fitzgibbons, G. L., Gombola, P. P., & Shepherd, D. W. 1988, AJ, 95, 374
Weiler, K. W., & Johnston, K. J. 1980, MNRAS, 190, 269
White, N. E., & Giommi, P. 1991, in Database and On-Line Data in Astronomy, ed. D. Egret & M. Albrecht (Dordrecht: Kluwer), 11
White, N. E., & Peacock, A. 1988, Mem. Soc. Astron. Ital., 59, 7
Wilkes, B. J. 1986, MNRAS, 218, 331
Wills, D., & Wills, B. J. 1976, ApJS, 31, 143
Wlerick, G., Westerlund, B., & Garnier, R. 1979, A&A, 72, 277
Wolfe, A. M., 1978, in Pittsburgh Conf. on BL Lac Objects, ed. A. M. Wolfe (Pittsburgh: Univ. Pittsburgh Press) 1
Wolter, A., Caccianiga, A., Della Ceca, R., & Maccacaro, T. 1994, ApJ, 433, 29
Worrall, D. M., et al. 1984a, ApJ, 278, 521
Worrall, D. M., Puschell, J. J., Rodriguez-Espinosa, J. M., Bruhweiler, F. C., Miller, H. R., Aller, M. F., & Aller, H. D. 1984b, ApJ, 286, 711
Worrall, D. M., Giommi, P., Tananbaum, H., & Zamorani, G. 1987, ApJ, 313, 596
Zensus, J. A. 1989, in BL Lac Objects, ed. L. Maraschi, T. Maccacaro, & M.-H. Ulrich (Berlin: Springer), 3